MECHANISMS AND MODELS OF DEHYDRATION AND SLOW FREEZING DAMAGE TO CELL MEMBRANES

A DISSERTATION
SUBMITTED TO THE FACULTY OF THE GRADUATE SCHOOL
OF THE UNIVERSITY OF MINNESOTA
BY

Vishard Ragoonanan

IN PARTIAL FULFILLMENT OF THE REQUIREMENTS
FOR THE DEGREE OF
DOCTOR OF PHILOSOPHY

Adviser: Alptekin Aksan

October 2010

Acknowledgments

I would like to thank my adviser, Professor Alptekin Aksan, for his advice and for pushing me to scrutinize and dissect everything. His guidance for the past five years has made me grow both as a researcher and as a person.

I would like to acknowledge all the people who have contributed to the studies that form part of this thesis: Professor Allison Hubel, Professor Timothy Wiedmann, Jason Malsam, Lily Zhang, Dario Canelon, Eduardo Reategui, Rebekah Less, Cally Scherber. Without their help, this thesis would not have been possible. I would also like to thank Professor John Bischof for useful discussions regarding damage to cell membranes due to osmotic and thermal stresses. I am grateful to my doctoral committee, Professor Allison Hubel, Professor John Bischof and Professor Jonathan Sachs, for their valued critique and feedback.

I would like to thank my colleagues and friends at the University of Minnesota who have supported me during my time there. I would especially like to thank Ms. Neha Shah for the many enjoyable conversations that we have had.

I owe my deepest gratitude to my parents, Mr. Lally Ragoonanan and Mrs. Carol Ragoonanan, and my sister, Dr. Vindra Ragoonanan. Withour their support and belief in me, I would never have been able to achieve what I have. I would also like to my father-in-law, Mr. Vinod Nagpal and my mother-in-law, Mrs. Uma Nagpal, for their support.

I am indebted to my wife, Ashima. Her love and support is the most precious thing in my life. Her strength and encouragement have been my inspiration.

Dedication

This dissertation is dedicated to my parents, my wife, Ashima, and my son, Aarav. It would not have beeen possible without you.

Abstract

Cell preservation is accomplished primarily by two methods: cryopreservation and dehydration, with the former being the standard technique used. In order to optimize and develop cell preservation protocols for cells that are difficult to preserve or whose end application is incompatible with current cell preservation protocls and to advance preservation by dehydration, a better understanding of the freeze- and dehydration-induced changes to the cell membrane is required. Despite a large body of literature on the topic, the mechanisms of damage to cells during slow freezing and dehydration are still ambiguous. The objective of this study is to investigate the mechanisms of damage to the cell membrane during slow freezing and dehydration and expand our outlook beyond the cell membrane to its underlying support, the cytoskeleton. In this study, we used several model systems to investigate slow freezing and dehydration. We used a liposome model to gather basic information on changes that can occur to a simple membrane system during freezing. This study revealed that eutectic formation was capable of dehydrating the membrane at low temperatures which may be contribute to alteration of the post-thaw membrane structure. We used a bacteria model to investigate the role of the phase transition and immediate versus slow osmotic stress on post-rehydration viability. This study revealed that going through a lyotropic membrane phase transition was detrimental to post-rehydration viability. This study also demonstrated that a rapidly applied osmotic stress was more detrimental to the structure/ organization of the

membrane than gradual osmotic stress. We then subjected a model mammalian cell to both hyperosmotic stress and freeze-thaw and investigated both the membrane and cytoskeletal responses. Osmotic stress experiments suggested that alterations in membrane structure (i.e., surface defects and lipid dissolution) were directly dependent on the change in the chemical potential of water. These experiments also suggest that cell shrinkage and the resulting formation of membrane protrusions negatively affect viability upon return to isotonic conditions. It was found that membrane morphology in the dehydrated state and post-hyperosmotic viability was dependent on the stiffness of the cytoskeleton. Freeze/ thaw experiments suggested that ice-cell interaction decreases post-thaw viability. However, similar to osmotic stress experiments, cell shrinkage and cytoskeletal stiffness negatively impact post-thaw viability. We suggest the resulting membrane morphology due to cell shrinkage is also responsible for damage during freeze/ thaw. The various mechanisms discovered and the models proposed can be used in developing new protocols for cell preservation and for cell destruction (e.g. cryosurgery).

Table of Contents

List of tables x
List of figures xi
Chapter 1: Introduction 1
1.1 Cell preservation 1
1.2 Water transport during dehydration 7
1.3 The lipid bilayer membrane 9
1.3.1 Membrane hydration 9
1.3.2 Phases of the lipid bilayer 10
1.4 Structure of the cell membrane and its interaction with the cortical cytoskeleton 13
1.5 Dehydration damage to lipid vesicles and cell membranes 15
1.6 Factors that determine the degree of membrane damage during dehydration 19
1.7 Additional damage mechanisms during freezing 21
1.8 Response of cytoskeleton during dehydration and freezing 22
1.9 Models of membrane damage 24
1.10 Outline of thesis 26
Chapter 2: Characterization of the effect of NaCl and trehalose on the thermotropic hysteresis of DOPC lipids during freeze/thaw 30
2.1 Summary and introduction 30
2.2 Materials and methods 33
2.2.1 Preparation of liposomes 33
2.2.2 FTIR spectroscopy 34
2.3 Results and discussion 36
2.4 Conclusion 52
Chapter 3: Roles of membrane structure and phase transition on the hyperosmotic stress survival of *Geobacter sulfurreducens* 53

3.1 Summary and introduction....53
3.2 Materials and methods....58
3.2.1 Bacterial culture....58
3.2.2 Application of hyperosmotic shock and slow dehydration....59
3.2.3 G. sulfurreducens viability measurements....60
3.2.4 Determination of the phase, lipid order and thermodynamic transitions of the membrane....61
3.2.5 Water content analysis....62
3.3 Results....62
3.3.1 Effect of hyperosmotic shock on G. sulfurreducens viability and membrane phase transition behavior....62
3.3.2 Effect of dehydration on G. sulfurreducens viability and membrane phase transition behavior....65
3.3.3 Thermotropic and lyotropic phase transitions....69
3.3.4 Membrane structure change with lyotropic phase change (T_d = 30°C group)....71
3.3.5 Membrane structure change with thermotropic phase change (T_d=5°C group)....71
3.3.6 Effects of thermotropic and lyotropic membrane phase transitions on post-rehydration viability....73
3.3.7 Effect of the lyotropic phase change during re-hydration on G. sulfurreducens viability....73
3.3.8 Effect of the lyotropic phase change during dehydration on G. sulfurreducens viability....75
3.4 Discussion....75
3.5 Conclusion....81
Chapter 4: Hyperosmotic stress of human foreskin fibroblasts....82
4.1 Summary....82
4.2 Part I – Hyperosmotic stress exposure with sorbitol or NaCl....83

4.2.1 Materials and methods 84
4.2.1.1 Cell culture 84
4.2.1.2 Isothermal osmotic stress experiments 85
4.2.1.3 Measuring changes in actin cytoskeleton 86
4.2.1.4 Characterization of the membrane structure using FTIR 87
4.3 Results 88
4.4 Part II – Hyperosmotic stress exposure with PEG 600 96
4.4.1 Materials and methods 96
4.4.1.1 Isothermal osmotic stress experiments 97
4.4.1.2 Measuring changes in actin cytoskeleton 97
4.4.1.3 Monitoring changes in cell membrane 98
4.4.1.4 Scanning electron microscopy (SEM) 100
4.4.2 Results 102
4.5 Discussion 112
4.6 Conclusion 117
Chapter 5: Slow Freezing of human foreskin fibroblasts 119
5.1 Summary 119
5.2 Part I – Freeze/ thaw in media 120
5.2.1 Materials and methods 121
5.2.1.1 Freeze/thaw experiments 122
5.2.1.2 Change in ice structure 123
5.2.1.3 Measurement of the degree of actin polymerization 123
5.2.1.4 Characterization of the membrane structure using FTIR spectroscopy 125
5.2.1.5 Characterization of the membrane viscosity using DCVJ fluorescence 125
5.2.1.6 Statistical analysis 127
5.2.2 Results 127
5.2.2.1 The cell membrane response to freeze/thaw 132

5.3 Part II – Freeze/thaw in PEG solutions 136
5.3.1 Materials and methods 137
5.3.1.1 Freeze/thaw experiments 137
5.3.1.2 Increase in membrane stiffness using wheat germ agglutinin 137
5.3.1.3 Decreasing the cytoskeleton stiffness 138
5.3.1.4 Scanning electron microscopy 138
5.3.1.5 Statistical analysis 139
5.3.2 Results 140
5.4 Discussion 144
5.5 Conclusion 148
Chapter 6: Mechanisms and models of dehydration- and slow freezing-induced damage 150
6.1 Summary 150
6.2 Thermodynamic mechanisms of damage 151
6.2.1 Slow dehydration damage 152
6.2.1.1 Surface defects and lipid desorption 160
6.2.1.2 Effect of osmolyte 161
6.2.2 Fast dehydration damage 162
6.3 Damage due to cell shrinkage and cytoskeleton stiffness 168
6.3.1 Cell stiffness and membrane morphology during dehydration 169
6.3.2 Membrane protrusions and membrane damage 171
Chapter 7: Conclusion 174
7.1 Damage mechanisms from osmotic stress 174
7.2 Possible strategies to alleviate dehydartion damage 175
7.3 Damage mechanisms from slow freezing 176
7.4 Possible strategies to alleviate slow freezing damage 176
7.5 Suggestions for future work 177
7.6 Final conclusion 178
Chapter 8: Bibliography 180

LIST OF TABLES

Number *Page*

Table 1.1 Factors that determine the structure of the membrane and its osmotic response....4

Table 2.1 Summary of measured transition temperatures [°C] (average ± s.d.) for DOPC liposomes in buffer and in buffer with NaCl and trehalose (n = 3 experiments)....40

Table 2.2 Hysteresis area (see inset in Figure 2.1) for DOPC liposomes in buffer and in buffer with NaCl and trehalose (n = 3 experiments) 49

Table 3.1 Effect of Hyperosmotic Shock on G. sulfurreducens Viability (n: number of samples in each group)....64

Table 3.2 Effect of Drying Conditions on Membrane Phase Transition Cooperativity (units= $cm^{-1}°C^{-1}$) 73

Table 4.1 Cell response and measurements 84

Table 5.1 Cell response and measurements 121

Table 6.1 Rate Constants for FM1-43 dye partitioning at various osmotic pressures for data shown in Figure 4.14 157

LIST OF FIGURES

Number *Page*

Figure 1.1 Magnitude of osmotic pressure experienced by cells in different dehydration processes 2

Figure 1.2 Schematic showing freeze-induced dehydration (blue dots – water molecules; red dots – non-permeating solute). Adapted from http://www.me.umn.edu/labs/bhmt/tutorial/ 3

Figure 1.3 (a) Crystalline phase of lipid bilayer (b) Gel phase of lipid bilayer; (c) Liquid crystalline phase of lipid bilayer. Headgroup patterns are shown to the right of the respective sketch of the bilayer for each phase. Adapted from Cevc [71]. 11

Figure 2.1 **A)** Variation of ν-CH_2 peak (◇ - cooling, ○ - heating) (hatched area indicates hysteresis between lipid phase transitions during cooling and heating), **B)** Change in ν_s-PO_2^- (~1088 cm^{-1}) (◇ - cooling, ○ - heating), **C)** Variation in the 1160 – 1220 cm^{-1} spectral range (dashed arrows indicate direction of temperature change; dashed circles indicate ν-C=O and ν_a-C-O-CO bands) with temperature in DOPC liposomes in buffer during a freeze/thaw cycle (T = 20→ -80→ 20°C at 1°C/min). (n=3). 35

Figure 2.2 Change in area of water combination band with temperature during cooling of DOPC liposomes in buffer (The area is normalized to the value at -80°C) (representative data set). 41

Figure 2.3 Variation of ν-CH_2 peak with temperature in, ***A)*** 0.5M NaCl, and ***B)*** 4M NaCl solutions during a freeze/thaw cycle (T = 20→ -80→ 20°C at 1°C/min) (◇ - cooling, ○ - heating). ***C)*** Spectral changes in the 1160 – 1220 cm^{-1} spectral range with temperature (dashed arrows indicate direction of temperature change; dashed circles indicate ν-C=O and ν_a-C-

O-CO bands) for 0.5M NaCl ***D)*** Spectral changes in the 1160 – 1220 cm^{-1} spectral range with temperature for 0.5M NaCl.(n=3) 43

Figure 2.4 Comparison of the spectra at T = -29°C during cooling and warming of the DOPC liposomes in 4M NaCl.....45

Figure 2.5 Changes in the δ-OH peak of water in 0.5M NaCl solution with temperature. *Note the spectral changes during supercooling, freezing and* $NaCl{\cdot}2H_2O$ *formation.* 46

Figure 2.6 Variation of ν-CH_2 peak with temperature in, ***A)*** 0.5M NaCl + 5% TRE, and ***B)*** 4M NaCl + 5% TRE solutions during a freeze/thaw cycle (T = 20→ -80→ 20°C at 1°C/min) (◇ - cooling, ○ - heating). ***C)*** Spectral changes in the 1160 – 1220 cm^{-1} spectral range with temperature (dashed arrows indicate direction of temperature change; dashed circles indicate ν-C=O and ν_a-C-O-CO bands) for 0.5M NaCl + 5% TRE D***)*** Spectral changes in the 1160 – 1220 cm^{-1} spectral range with temperature for 4M NaCl + 5% TRE.(n=3). 47

Figure 3.1 Change in νCH_2 band maxima with temperature for *G. sulfurreducens* in growth medium (◆),growth medium + 6.75% w/w sucrose (▲), growth medium + 13.5% w/w sucrose (■), and growth medium + 27% w/w sucrose (●). (Representative data set).....63

Figure 3.2 Change in *G. sulfurreducens* **A)** viability, and **B)** T_m with drying time for samples dried at 30°C and 65% RH for up to 60 minutes in growth medium (◇) and growth medium containing 13.5% w/w sucrose (□) (n=3 in all data points. Lines are guides for the eye).....66

Figure 3.3 Membrane phase transition temperature versus water content as measured by the ratio of the amount of water to CH (see methods).....67

Figure 3.4 Change in Viability with T_m for *G. sulfurreducens* samples dried at 30°C and 65% RH for up to 60 minutes in growth medium (◇) and growth medium + 13.5% w/w sucrose (□) (lines are drawn as guides for eye; error bars for T_m are not shown for clarity; range of error: 1°C – 3.5°C).....68

Figure 3.5 Comparison of the membrane phase behavior of *G. sulfurreducens* dried in growth medium containing different concentrations of sucrose. (A) Change in νCH_2 maxima with temperature for *G. sulfurreducens* in growth medium (hydrated control) (◆), dried in growth medium (◇), dried in growth medium + 6.75% w/w sucrose (△) and dried in growth medium + 13.5% w/w sucrose (□) (samples were dried at 30°C for 45 minutes). (B) Change in νCH_2 maxima with temperature for *G. sulfurreducens* in growth medium (hydrated control) (◆), dried in growth medium (◇) and dried in growth medium + 6.75% w/w sucrose (△) (samples were dried at 5°C for 45 minutes). (Representative data sets).....70

Figure 3.6 Post re-hydration viability of *G. sulfurreducens* dried for 45 min at 65% RH. (T_d: drying temperature, T_r : re-hydration temperature) (n>3).....72

Figure 3.7 Schematic showing the two modes of osmotic stress and the respective suggested mechanisms of membrane damage (associated FTIR spectroscopy measurements are also shown).....81

Figure 4.1 Schematic representations of: (a) the osmotic stress experiments conducted; (b) Microfluidic flow-through device used in the osmotic stress experiments. The device was made from poly(dimethylsiloxane) (PDMS) made from an SU-8 mold cast on a silicon wafer. The inner chamber height was 70μm. Solutions were exchanged using a syringe pump;(c) Linkam cryostage block on which samples were cooled.....83

Figure 4.2 Phase contrast microscopy images of (a) cells in suspension using a microfluidic device [238], and attached rounded cells that were exposed to rapid hyperosmotic shock. (b) The osmotic stress history for the cells in (a) and (c) (dashed line). (c) Attached, rounded cells that experienced stepwise decrease in osmolality back to isotonic.....88

Figure 4.3 GFP-actin fluorescence microscopy with attached spread cells exposed to hyperosmotic stress. Arrows indicate the increased definition of the stress fibers. The increase in lamllelipodia is indicated by the circle.....90

Figure 4.4 Transmitted light (left column) and GFP-actin fluorescence (right column) microscopy with attached spherical cells exposed to stepwise hyperosmotic stress (the cell was exposed to 4300 mOsm for 10 minutes). ...91
Figure 4.5 F-actin content at isotonic conditions as determined by rhodamine-phalloidin fluorescence intensity for attached spherical cells before and after stepwise hyperosmotic stress exposure. Fixation was performed ~5 minutes after start of rehydration. Cells were on poly-lysine coated glass. Statistical differences ($p < 0.05$) are marked with *. $n > 30$ cells.....92
Figure 4.6 Transmitted light microscopy of a cell subject to an osmotic stress cycle using 2.5 M NaCl.....93
Figure 4.7 Change in νCH_2 band maxima for cells undergoing osmotic stress with exposure to NaCl solutions (n=1 experiment). 95
Figure 4.8 Ratio of the radius of the largest bleb to the cell radius for cells that were exposed to osmotic stress using sorbitol and 48% w/w PEG 600 for 10 minutes before returning to isotonic conditions.....101
Figure 4.9 Viability upon return to isotonic conditions after stressing with Π = 10 MPa PEG 600 at 22 °C, 4 °C, and at 4 °C in the presence of 20μM Y27632.....102
Figure 4.10 F-actin content determined by rhodamine-phalloidin fluorescence intensity at (a) isotonic conditions before and 10 minutes after hyperosmotic stress with 48% w/w (Π = 10 MPa) PEG 600 (hatched), and at (b) 10 minutes exposure to the same hyperosmotic stress.....104
Figure 4.11 SEM images (a) before and (b,c,d) after dehydration with 48% w/w (Π = 10 MPa) PEG 600 at 22 °C and at 4 °C and with Y27632 105
Figure 4.12 SEM images after return to isotonic conditions after dehydration with 48% w/w (Π = 10 MPa) PEG 600 at (a,b) 22 °C and at (c,d) 4 °C 106
Figure 4.13 (a) Fluorescence and (b) Transmitted light confocal microscopy images of HFF after 10 minutes exposure to Π = 30 MPa (67 % w/w) PEG 600

showing FM1-43 dye location in cell membrane. Scale bar represents 10μm. 106
Figure 4.14 FM1-43 uptake for cells subject to osmotic stress using 48.3% w/w (▲),54.7% w/w (●) , 59.6% w/w (■), 67% w/w (◆) PEG 600 at 22 °C. n ≥ 60 cells. Lines are drawn as guides for eyes.....107
Figure 4.15 Cellmask dye exiting cell soon after start of osmotic stress using 67% w/w (Π=30MPa) PEG 600. Arrows indicate streaklines of dye coming from cells. 108
Figure 4.16 (a) Fluorescence and (b) Transmitted light images of HFF at isotonic conditions in PBS after loading with Cellmask dye (exposure time = 1s). Scale bar represent 10μm.....108
Figure 4.17 Decrease in Cellmask concentration in membrane after osmotic stress with (◆) 48% w/w (Π=10MPa) and (■) 67% w/w (Π=30MPa) PEG 600. n ≥ 60 cells. Lines are drawn as guides for eyes. Both conditions start at the same point. 109
Figure 4.18 Ratio of Cellmask dye intensity 1 minute after (using 100 ms exposure) the end of the applied osmotic stress (Π=10MPa), to the dye intensity before (using 1000 ms exposure) at isotonic conditions. n ≥ 100 cells 110
Figure 4.19 Cellmask concentration in membrane in dehydrated state after dehydration at (◆) 22 °C and (■) 4 °C using 48% w/w (Π=10MPa) PEG 600. n ≥ 60 cells. Lines are drawn as guides for eyes. 111
Figure 5.1 Schematic representations of (a) experiments conducted (freeze/thaw), (b) Linkam cryostage block on which samples were frozen/thawed. Samples were either manually nucleated using a chilled needle or using *Pseudomonas syringae*,.....120
Figure 5.2 (a) Phase contrast microscopy with HFF cells suspended in (a) 1xPBS at room temperature; and after exposure to a freeze/thaw cycle while suspended in PBS. Ice was nucleated at -2°C. (b) Schematic showing the different cell populations observed after freeze/thaw. Some of the

darkened blebbing cells were PI^- and some were PI^+. (c) SEM images of cells taken (I) before freeze/thaw and (II), (III), (IV) after freeze/thaw. Scale bars represent 5 μm. Illustrations of cells in upper right corners depict the cell population which the cell is likely to belong to based on its appearance.....126

Figure 5.4 GFP-actin fluorescence intensity of cells before and 15 minutes after freeze-thaw to -8°C (n=2 for blebbing cells; n=3 for other conditions) and of cells treated with 10 μM CD for 30 minutes (n=3). Fluorescence is normalized with respect to initial value. 128

Figure 5.5 Cytoplasmic crowding as measured by CCVJ fluorescence readings taken at 22°C for cells before and immediately after freeze/thaw and of cells treated with 10 μM CD for 30 minutes. Sample was cooled at 2°C/min to -30°C and thawed 130°C/min to 22°C. Values of CCVJ fluorescence were normalized to pre-freeze values. Statistical differences ($p < 0.05$) are marked with *. 129

Figure 5.6 (a) Comparison of F-actin content for live cells (before freeze/thaw) and dead cells (after freeze/thaw) at room temperature as determined by rhodamine-phalloidin fluorescence intensity. A statistical difference ($p < 0.05$) is marked with *. n = 20 cells. Sample was cooled and thawed at 2°C/min to from 22°C to -30°C; (b) Typical morphology of actin cytoskeleton for membrane-compromised (+) cells and intact (-) cells. Membrane compromised cells were determined using the LIVE⁄DEAD® Fixable Blue Dead Cell Stain Kit from Invitrogen Corporation. 131

Figure 5.7 Change in DCVJ fluorescence (■) (n=150 cells) and νCH_2 band maxima (◆) (n=3 experimentss) with temperature for cells under going freezing 132

Figure 5.8 DCVJ fluorescence (■) (n=67 cells) and FTIR νCH_2 band maxima (◆) with temperature for during cooling. Both DCVJ and FTIR data show a small thermotropic phase transition indicated by arrows 133

Figure 5.9 Change in νCH_2 band maxima with temperature for cells under going freeze-thaw with cryoprotectant (▲,△10% DMSO; ■,□10% glycerol) and without cryoprotectant (◆,◇ media). Filled symbols represent cooling while open symbols represent warming.....134
Figure 5.10 Difference in νCH_2 band maxima at room temperature for cells under going freeze-thaw with and without cryoprotectant and for cells treated with CD that did not undergo freeze/thaw. n=3 for each experimental condition. 135
Figure 5.11 Post-thaw cell viability for cells that were cooled and thawed at 2°C/min to from 22°C to -20°C. n=3 138
Figure 5.12 Post-thaw cell viability for cells in media and various 300 mOsm PEG 600 solutions that were cooled at 2°C/min to from 22°C to -20°C and thawed at 130°C/min. n≥3 139
Figure 5.13 Appearance of PI^+ cells in PEG 600 (left) versus media (right). PI^+ cells are outlined in red. The scale bar represents 10 µm. 140
Figure 5.14 SEM images of HFFs frozen to -20 °C in 300 mOsm PEG 600 140
Figure 5.15 Comparison of cell radii for cells in media, 300 mOsm PEG 600 and 300 mOsm PEG 200. 142
Figure 5.16 SEM images of HFFs frozen to -20 °C in 300 mOsm PEG 200 143
Figure 5.17 Post-thaw cell viability for cells in media and various 300 mOsm PEG 200 solutions that were cooled at 2°C/min to from 22°C to -20°C and thawed at 130°C/min . Groups marked with # are not statistically different. All other groups are statistically different ($p<0.05$). 144
Figure 6.1 Free energy diagram describing lipid desorption/ adsorption process. Adapted from [285]. $\Delta G_d^{\neq o}$,and $\Delta G_a^{\neq o}$,represent the free energy for desorption and adsorption respectively.....153
Figure 6.2 Free energy diagram describing lipid desorption/ adsorption process when there is a change in the chemical potential of water 155

Figure 6.3 Plot of the negative natural log of the rate constant of FM1-43 dye insertion during osmotic stress versus the decrease in the chemical potential of water for (▲) 48.3% w/w (Π=10MPa), (●) 54.7% w/w (Π=15MPa), (■) 59.6% w/w (Π=20MPa), (◆) 67% w/w (Π=30MPa) PEG 600 157

Figure 6.4 Abuin et al [247] data for partitioning of MC540 into DPPC vesicles. The amount of dye in the membrane is directly related to the A_{570}/A_{530} ratio..... 158

Figure 6.5 Plot of the negative natural log of the rate constant of MC540 dye insertion into DPPC vesicles [247] during osmotic stress versus the decrease in the chemical potential of water. 159

Figure 6.6 SEM images of cells that were pretreated with various drugs and then subjected to hyperosmotic stress at 4°C using 48% w/w PEG 600. 169

CHAPTER 1: INTRODUCTION

1.1 CELL PRESERVATION

Stabilization and storage of cells, tissues and whole organisms is used as an enabling technology for applications in pharmaceutical, medical, agricultural, biotechnology, and food industries. Conversely, destruction of cells, such as cancer cells, is important for therapeutic applications such as cryosurgery [1]. Therefore, establishing the mechanisms of cell injury and death is crucial for optimizing the conditions to ensure the best outcome for both preservation and destruction of cells.

Although there have been great advances in the field of cell preservation, not all cell types and applications are compatible with current preservation protocols. Cryopreservation, which is the method of choice for cell preservation [2], has had limited success in preserving certain types of cells such as hepatocytes [3] and certain species of sperm cells [4]. Also, some applications are not compatible with current cryopreservation protocols, e.g. in stem cell therapy the use of dimethyl sulfoxide (DMSO), a very popular cryoprotectant, can cause adverse reactions to patients. Desiccation/ lyopreservation, which involves removal of water from the specimen, is another technique used for the preservation of cells. There has also been great interest in the lyopreservation of eukaryotic cells, especially mammalian cells, motivated by the need for improved storage, ease of transportation and the usage of cell types such as red blood cells, platelets, stem cells [5]. However, cell preservation using lyopreservation has been

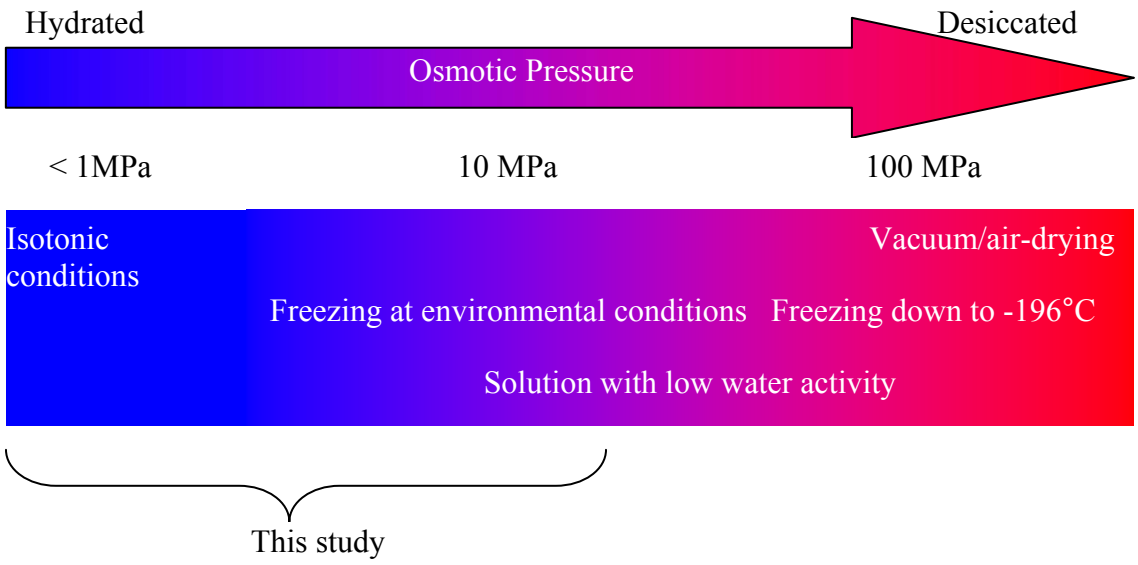

Figure 1.1 Magnitude of osmotic pressure experienced by cells in different dehydration processes

mostly limited to germplasm [6] and to bacteria, which have a certain degree of desiccation tolerance [7]. The precise mechanisms of damage and stabilization for both cryopreservation and lyopreservation have yet to be fully elucidated. Instead, preservation protocols are often developed through a trial and error process.

The common endpoint in both cryopreservation and lyopreservation is the reduction of the chemical potential of water (μ_w), or correspondingly, an increase in osmotic pressure (Π) (Figure 1.1) or a decrease in water activity (a_w). Reduction in the water activity dampens the molecular motions thereby reducing the degradation of the biological material [8]. The relationship between the reduction in the chemical potential of water ($\Delta\mu_w$), osmotic pressure, water activity and sample temperature (T_s) is given by

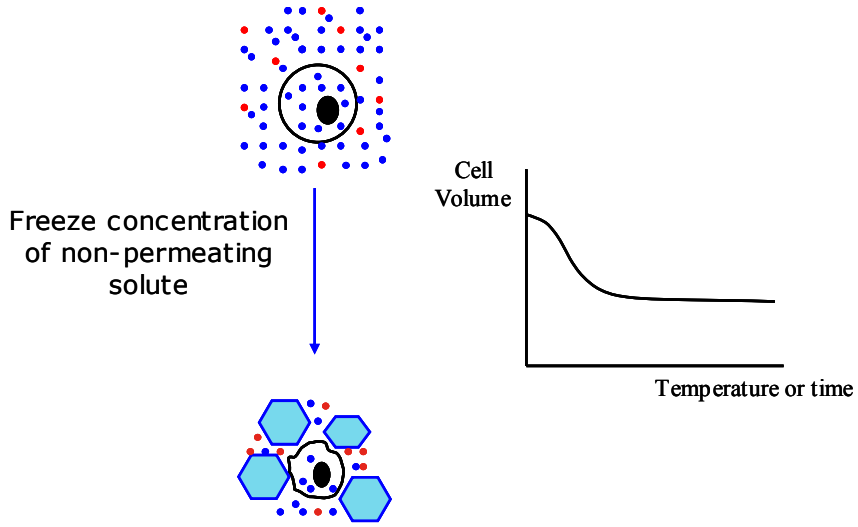

Figure 1.2 Schematic showing freeze-induced dehydration (blue dots – water molecules; red dots – non-permeating solute). Adapted from
http://www.me.umn.edu/labs/bhmt/tutorial/

$$\mu_w - \mu_w^o = \Delta\mu_w = RT_s \ln a_w = -\nu_w \Pi \qquad (1.1)$$

where μ_w^o, v_w and R are the standard chemical potential of water, molar volume of water and the ideal gas constant, respectively. Osmotic pressure, is equivalent to a hydrostatic "suction" pressure that pulls water through the membrane. During freezing, the increase in osmotic pressure is related to the difference in the temperature of the sample and the phase change temperature (T_{ph}) and the enthalpy of freezing (ΔH_f),

$$\mu_w - \mu_w^o = \Delta\mu_w = RT_s \ln a_w = -\nu_w \Pi = \frac{\Delta H_f}{T_{ph}}\left(T_s - T_{ph}\right). \qquad (1.2)$$

Table 1.1 Factors that determine the structure of the membrane and its osmotic response.

Factor	Example	Effect on cell membrane
Biological	Cholesterol content	Alters membrane fluidity [9, 10], permeability [9, 10], and compressibility [11]
	Degree of polymerization of actin	Alters volume regulation response of the cell [12], lipid head group spacing [13], membrane permeability [14]
	Cytoskeleton-membrane interactions (via transmembrane proteins)	Facilitates lipid/ protein compartmentalization [15], alters membrane morphology [16-18] and membrane strength [19]
	Lipid composition	Phase separation of lipids [20], formation of non-lamellar phases [21]
Mechanical	Compressibility of the membrane	Decrease in compressibility leads to a reduction in membrane permeability [22]
	Regions of different membrane curvature [23]	Formation of domains [23] and phase separation of lipids [24] (larger curvature favors the liquid crystalline phase [25])
	Membrane interfacial tension	Increase in interfacial tension increases lipid packing [26]
	Intermembrane hydration forces	Changes membrane phase transition temperature and influences phase separation [27]
Chemical	Change in chemical potential of water	Change in lamellar phase of the membrane [28], facilitates membrane fusion [29, 30], vesiculation [31-34], phase separation of lipids [35-37], lipid desorption [38], formation of non-lamellar phase [35, 39-41]
	Specific interactions	Interaction of solutes (e.g. trehalose) with lipids can reduce the extent of phase separation and fusion [42, 43], interactions with amphipaths can increase leakage [44]

Cryopreservation of cells typically consists of two steps: (i) Loading of a permeating cryoprotective agent (CPA) into the cells, and (ii) Cooling the cells to cryogenic levels. During CPA loading, cellular dehydration occurs as water and CPA are transported out of and into the cell respectively. This leads to an initial reduction in cell volume followed by volume recovery as CPA enters the cell. The freezing process generally consists of

slowly cooling (<10 °C/min) the cell suspension to the storage temperature, usually between -80 °C and -196 °C. Some of the protocols also include a nucleation step where extracellular ice is nucleated at a high subzero temperature. During freezing, extracellular ice formation and the resultant freeze-concentration causes water to exit the cell (Figure 1.2) resulting in cellular dehydration.

During lyopreservation, the water surrounding the macromolecules in the cell, tissue or organism is substantially reduced leading to a reduction in water activity. In order to survive this extreme dehydration, anhydrobiotic organisms synthesize chemical agents such as carbohydrates [45]. The carbohydrates are hypothesized to "replace" the water [46, 47] and provide the necessary hydrogen bonding interactions to stabilize the structures of macromolecules such as proteins and cellular membranes [45]. This concept has been employed in the lab for the freeze-drying of platelets where the cell membrane was stabilized in the presence of trehalose [48].

The cell membrane, which forms the barrier between the cell and its environment, is a primary site of dehydration-induced injury [39, 49] during desiccation and cryopreservation. The change in chemical potential of water during cryopreservation or lyopreservation results in several changes in membrane structure including: lyotropic phase transitions [28]; phase separation [35-37]; fusion [29, 30]; formation of non-lamellar phases [35, 39-41]; vesiculation [31-34]; lipid desorption [38] (see Table 1.1 and Section 1.5). These structural changes in the cell membrane can lead to a loss in membrane integrity/ increased permeability to solutes either in the dehydrated state or

during rehydration [42, 50]. Membrane integrity has been identified as one of the key factors that allows anhydrobiotic organisms to survive desiccation [51].

Understanding the factors that determine dehydration-induced membrane damage is of key importance in order to develop a systematic approach to cell preservation. It has been proposed that the kinetics and temperatures of dehydration and rehydration [31, 52, 53] and their effect on the physical state of the membrane is central in determining the organism's survival (see Sections 1.5 and 1.6). These parameters have been shown to be important to viability for gram negative bacteria such as *Escherichia coli* [31, 52] and *Bradyrhizobium japonicum* [53] and for *Saccharomyces cerevisiae* (yeast) [54]. There has been little research conducted into how the kinetics of dehydration affects the membrane integrity of mammalian cells (except for one study [55] which demonstrated that high rates of dehydration and osmotic stress at higher temperatures was detrimental to cell survival). Most studies on mammalian cells focus on the extent of cellular dehydration and its relation to post-rehydration or post freeze-thaw membrane integrity.

Due to its interaction with the cell membrane, the cortical cytoskeleton may also have a significant role in determining post-dehydration and post-thaw viability. The cortical cytoskeleton is "linked" almost continuously to the cell membrane [56] and is capable of modifying membrane structure [13] (see Table 1.1), altering the shape/ morphology of the membrane [16, 17], changing the mechanical properties of the cell [19, 57-59] (see Section 1.4) and influencing the membrane water transport [14, 57] (see Section 1.8). It has also been observed that disruption of the actin cytoskeleton increases the post-thaw viability of certain plant cells [60] and mammalian embryos [61-63]. As such, we

hypothesize that the cytoskeleton would play a significant role in determining the cell's response to freeze/thaw and dehydration stresses and its survival.

Both the physical conditions and the membrane-associated biological factors need to be addressed to develop successful preservation protocols. Factors that affect the structure of the membrane and its osmotic response are given in Table 1.1. In this thesis, we primarily focus on the changes in the structure of the membrane and the cortical cytoskeleton during freeze/ thaw and during osmotic dehydration.

1.2 WATER TRANSPORT DURING DEHYDRATION

An essential process in cellular dehydration is the transport of water from the inside of the cell to the extracellular environment. Water transport through a semipermeable lipid membrane in response to osmotic stress proceeds in two steps [28]. Initially, the transmembrane osmotic pressure gradient causes flux of water through the membrane. Secondly, the resulting dehydration forces the lipid molecules together and water transport becomes more constrained.

Transport of water through the hydrophobic region of the lipid bilayer may result in changes in the structure of the membrane. Sogami et al [64] suggested that the positive change in entropy (ΔS) for permeation through bilayers and cell membranes is related to the lipid chain disordering and they intimate that higher ΔS values may indicate irreversible breaking of the membrane. The positive ΔS values may be a result of the

creation of free volume within the bilayer necessary for transport through the bilayer, as shown by molecular dynamics simulations [65]. This creation of free volume for transport is described by the "kink model" which states that transmembrane water transport depends on the presence of free volume formed by the kinks in adjacent lipid acyl chains [28, 66].

The biophysical volumetric response of the cells in response to osmotic stress can be characterized using the Kadeem and Katchalsky model [67] developed using irreversible thermodynamics. In the K-K model, three parameters, the hydraulic conductivity (L_p), the solute permeability (P_s), and a reflection coefficient (σ), are used to characterize the membrane. σ characterizes the co-transport of water and solute through a common channel in the membrane. When there is no co-transport, a two-parameter model can also be utilized [68, 69] as follows;

$$\frac{dV_w}{dt} = -L_p A\left(\Pi^e - \Pi^i\right) \tag{1.3}$$

where A is the cell's surface area, V_w is the volume of water inside the cell and Π^e and Π^i represent osmotic pressure outside and inside the cell, respectively. During dehydration the values of Π^e increases, leading to a decrease in the volume of intracellular water. Limitations of this model are that it does not account for changes in the membrane either due to lyotropic phase change or during water transport.

1.3 THE LIPID BILAYER MEMBRANE

The key step in understanding how changes in hydration affect the structure of the membrane is identifying the driving forces behind membrane formation. The curved, bilayer structure of membranes in cells and vesicles is largely due to a combination of the amphiphilic (water-loving/ water-hating) nature of lipids and the shapes of the lipid molecules. Bilayers are generally formed from lipids that have a cylinder-like or slightly conical shape [70]. In order to minimize the free energy, the heads of the lipid molecules face the polar, aqueous environment, while the hydrophobic tails tend to minimize their contact with water. The hydrophobic effect is the major driving force behind the self-assembly of lipid molecules into lipid bilayers. The minimization of free energy is also the reason for the formation of a closed surface for vesicles and cells. Lipid molecules can also adopt other configurations such as micelle and inverted phases depending on the lipid head group size, the alkyl chain characteristics (length; saturated/ unsaturated bond content), salt concentration, pH and lipid concentration [70, 71].

1.3.1 MEMBRANE HYDRATION

Phospholipids (the most commonly found lipid in biological membranes) can bind significant amounts of water. It was shown using Atomic Force Microscopy (AFM) that a phosphatidylcholine (PC) lipid bilayer surface has 2-3 hydration layers [72]. In the inner hydration shell phospholipids have about 0.5-3 n_w/n_L (n_w – moles of water; n_L – moles of lipid) [73]. The existence of further hydration shells is dependent on the type of

lipid head group [42]. For PC lipids the bilayer surface is found to be saturated at 22 n_w/n_L [74].

Due to the amount of water that binds to lipid head groups, a decrease in hydration decreases the effective size of the headgroup which increases lipid packing [75] and decreases lipid diffusion [76]. In turn, the structure of water is also influenced by the presence of lipid molecules. In phospholipid bilayers the water molecules bound to the lipids have fewer hydrogen bonds than those in the bulk and the water molecules at the interface are highly ordered (having a single orientation) [77]. Water near the membrane (at the interface) becomes increasingly more network-like (making four hydrogen bonds with other water molecules) with a decrease in temperature or hydration [78]. It has been proposed that the structure of water near the membrane may also mediate interactions between the membrane and cytoplasmic components (see [79] for a review).

Due to interactions between the water and lipid molecules, a reduction in the number of water molecules instigates changes in membrane structure. These changes typically first manifest as a change in phase where lipid molecules are more tightly packed but the can also take the form of phase separation [35-37], fusion [29, 30], formation of non-lamellar phases [35, 39-41], vesiculation [31-34] and lipid desorption [38] (see Section 1.5).

1.3.2 PHASES OF THE LIPID BILAYER

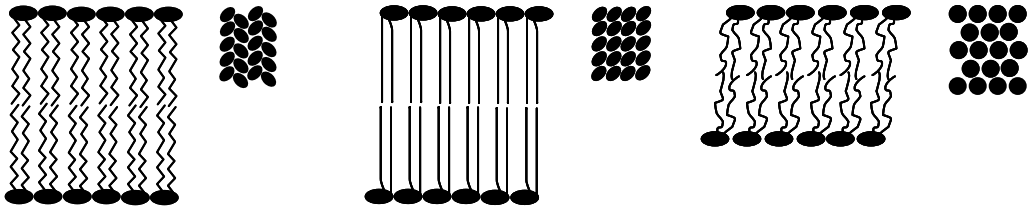

Figure 1.3 (a) Crystalline phase of lipid bilayer (b) Gel phase of lipid bilayer; (c) Liquid crystalline phase of lipid bilayer. Headgroup patterns are shown to the right of the respective sketch of the bilayer for each phase. Adapted from Cevc [71].

Single component (i.e., one type of lipid) bilayers have three main phases whose formations are a function of both temperature and hydration. A phase change due to a change in temperature is termed a thermotropic phase transition while a phase change due to a change in hydration is termed a lyotropic phase transition. The lowest temperature or hydration phase is a condensed/ sub-gel/ crystalline-like phase (Figure 1.3a) where the lipid acyl chains are ordered (all-*trans* configuration) and the lipids are arranged in a well-ordered lattice [71, 80]. With an increase in temperature or hydration the bilayer transitions to a gel phase (Figure 1.3b) where the head group lattice become disordered. With a further increase in temperature or hydration the bilayer transitions to a liquid-crystalline phase (Figure 1.3c) characterized by increased lipid head group spacing (approximately 25% increase compared to the gel phase), increasingly disordered acyl chains and a decreased bilayer thickness (approximately 16% decrease compared to the gel phase) [81-83]. Some phospholipids, especially phosphocholines, also exhibit a pretransition to a rippled gel phase before the main phase transition (gel $\rightarrow$ liquid-crystalline) [84].

Phase behavior of the lipid membrane is also affected by molecules associating with the lipid headgroups [71]. For example, binding of ions to lipid head groups can create ionic bridging which stabilizes ordered phases [71]. Direct interaction with the lipid head groups is also one of the main mechanisms hypothesized to enable stabilization of the liquid crystalline phase by trehalose during dehydration [85].

During the transition between phases, several membrane properties show discontinuities. For example, while water permeability decreases [10] and membrane compressibility increases [86] from the liquid crystalline phase to the gel phase, the maximum values exist at the membrane phase transition temperature (T_m) [22, 87]. The heat capacity of the membrane also has a maximum at T_m [22, 87]. The discontinuities in membrane properties at T_m indicate that the membrane structure at T_m differs significantly from that in either the liquid crystalline phase or gel phase.

It has been observed that the membrane is more susceptible to damage at the membrane phase transition (and the associated changes in membrane properties at the transition). For example, Hays et al [88] observed an increased leakage of intravesicular content at T_m for vesicles of various lipid compositions. Similarly, Drobnis et al. [89] observed that solute leakage during cooling of sperm occurred at the T_m. For cold shock hemolysis of erthrocytes, damage to the cell membrane is a result of the combination of a decrease in hydration and membrane phase change - the temperature at which cold shock hemolysis of hyperosmotically stressed erythrocytes starts to occur (~10°C) is the same temperature at which a membrane phase transition is observed in unstressed erythrocytes [90].

1.4 STRUCTURE OF THE CELL MEMBRANE AND ITS INTERACTION WITH THE CORTICAL CYTOSKELETON

The cell membrane exhibits a more complex behavior than the single component lipid bilayer due to its varied composition of many different types of lipids and proteins. Mammalian cells contain lipids with varying headgroups and fatty acid chains (see [91] for lipid composition of mammalian cell membranes). The fluid mosaic model [92] describes the membrane lipid bilayer as a dynamic, two dimensional fluid environment with a great degree of molecular mobility. This perspective has since changed due to accumulating evidence for the existence of lipid rafts [93] and compartmentalization of the membrane [94] implying that the cell membrane has a highly heterogeneous structure. The heterogeneous nature of the cell membrane is evident from the existence of complex diffusion behavior (i.e., confinement [94], directed motion and free random diffusion [95]) of membrane constituents.

One theory for the confined diffusion behavior in the cell membrane proposes the restriction of phospholipid movement by transmembrane proteins anchored to the cortical cytoskeleton [15]. The imposed ordering within the membrane plane is only one aspect of cytoskeleton-membrane interaction. Due to the almost continuous adhesion between the membrane and the cytoskeleton [56], the cortical cytoskeleton can also alter the shape/ morphology of the membrane [16, 17], the membrane tension [17] and the available membrane material (referred to as the membrane reservoir) [58]. In the last instance, it has been found that disruption of actin filaments increases the membrane

reservoir (a collective term for the membrane invaginations and the surface folds) [58]. The cytoskeleton also increases the stability of the cell membrane, e.g., defects in cytoskeletal proteins of red blood cells result in membrane instability [96], and cells with an intact cytoskeleton exhibited a lower incidence of cell lysis at larger compressive loads [19]. Adhesion between the cytoskeleton and membrane has also been theorized to be important in membrane events such as endocytosis [23, 97], membrane extension and membrane resealing [98]. The adhesion between the cytoskeleton and membrane can be broken due to defects in the cytoskeleton [16] or even by physical forces such as suction [99]. The loss of adhesion between the cytoskeleton and membrane can lead to the formation of blebs [100], which causes the membrane to have higher permeability to solutes [101, 102]. Even though the cytoskeleton is ubiquitous in mammalian cells, the structure and mechanical properties of the cytoskeleton and therefore its effect on the membrane varies with the cell type. For fibroblasts, neutrophils and red blood cells the cortical cytoskeleton has been found to behave like an elastic shell under tension and can be modeled as a "liquid drop" [103, 104]. On the other hand, some of the same cells, i.e. neutrophils and fibroblasts, as well as endothelial cells and chondrocytes have been modeled using a viscoelastic solid model [105]. Changes in the mechanical properties of the cytoskeleton can have profound effects on membrane morphology; As demonstrated by Tinevez et al. [59], the maximum bleb size is dependent on the magnitude of the tension in the cell cortex.

The most dominant and ubiquitous protein in the cortical cytoskeleton is actin. Actin has been shown to interact directly with lipid membranes through electrostatic interactions

[106, 107] and also through membrane associated proteins [108]. This close association between actin and the membrane [109] can result in changes to both the membrane and actin network. Increasing concentrations of F-actin can increase the head group spacing between phospholipids to a greater extent than that of actin monomers (G-actin) [13]. F-actin networks in giant unilamellar vesicles (GUVs) have also been shown to affect lipid organization [110]. Conversely, it has been observed that the membrane can affect the structures formed by actin filaments, e.g. actin filaments are bundled into membrane protrusions in GUVs containing actin, neural-Wiscott Aldrich Syndrome Protein (N-WASP), and the seven-subunit Actin-related protein 2/3 (Arp2/3) complex [111]. Also, the electrostatic interactions between the membrane and actin can result in the formation of highly ordered arrays of F-actin [106].

1.5 DEHYDRATION DAMAGE TO LIPID VESICLES AND CELL MEMBRANES

Several changes occur in pure lipid bilayers during dehydration that can cause a loss of membrane integrity / increased permeability to solutes upon rehydration. Some examples of systems that exhibit this damage after rehydration are chloroplasts in leaves [112], seeds [113], bacteria [31] and cells [114]. The loss in integrity has been observed in both dehydration and freezing [39]. There are several proposed mechanisms for the loss of membrane integrity due to dehydration. These included phase separation, membrane fusion, phase transition, lipid desorption/ dissolution, formation of non-lamellar phases and partitioning of amphiphilic molecules into the membrane. In some

instances more than one mechanism of damage exist, for example sarcoplasmic reticulum vesicles dried without trehalose exhibit extensive fusion, undergo phase transitions and experience lateral phase separation [42].

Membrane phase transition during dehydration and rehydration have been highlighted as responsible for the loss of membrane integrity [115]. This is based on research involving the leakage of vesicles during thermotropic phase change which showed that the rate of leakage is greatest at T_m [88]. The increase in permeability is attributed to packing defects due to the co-existence of gel and liquid crystalline domains at T_m [88]. These packing defects at T_m can also make the membrane mechanically unstable: This is demonstrated by the increased penetration of an AFM tip into the membrane at T_m [116]. Similarly, the loss in membrane integrity during lyotropic phase change is attributed to the membrane defects induced by co-existence of multiple phases. An example of the importance of membrane phase change is the loss in viability observed in *Saccharomyces cerevisiae* (yeast) due to the lyotropic phase change during rehydration at temperatures below the depressed T_m (T_m is lowered due to the presence of trehalose in yeast) [117].

Formation of a non-lamellar inverse hexagonal (hex II) phase at low water activities is another phenomenon that has been observed and correlates to dehydration-induced membrane damage [35, 39, 40]. Formation of the hex II phase is promoted by the presence of certain lipids, for example phosphatidylethanolamine [21]. The occurrence of the hex II phase in the plasma membrane destroys the lamellar structure of the membrane as the lipid hydrophobic tails become exposed to the environment. This configuration is accompanied by a decrease in lipid order [118]. The loss of lamellar

structure inhibits the membrane's ability to form an effective barrier between the cell and its external environment.

Phase separation has also been hypothesized to be related to the loss in semi-permeability of the membrane [119]. Two mechanisms have been proposed for the lateral phase separation of lipids in bilayer membranes. One mechanism is based on the different liquid-crystalline to gel phase transition temperatures of the various types of lipids in the membrane [35]. Phase separation via this mechanism involves the transition of one type of lipid to the gel phase with a decrease in temperature thereby concentrating the other type of lipid. It has also been shown both theoretically and experimentally that a fluid-fluid phase separation is possible for multi lipid bilayer membranes which are approximately nanometers apart. This separation is due to the existence of different strong repulsive forces for the different types of lipids [36, 37]. The repulsive force was first attributed to hydration of phospholipids, but other factors such as steric interactions [120] and coupling between osmotic stress and elasticity of the membrane [121] have also been implicated. Membrane damage due to phase separation of different types of lipids has been attributed to the resulting concentration of non-lamellar forming lipids and therefore formation of a non-lamellar phase [122]. Membrane damage has also been attributed to the creation of packing defects between phases [123]. Interestingly phase separation is not only seen during dehydration of membrane but also during freeze fracture experiments for samples that are cooled too slowly [42].

Fusion of the membrane also can cause a loss in membrane integrity. Osmotically stressed large unilamellar vesicles (LUVs) experience a loss in membrane integrity just

prior to fusion [124]. Some researchers interpret fusion as a side effect of phase separation. However, it has been shown that phase separation may assist fusion without actually being responsible for it [30]. The facilitation of fusion by phase separation was attributed to Marangoni flows within the outer leaflet of the membrane which caused the lipids to expose their hydrophobic tails [125]. It has been suggested that dehydration also facilitates fusion, as demonstrated for LUVs [29, 30] due to the formation of membrane defects [30, 126]. This hypothesis is supported by work performed by Cevc et al. [127] who showed that freshly prepared vesicles (with more defects) experienced a larger extent of fusion that aged vesicles (with less defects).

Vesiculation is another form of damage that has been observed during dehydration. For example, formation of vesicles has been observed for *E. Coli* bacteria [31], protoplasts [32] and LUVs [33, 34] exposed to osmotic stress. Vesiculation is attributed to fusion events in the membrane [128]. The resultant loss of membrane area in the form of vesicles restricts the cell's ability to return to its original volume upon rehydration thereby causing a loss in membrane integrity.

The loss of membrane integrity during dehydration has also been attributed to a loss of membrane constituents to the external environment [129]. This hypothesis was based on the increase in the dissolution of membrane components [38] and the increase in the rate of hemolysis of erythrocytes with an increase in osmotic stress [129]. This dissolution of membrane constituents has also been observed for cryopreserved goat epididymal sperm where hydrophilic membrane constituents were shed [130].

The loss of membrane integrity due to dehydration has also been attributed to the partitioning of amphiphilic substances into the membrane upon drying [44]. Golvina et al [44] showed that amphipaths extracted from pollen had a fluidizing effect on the membrane of dried pollen and increased membrane permeability.

One common aspect in most damage mechanisms, such as fusion, vesiculation, hex II phase formation and membrane constituent dissolution, is the exposure of the lipid hydrophobic chains to the environment. Exposure of the hydrophobic chains requires a change in the free energy of transfer of the tail groups into solution. As such, the degree of damage caused by these mechanisms may be influenced by solutions properties (e.g. surface tension). Another recurring factor is the formation of membrane defects which are involved in fusion, increased permeability during a phase transition and partitioning of amphipaths into the membrane [79]. The formation of membrane defects is attributed to geometric packing constraints that arise in the membrane during either a thermotropic or lyotropic phase change [79].

1.6 FACTORS THAT DETERMINE THE DEGREE OF MEMBRANE DAMAGE DURING DEHYDRATION

In addition to temperature, there are other factors that change the post-dehydration membrane state. Puhlev et al. [114] found that vacuum promotes desiccation tolerance of human fibroblasts. They suggested the increase tolerance was due to either: 1) elimination of meniscus effects that could damage the cells due to the removal of air prior

to the final stage of drying [114]; 2) Reduction in the amount of oxygen available to generate oxygen free radicals/ reactive oxygen species. One possibility not considered by the authors is the change in the thermodynamic state of the system, and resultant change in membrane structure, due to the decrease in pressure. Interestingly, the opposite effect has been observed, i.e. an increase in pressure alters the structure of the membrane, thereby yielding an increase in permeability [131].

As mentioned previously, the rate of drying has been found to be important in determining the survival of dehydrated cells and microorganisms [7, 132]. Puhlev et al. [114] also found that high initial rates of dehydration resulted in lower survival of human fibroblasts and stem cells in the desiccated state. Yeast, another eukaryotic organism, also demonstrates lower survival at higher rates of dehydration [133]. The mechanism behind the effect of the rate of dehydration on membrane structure has yet to be elucidated.

Research on the dehydration tolerance of anhydrobiotic organisms has led to the discovery that carbohydrates are capable of affording desiccation tolerance to lipid vesicles and isolated biological membranes [134], isolated organelles [135], bacteria [136, 137] and mammalian cells [5, 138]. Desiccation of model membranes in the presence of trehalose decrease the extent of fusion, phase transitions and lateral phase separation [42].

1.7 ADDITIONAL DAMAGE MECHANISMS DURING FREEZING

Dehydration-induced membrane damage is only one of many factors that determines the survival of the cell during slow cooling [139]. Other factors that affect post-thaw cell survival at slow cooling rates include:

1. Cell shrinkage - the minimum volume hypothesis [140] attributes damage during slow freezing to cell shrinkage and the resulting physical compression forces that develop in the membrane. Cell shrinkage has also been implicated in the loss of cell membrane area due to vesiculation [141].

2. Mechanical damage due to compression and shear due to interaction with ice crystals [142-144]

3. Denaturation of lipoproteins in the cell membrane due to elevated salt concentration [145]

4. Damage due to eutectic formation [146] – damage is postulated to be due to two possible mechanisms: (i) mechanical damage by eutectic crystals; or (ii) formation of intracellular eutectic crystals

The above collection of damage mechanisms during slow cooling rates fall under the general classification of “solution effects”. Due to the various phenomena that occur simultaneously during slow freezing it has been difficult to ascertain the exact damage mechanisms to cell membranes.

According to the two-factor hypothesis, damage also occurs at the other end of the spectrum, i.e., at rapid cooling rates, due to the formation of intracellular ice [139]. If the cooling rate is too fast, such that an osmotic balance cannot be maintained between the cell and its environment, then the intracellular water becomes supercooled. Intracellular ice formation results from nucleation of the super-cooled intracellular water [147]. The formation of intracellular ice is usually associated with cell death [147] although the formation of innocuous intracellular ice has also been observed [148].

1.8 RESPONSE OF CYTOSKELETON DURING DEHYDRATION AND FREEZING

Dehydration triggers several changes in the cytoskeleton. Actin, the most abundant protein in the cortical cytoskeleton, typically undergoes polymerization under hyperosmotic conditions [12]. There are two possible pathways for actin polymerization, one is the thermodynamic favorability of the filamentous actin at low water activity [149] while the other is the biochemical pathways activated for actin polymerization [150]. Hyperosmotic stress also causes remodeling of the cytoskeleton in the form of increased cortical actin networks [151, 152]. It has also been shown *in vitro* that hyperosmotic stress can crosslink actin filaments into actin bundles [153]. Damage to the actin cytoskeleton could also potentially occur during dehydration due to the high osmotic pressures experienced (on the order of megapascals): Cross-linking of actin filaments leads to cessation of water transport across a semi-permeable membrane at low

hyperosmotic pressures, but at an osmotic pressure greater than 40 cm·H_2O (Π = 4 kPa) water transport resumes as the actin network breaks down [154].

The cytoskeleton may also affect the response of the cell to dehydration in terms of volume regulation, water permeability and membrane morphology. The actin cytoskeleton has been reported to interact with several enzymes and transporters that may be involved in cell volume regulation [12]. The cross-linking of actin in cells has also been observed to affect volume regulation [155]. Cells lacking an actin cross-linking protein (ABP280) failed to regulate the cell volume under hypotonic conditions [156]. Disruption of the cell's actin cytoskeleton by cytochalasin D can also increase the hydraulic permeability of the cell membrane [14, 57]. Changes in the structure of the cytoskeleton can also affect membrane shape as seen in earthworm coelomocytes where filiopodial formation during hyperosmotic stress depends on the disruption of the cortical actin ring [18].

Due to the interactions between the cytoskeleton and the membrane, the effect(s) of actin on water properties, and given that actin polymerization is favored at low water activity [12], it is reasonable to postulate that the actin cytoskeleton has an impact on changes in the cell membrane structure during dehydration and hence, cell viability upon rehydration or thawing. However, this impact/ response will likely be dependent on cell type, e.g. human fibroblasts show an increase in filamentous actin (F-actin) content with hyperosmotic stress [157] whereas chondrocytes do not [158].

Even though the actin polymerization response to dehydration is inhibited at low temperatures [159], the structure of the actin cytoskeleton has been shown to affect post-thaw outcome during cryopreservation. There are several examples in the literature where disruption of the actin cytoskeleton leads to increased post-thaw viability following cryopreservation [61-63]: Hosu et al. [63] report that mouse oocytes demonstrate a significant increase in post-thaw stiffness, which if negated by using latrunculin A to disassemble the cytoskeleton prior to freezing, leads to a higher post-thaw viability. It is hypothesized that disruption of the actin cytoskeleton allows the membrane to become less rigid such that the F-actin filaments are not disrupted during freezing [160]. Conversely, Liu and McGrath have proposed, based on the analysis of the freezing response of attached osteoblasts, that an intact cytoskeleton is required to support the cells against freeze/thaw stresses [161]. Additionally, an intact actin cytoskeleton has been shown to be crucial for *Arabidopsis thaliana* (plant cells) to survive hyperosmotic stress exposure [162]. Clearly, the structure of the cytoskeleton does influence post-thaw or post-hyperosmotic membrane damage but the mechanism is still unknown.

1.9 MODELS OF MEMBRANE DAMAGE

Muldrew and McGann [163] proposed a mechanistic model to explain intracellular ice formation based on the assumption that the water efflux during dehydration was responsible for membrane rupture. This theory was later modified to the efflux being

responsible for membrane poration rather than membrane rupture [57]. However, experimental evidence in support of this theory is lacking.

McGrath [129, 164] proposed a thermodynamic/ kinetic model for the hemolysis of red blood cells during osmotic stress. In this model, McGrath assumed that the key activation step in membrane damage due to osmotic stress is the exposure of the hydrophobic tail groups to the external environment. This model uses the Gibbs-Duhem equation,

$$n_{LPS} d\mu_{LPS} = -n_w d\mu_w - A d\gamma - S dT + V dP , \qquad (1.4)$$

to relate the change in chemical potential of water (μ_w) to the change in chemical potential of a theoretical lipo-protein species (LPS) involved in damage. The terms n_{LPS}, n_w, μ_{LPS}, A, γ, S, V and P in Eq 1.4 represent the number of the LPS molecules, the number of the water molecules, the chemical potential of the LPS molecules, the area of the membrane, the surface tension, entropy, volume and pressure, respectively. Using absolute reaction rate theory, the change in the chemical potential was incorporated into a rate equation that can be used to predict the membrane damage. The model has shown excellent agreement with the hemolysis data for red blood cells [129, 164]. This model attributes dehydration damage to increased lipid dissolution at low water activity: The decrease in chemical potential of water leads to an increase in the chemical potential of LPS promoting the transfer of LPS molecules from the membrane into the extracellular solution therefore increasing membrane damage [129, 164]. This model can also be used to explain reduced membrane damage observed during dehydration at low pressure

(vacuum) [114]: A decrease in pressure decreases the chemical potential of LPS, which stabilizes membrane structure. However, this model is limited as it assumes an instantaneous equilibration of the chemical potential of water across the membrane and therefore does not take into account the transmembrane osmotic pressure gradient and the effect of the resulting water efflux. Also, the model only considers the membrane as a system rather than the membrane and the external solution. Therefore, the effect of the decrease in the chemical potential of water was on LPS transfer was only examined in terms of LPS molecules leaving the bilayer never the reverse. To the best of our knowledge, this model has never been applied to any other cell type other than the one it was originally developed for, the red blood cells.

Leekumjorn et al. [165] used molecular dynamic simulations to model the dehydration of dipalmitoylphosphatidylcholine (DPPC) lipid bilayers by using Argon to replace the water surrounding the bilayer. As expected, the bilayer transformed into a non-bilayer structure due to the absence of the stabilizing hydrophobic effect. The simulation provided evidence for the exposure of the hydrophobic tail groups to the external environment during dehydration - this is one of the main assumptions of McGrath's model.

1.10 OUTLINE OF THESIS

Although the literature provides a wealth of information on the response of the cell or vesicle membrane to osmotic and freezing stresses there are several gaps that

exist. There is little information regarding the effect of dehydration kinetics on membrane structure at the molecular level even though the kinetics of dehydration and rehydration have been shown to be important to the post-thaw and post-rehydration survival of various organisms [31, 52, 53, 114]. There are also very few studies investigating the effect of freezing on membrane structure at the molecular level. Another factor that determines the extent of membrane damage, which has not received much attention, is the interaction between the membrane and cytoskeleton. We seek to address these gaps by investigating the effects of slow freezing and osmotic stress on membranes in simple systems (vesicles and bacteria) and the more complicated system of a mammalian cell. We also investigated the role of the cytoskeleton in determining the damage that occurs during dehydration and slow freezing of a model mammalian cell.

In the second chapter, slow freezing of liposomes/ LUVs is investigated using IR spectroscopy, which gives direct information on the membrane structure. Thermotropic hysteresis was observed for changes in both lipid head group hydration and lipid packing during cooling and heating. It was also observed that eutectic (sodium chloride dihydrate) formation during heating enhanced dehydration of the lipid bilayer. The presence of trehalose in the solution suppressed eutectic formation and the resulting dehydration phenomenon as well as enhancing recovery of pre-freeze membrane structure.

In the third chapter, dehydration of a model bacterium (*Geobacter sulfurreducens*) was performed. Using IR spectroscopy, it was observed that hyperosmotic shock and slow dehydration resulted in different cell membrane structures. It was also shown that the

post-rehydration viability could be maximized if the lyotropic phase change of the cell membrane was eliminated during dehydration.

In the fourth chapter, we investigated the response and interaction of the cell membrane and cytoskeleton of human foreskin fibroblast cells during application of osmotic stress. Our data suggest that the cells experienced a decrease in the availability of membrane material which may have reduced the cell's ability to expand during return to isotonic conditions. We also observed that hyperosmotic stress was responsible for increased rate of transfer of lipophilic dyes into and out of the membrane. The increased rate of insertion of the lipophilic styryl dye, FM1-43, into the membrane with increasing osmotic stress suggests the formation of membrane defects. It was observed that reducing crosslinking between actin filaments by inhibiting myosin motors yielded a more lamellae-like (vs. villi-like) dehydrated membrane morphology, and superior viability upon return to isotonic conditions.

In the fifth chapter, we investigated the response of the cell membrane and cytoskeleton of human foreskin fibroblast cells during slow freezing. From the results obtained, we suggest that mechanical damage due to shear and compression by ice crystals significantly decreases post-thaw viability. However, if this interaction is minimized, by increasing the unfrozen fraction using polyethylene glycol (PEG), dehydration-induced cell shrinkage also caused a significant decrease in viability. It was observed that inhibition of myosin motors enhanced post-thaw viability and reduced the incidence of post-thaw blebbing for cells frozen and thawed in isotonic solutions of PEG 600.

In the sixth chapter, the mechanisms behind osmotically induced alterations to the membrane are discussed. A model is proposed to explain the increased rate of lipophilic dye transfer observed in Chapter 4 and similar observations made in the literature. The model uses thermodynamics and a transition state theory model for lipid transfer [166] to relate the increased rate of lipid transfer and the formation of membrane surface defects to the decrease in the chemical potential of water. The role of the cytoskeleton in determining membrane morphology during dehydration damage is also discussed with respect to cytoskeletal stiffness. It is proposed that at the stiffness of the cytoskeleton affects the membrane morphology in the dehydrated state and the ability of the membrane to expand during return to isotonic conditions or during thawing.

The seventh chapter contains the conclusions of our studies and includes suggestions for improvements in dehydration and slow freezing protocols of cells based on our findings. Suggestions for future work are also given.

CHAPTER 2: CHARACTERIZATION OF THE EFFECT OF NACL AND TREHALOSE ON THE THERMOTROPIC HYSTERESIS OF DOPC LIPIDS DURING FREEZE/THAW

2.1 SUMMARY AND INTRODUCTION

This study characterizes the freeze/thaw behavior of large unilamellar DOPC vesicles in the presence of 0.5, 2, or 4M NaCl and 73 to 146 mM trehalose using Fourier transform infrared (FTIR) spectroscopy. Differences in hydration history during cooling and heating contributed to hysteresis in lipid phase change behavior. There was also an increase in post-thaw lipid chain order. Lipids transitioned to a more ordered state during cooling. However with heating, there was further conversion to a more ordered state at temperatures lower than the chain melting temperature. This conversion during heating became even more pronounced with increasing concentrations of NaCl due to the formation of NaCl dihydrate crystals and the resulting changes in lipid hydration. When trehalose was present in the solution, it was capable of abrogating the severe dehydration effect at high trehalose/ NaCl concentrations by suppressing the formation of the dihydrate crystals. Addition of trehalose enhanced recovery of pre-freeze membrane structure. Reasons for the protective mechanism of trehalose during freeze/thaw of DOPC liposomes in the presence of NaCl are discussed.

Understanding the structural and dynamic changes of the cell membrane is pivotal for cryopreservation [167]. Cryopreservation induces a variety of stresses such as low temperatures, phase change (i.e. freezing and melting), vitrification, exposure to ice

crystals, and increased osmotic stress (due to solute rejection in the frozen extracellular medium), which directly affect the cell membrane. Therefore, it is not surprising that the plasma membrane has long been identified as one of the primary sites of irreversible injury during cryopreservation [89, 168]. To minimize the detrimental effects of these stresses on the membrane, various cryoprotectant agents (such as dimethylsulfoxide, glycerol, and carbohydrates such as trehalose) have been used with significantly successful outcomes [167, 169, 170]. However, the mechanism of protection offered by these agents has not yet been determined, while the validity of two opposing hypotheses, "the water replacement hypothesis" [46, 47, 171] and the "preferential exclusion hypothesis" [172, 173] is still being debated.

Membrane model systems (mainly liposomes) have frequently been used to explore the biophysical response of the lipid bilayers to changes in temperature and osmotic stress [27, 37, 78, 174-183]. At room temperature, when the lipid bilayer is in a fully hydrated state, it is in the liquid crystalline (L_α) phase [82]. The membrane transitions into more ordered gel (L_β) or condensed (L_c) states with reduction in temperature (thermotropic transition) or hydration (lyotropic transition) [81, 82]. The L_α state is characterized by a relatively large lipid head group spacing and high disorder in the lipid acyl chains and consequently, a smaller bilayer thickness [81, 82]. In the gel (L_β) and condensed (L_c) phases, the lipid head groups are very tightly packed, and the lipid acyl chains are highly ordered, giving rise to a larger bilayer thickness [81, 82]. In the L_c phase, the lipids are arranged in a well-ordered lattice [71, 80] as compared to the gel or liquid crystalline phases. DOPC lipids are known to transition directly from the L_α phase to the L_c phase,

bypassing the intermediate L_β phase [184]. The structure of the lipid bilayer, and its lyotropic and thermotropic phase transitions can be monitored using NMR spectroscopy, X-ray diffraction, fluorescence microscopy [185], differential scanning calorimetry [186], and Fourier Transform Infrared (FTIR) spectroscopy [187]. Among these methods, FTIR spectroscopy offers a significant advantage by supplying independent information on the structural transitions of the lipid tail and head groups as well as the state of the surrounding environment [188-190]. Therefore, FTIR spectroscopy has extensively been used to analyze the phase transition behavior of liposomes [50, 176, 191], as well as the membrane transitions of pollen [192], yeast [193], sperm [89] and bacteria [137, 188, 194].

Despite the fact that lipid phase transitions have been intensively studied for many years, the detailed intermolecular interactions that give rise to the structural/dynamic changes remain elusive. This is important because a better understanding of how membranes behave at low temperatures (as well as during extracellular medium phase change) is crucial for improving cryopreservation.

In this study, to obtain a more clear description of the role of water on the lipid behavior, IR spectra have been obtained when DOPC liposomes were subjected to a freeze/thaw cycle. Differential scanning calorimetry (DSC) study of DOPC liposomes by Ulrich et al. [195] and the recent X-ray diffraction study of DOPC multilayers by Zhang et al. [196] provided an excellent framework for interpreting the FTIR spectroscopy results presented here. In the studies by Ulrich et al. and Zhang et al., lipid phase behavior was examined for multibilayer systems versus unilamellar liposomes in our study. Additionally, in the

X-ray diffraction study conducted by Zhang et al., the phase behavior was determined under equilibrium conditions. Therefore, there are slight differences among our and their results. Nevertheless, FTIR analysis complemented the DSC and X-ray diffraction studies by providing a more complete picture of the phase transition of DOPC liposomes and by extending the analysis to the dynamic changes that occur during freeze/thaw, which are more relevant to practical issues in cryopreservation.

2.2 MATERIALS AND METHODS

DOPC-cis (1,2-dioleoyl-sn-glycero-3-phosphocholine 18:1 cis) in chloroform was purchased from Avanti (Avanti Polar Lipids Inc., Alabaster, AL). Trehalose dihydrate (TRE) at ≥ 99% purity was purchased from Ferro-Pfanstiehl Laboratories (Waukegan, IL). All other chemicals were purchased from Sigma (Sigma-Aldrich Corp., St. Louis, MO).

2.2.1 PREPARATION OF LIPOSOMES

Chloroform was evaporated from DOPC by exposing the sample to a steady stream of ultrapure N_2 for 24 hours followed by vacuum exposure for 30-60 minutes to ensure complete removal of the solvent. The dried lipids were re-hydrated by mixing 2.5 ml of buffer composed of 50 mM NaCl and 10 mM TES (pH = 7.29), with 100 mg of lipids. The resulting dispersion was repetitively passed through a 100 nm pore polycarbonate filter (a total of 41 passes) sandwiched between two filters (Avanti extruder). The dispersion was modified by adding 0.5, 2 or 4M NaCl. To selected samples, either 73 or

146 mM TRE was added. All experiments were conducted at least in triplicate within 3 days of the preparation of the liposome stock solution (stored at 4°C).

2.2.2 FTIR SPECTROSCOPY

1 µl experimental solutions were sandwiched between two 16 mm diameter CaF_2 windows, which were then sealed with vacuum grease, and placed on a freeze-drying cryostage (FDC-196, Linkam Scientific Instruments Ltd., UK). The cryostage was exposed to N_2 for 10-15 minutes at 45^{o}C to remove the moisture. All samples were exposed to identical thermal treatment; cooling from T = 20^{o}C down to T = -80^{o}C followed by heating back to T = 20^{o}C at a rate of 1^{o}C/min. IR spectra were collected in the spectral range of 930 - 8000 cm^{-1} at 4 cm^{-1} resolution with 128 co-added interferograms using a Nicolet Continuum FTIR microscope (equipped with an MCT micron detector, Thermo Electron Corporation, LLC., Waltham, MA). Spectral analysis was carried out using OMNIC software (Thermo Electron). The spectral changes in the acyl chain CH_2 symmetric stretching band (ν-CH_2) located in the region near 2850 cm^{-1} , the phosphorus head group (PO_4) and the glycerol back bone vibrations (ν-C=O and ν_a-C-O-CO) located at 1088 cm^{-1} and 1160-1220 cm^{-1}, respectively were monitored. When examining the shifts in the ν_s-PO_2^- peak, the change in wavenumber was normalized with respect to the difference between the initial and final wavenumber values of ν_s-PO_2^- peak. The δ-OH band of H_2O (1650 cm^{-1}) was monitored to determine the state of water. The water bending and libration combination band (1950-2680 cm^{-1}) was also monitored to determine the freezing and thawing temperatures of the solution. Note that the area of the

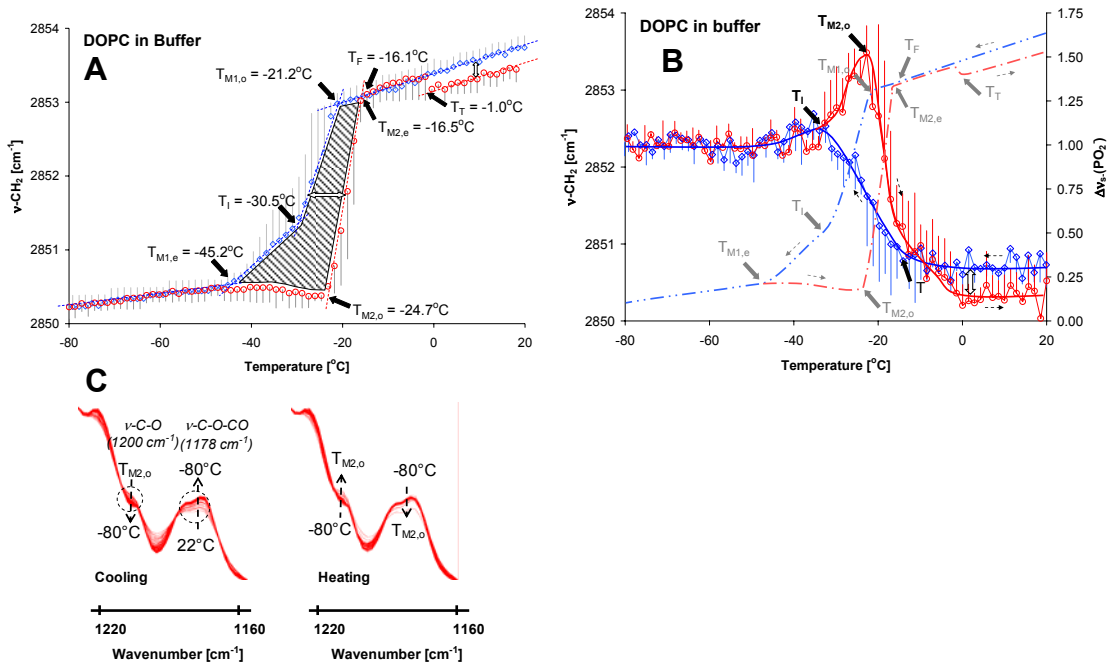

Figure 2.1 **A)** Variation of ν-CH_2 peak (◇ - cooling, ○ - heating) (hatched area indicates hysteresis between lipid phase transitions during cooling and heating), **B)** Change in ν_s-PO_2^- (~1088 cm^{-1}) (◇ - cooling, ○ - heating), **C)** Variation in the 1160 – 1220 cm^{-1} spectral range (dashed arrows indicate direction of temperature change; dashed circles indicate ν-C=O and ν_a-C-O-CO bands) with temperature in DOPC liposomes in buffer during a freeze/thaw cycle (T = 20→ -80→ 20°C at 1°C/min). (n=3).

water bending and libration combination band increases with increasing conversion of water to ice. Note that the freezing temperature of the experimental solutions was not controlled. However, freezing of the solutions was rapid and was completed within 1-2°C in all systems studied. In all of the experiments conducted here, during cooling freezing of water occurred at a higher temperature than lipid phase change.

2.3 RESULTS AND DISCUSSION

In this study, DOPC lipid phase transition was examined during freeze/thaw using FTIR spectroscopy. In addition to determining the relationship between the solution and the lipid phase transitions, the effects of NaCl and trehalose on lipid phase change have also been examined. This provided insight on the roles these components play in the freeze/thaw process, which is significant in biological (e.g. cryopreservation of microorganisms) and pharmaceutical (freeze-drying of proteins and liposome formulations) fields.

Freezing Response:

When DOPC lipids dissolved in buffer was cooled from room temperature, the frequency of the methylene groups decreased linearly with temperature (Figure 2.1A). DOPC in this region is in the liquid crystalline, L_α, state, and the continuous reduction in the peak frequency with temperature corresponds to a reduction in the gauche conformations in the acyl chain. This yields an increase in interlamellar spacing (distance between neighboring bilayers) of the multilayered DOPC bilayers as noted by Zhang et al [196]. A transition, $T_{M1,o}$, was noted at -21.2 ± 0.5 ºC, which was characterized by a more rapid decline in the methylene peak frequency with decreasing temperature following a sigmoidal path. A second transition, $T_{M1,e}$, was noted at -45.2 ± 3.2 ºC, beyond which the frequency remained nearly constant as the temperature was further decreased. In the region between $T_{M1,o}$ and $T_{M1,e}$, a frequency change of approximately 3 cm^{-1} was observed over a

temperature range of 24ºC. This is characteristic of a transition from the liquid crystalline to a more ordered phase. Note that an intermediate transition was detected at T_I = -30.5 ± 1.2 ºC.

In comparison, Zhang et al. [196] noted a major change in hydration (decrease in water layer thickness) at -7.5 ºC evidenced by a decrease in interlamellar spacing. However, there was no lipid phase transition at this temperature as evinced by the absence of change in the bilayer thickness. They also reported lipid phase transition from pure L_α to a mixture of L_α and $L_{c,}$ (L_α/L_c) at -15.4 ºC. The decrease in frequency observed in IR spectra beginning at $T_{M1,o}$ and ending at $T_{M1,e}$ is consistent with the conversion of L_α to L_α/L_c: A lower ν-CH_2 frequency indicates decreased lipid acyl chain order [197]. The discrepancy between the onset temperature of the transition and the range reported by Zhang et al. [196] and our results may be due to the non-equilibrium conditions in our experiment (Zhang et al. [196] study was conducted at equilibrium conditions while our study was conducted at a constant heating/cooling rate of 1^{o}C/min). The discrepancy may also be due to the fact that the system in the Zhang et al. [196] study was different in configuration (Zhang et al. [196] study was conducted with multibilayers versus unilamellar liposomes used in our study). Note that values reported in the literature for the phase transition temperature of DOPC lipids range from -21 ^{o}C to -15.4 ^{o}C [184, 195, 196, 198].

Initially, an increase in the peak frequency of v_s-PO_2^- (the head group peak) was observed during cooling (Figure 2.1B), which corresponded to the freezing of the buffer at T_F = -

16.1^{o}C. Freezing of the solution was also detected by the characteristic changes associated with the water bending peak located at 1650 cm^{-1} (data not shown). ν_s-PO_2^- frequency reached a climax at T_I = -30.5 ^{o}C, and decreased slightly with cooling until $T_{M1,e}$ was reached. At lower temperatures, there was no significant change in ν_s-PO_2^-. The climax reached at T_I indicated that there was no further change in lipid head group hydration for $T < T_I$. In contrast, for $T < T_I$, lipid tail group transitions continued down to $T_{M1,e}$. This suggests that the cooling induced increase in acyl chain order (as evidenced from the FTIR spectra and the interlamellar spacing measured using X-ray diffraction [196]) is not strongly dependent of the changes in the structure of the head group.

Thawing Response:

Upon reaching -80ºC, heating was initiated. The change in the methylene peak frequency (ν-CH_2) could be superimposed on the cooling curve until $T_{M1,e}$ was reached at -45.2 ^{o}C. At this temperature, the behaviors observed during cooling and heating differed significantly: In contrast to what was observed during cooling, the ν-CH_2 frequency decreased with heating up to $T_{M2,o}$, = -24.7 ± 2.4ºC. The significant difference in the ν-CH_2 behavior between cooling and heating in the region $T_{M1,e} < T < T_{M2,o}$ showed that during heating there was a significant increase in lipid order. Beyond this range, a rapid increase in the peak frequency was observed with increasing temperature until the transition was apparently completed at $T_{M2,e}$,= -16.5 ± 0.3 ºC. The temperature at which the lipid transition was completed during thawing was greater than the transition onset

temperature observed during freezing by about 5 ^{o}C ($T_{M2,e} > T_{M1,o}$). A significant hysteresis in lipid structural transition between the cooling and heating processes was present (as indicated by the horizontal white arrow in Figure 2.1A). Note that Zhang et al. also observed hysteresis (a difference in the L_c to L_α vs. L_α to L_c phase transition temperatures) in their experiments even though their experiments were conducted at equilibrium conditions. Similar hysteresis behavior has also been previously observed between lipid phase transitions during heating and cooling of DOPC lipids (and other types of lipids) at temperature ramp rates as slow as 0.3 ^{o}C/ min [184].

Finally, above $T_{M2,e}$, the frequency increased linearly with temperature, superimposible to the cooling curve until complete melting of the frozen phase (T_T) at -1.0 ^{o}C. At this temperature, a discontinuous decrease in the peak frequency of about 0.2 cm^{-1} was observed (vertical white arrow in Figure 2.1A). This indicates that the post-thaw structural/ dynamic properties of the liposomes were altered. Zhang et al. [196] also observed changes in the interlamellar spacing above the L_c to L_α phase transition temperature, but they attributed it to alterations in the hydration layer rather than in the lipid chain region.

During heating, the peak frequency of the ν_s-PO_2^- groups followed the path obtained during cooling until T_I was reached. Beyond T_I, increase in temperature caused an increase in frequency, differing very significantly from the path observed during cooling. At $T_{M2,o}$, corresponding to the minimum in frequency for the lipid acyl chains, a frequency maximum was observed for the ν_s-PO_2^- groups. The decrease in hydration of

Table 2.1 Summary of measured transition temperatures [°C] (average ± s.d.) for DOPC liposomes in buffer and in buffer with NaCl and trehalose (n = 3 experiments)

	Sample				
	buffer	**+ 0.5 M NaCl**	**+ 0.5 M NaCl + 146 mM Trehalose**	**+ 4M NaCl**	**+ 4M NaCl + 146 mM Trehalose**
T_F	-16.1 ± 5.6	-17.5 ± 4.7	-14.0 ± 3.3	-27.7 ± 2.4	-33.2 ± 2.9
$T_{M1,o}$	-21.2 ± 0.5	-20.7 ± 0.8	-19.6 ± 1.9	-20.1 ± 0.9	-21.4 ± 0.1
T_I	-30.5 ± 1.2	-30.0 ± 0.5	-30.9 ± 1.9	-30.1 ± 1.4	-28.5 ± 1.7
$T_{M1,e}$	-45.2 ± 4.3	-40.0 ± 0.4	-39.4 ± 1.2	-39.4 ± 1.0	-37.0 ± 0.9
$T_{M2,o}$	-24.7 ± 2.4	-21.3 ± 1.3	-21.9 ± 1.9	-22.7 ± 0.8	-21.5 ± 2.5
$T_{M2,e}$	-16.5 ± 0.3	-17.3 ± 0.4	-16.7 ± 1.5	-17.0 ± 0.8	-17.3 ± 0.8
T_T	-1.0 ± 0.5	-2.19 ± 0.5	-2.5 ± 0.3	-18.9 ± 0.8	-19.1 ± 1.6
T_E	-	-40.6 ± 1.1	-	-35.2 ± 2.9	-40.3 ± 2.2

T_F = Freezing temperature of the solution

$T_{M1,o}$ = Onset of rapid change in acyl chain frequency during cooling

$T_{M1,e}$ = End of rapid change in acyl chain frequency during cooling

T_I = The transition point between $T_{M1,o}$ and $T_{M1,e}$

$T_{M2,o}$ = Onset of rapid change in acyl chain frequency during heating

$T_{M2,e}$ = End of rapid change in acyl chain frequency during heating

T_T = Melting temperature of the solution

T_E = Eutectic Temperature (first observation of $NaCl{\cdot}2H_2O$ during cooling)

the lipid headgroups and the increase in packing of the acyl chains indicate that the maximum conversion of L_α to L_α/L_c was achieved at $T_{M2,o}$.

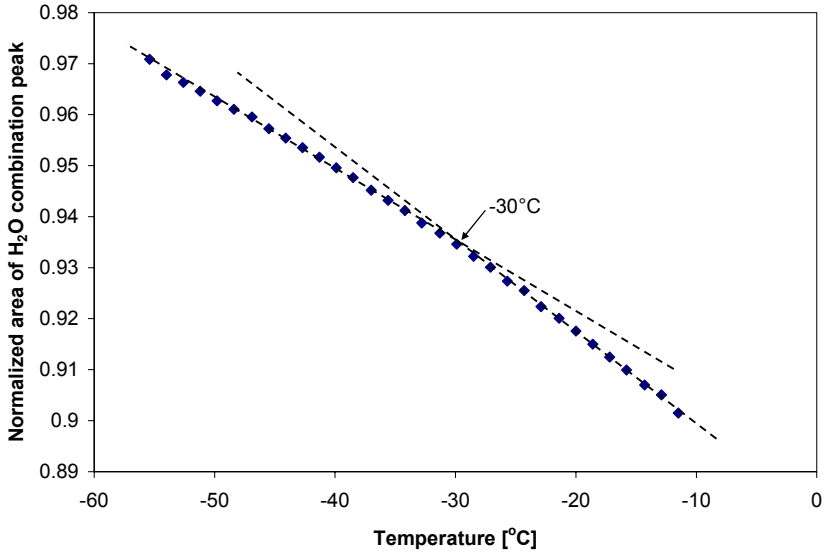

Figure 2.2 Change in area of water combination band with temperature during cooling of DOPC liposomes in buffer (The area is normalized to the value at -80°C) (representative data set).

With a further increase in temperature, the v_s-PO_2^- frequency rapidly decreased and eventually reached a plateau near -1°C. Similar to what is observed with the methylene peak, the frequency of the plateau was at a lower value than that observed prior to cooling. Thus, the changes in the phosphorus head group correlated with changes observed in the acyl chain suggesting a cooperative effect for the entire DOPC molecule with heating. A summary of the values of the transition temperatures are given in Table 2.1.

Although speculative, there is the possibility that the temperature, T_I, is the point at which further ice formation is not favored/ slowed down during cooling as observed from the decrease in slope of the water combination band area with decreasing temperature (Figure 2.2). This would allow the head groups to be maintained in a more hydrated state.

Alternatively, the decrease in the rate of conversion of water to ice may by due to the reduction in the rate of conversion of the lipids in the L_α to L_c state.

Finally, the peaks near 1178 and 1200 cm^{-1}, which correspond to the carbonyls in the glycerol backbone, underwent continuous changes with cooling which were largely reversed with heating (Figure 2.1C). These were attributed to the lipid phase transition and the corresponding changes in hydration levels. These changes became more distinct upon the addition of NaCl, which will be discussed in the following section.

One possible contributing factor towards the delay in the L_c to L_α transition and the hysteresis behavior was the comparative decrease in the availability of water during heating. DOPC lipids associate with 12-20 [195, 199] water molecules per lipid in the L_α state but with only 9 water molecules per lipid in the L_c state [195]. As a result, during L_α to L_c transition the DOPC head groups release 3-11 water molecules per lipid, which join the ice phase. Therefore, these water molecules may not be available to re-hydrate the headgroups during the (reverse) L_c to L_α phase transition during heating.

The cooperativity of L_c to L_α transition (i.e. the rate of change of ν-CH_2 with temperature) was greater than the L_α to L_c transition in all of the cases experimented. The increase in cooperativity in the gel phase is attributed to higher gel-gel lipid interaction energy (i.e., stronger interaction between the lipid acyl chains) [200].

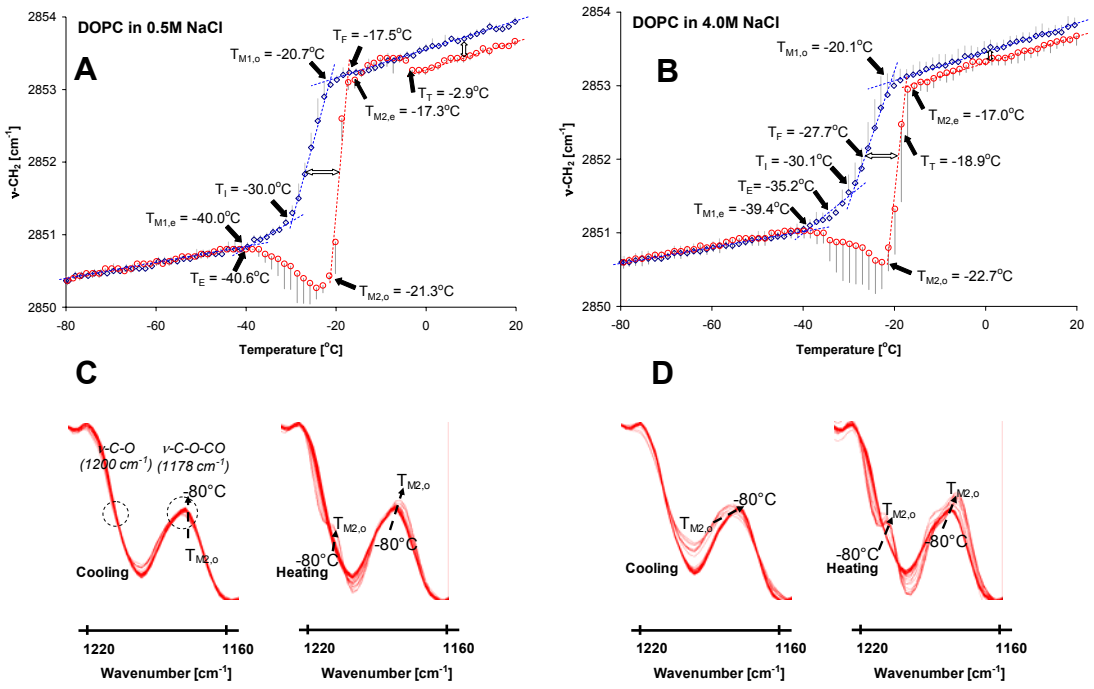

Figure 2.3 Variation of ν-CH_2 peak with temperature in, ***A)*** 0.5M NaCl, and ***B)*** 4M NaCl solutions during a freeze/thaw cycle (T = 20→ -80→ 20°C at 1°C/min) (◇ - cooling, ○ - heating). ***C)*** Spectral changes in the 1160 – 1220 cm^{-1} spectral range with temperature (dashed arrows indicate direction of temperature change; dashed circles indicate ν-C=O and ν_a-C-O-CO bands) for 0.5M NaCl ***D)*** Spectral changes in the 1160 – 1220 cm^{-1} spectral range with temperature for 0.5M NaCl.(n=3)

Effect of NaCl:

L_α to L_α/L_c transition was not affected by the decrease in water activity, a_w, for $a_w > 0.87$ (the water activity of the 4 M NaCl solution). This is indicated by the observations that during cooling of DOPC in 0.5 and 4 M NaCl solutions, the onset ($T_{M1,o}$) and the transition (T_I) temperatures did not change more than 1°C from those measured in TES buffer (Figure 2.3:A and B). However, $T_{M1,e}$ decreased by 5.2°C in the 0.5 M NaCl solution and by 5.8°C in 4 M NaCl solution. Phase transition cooperativity was less in 4 M NaCl than 0.5 M NaCl.

Additionally, in the presence of NaCl, ν-CH_2 values in the L_α/L_c state were slightly higher at -80°C relative to the 2850.2 cm^{-1} value measured in the buffer (2850.4 cm^{-1} in 0.5 M and 2850.6 cm^{-1} in 4 M NaCl solution). This suggests that NaCl either had a specific intermolecular interaction with DOPC or modified the solution properties (e.g., the amount of unfrozen solution). The increase in frequency in the L_α/L_c state indicates that there is more disorder in the lipids or more likely, an increase in the population of lipids in the L_α state vs. the L_c state.

During heating, ν-CH_2 peak frequency decreased markedly in the temperature range of $T_{M1,e} < T < T_{M2,o}$. Interestingly, in NaCl solutions, ν-CH_2 values at $T_{M2,o}$ were even below the values measured at T = -80°C (Figure 2.3). Analysis of the IR spectra in the range of 1600-1640 cm^{-1} indicated that in the $T_{M1,e} < T < T_{M2,o}$ range the amount of NaCl dihydrate crystals in the samples increased. The formation of the NaCl dihydrate crystals was also visually observed by the darkening of the sample at $T_{M1,e}$ during heating. The increase in the intensity of the dihydrate peaks (1600-1640 cm^{-1}) was accompanied by a decrease in the peak located at ~1665 cm^{-1}, which originated from the unfrozen interfacial water in the sample. The formation of NaCl dihydrate in aqueous NaCl during heating, starting at -40 °C, has been documented in NaCl-water inclusions [201]. We interpret these spectral observations as to indicate that NaCl dihydrate formation upon heating depleted the interfacial water, causing the lipids to become further dehydrated, inducing the hysteresis behavior observed in the freeze/thaw cycle. In Figure 2.3:C and D, the appearance of a significant ν-C=O peak only during heating ($T_{M1,e} < T < T_{M2,o}$) and the formation of asymmetry in the ν_a-C-O-CO peaks (tilting the peak towards lower

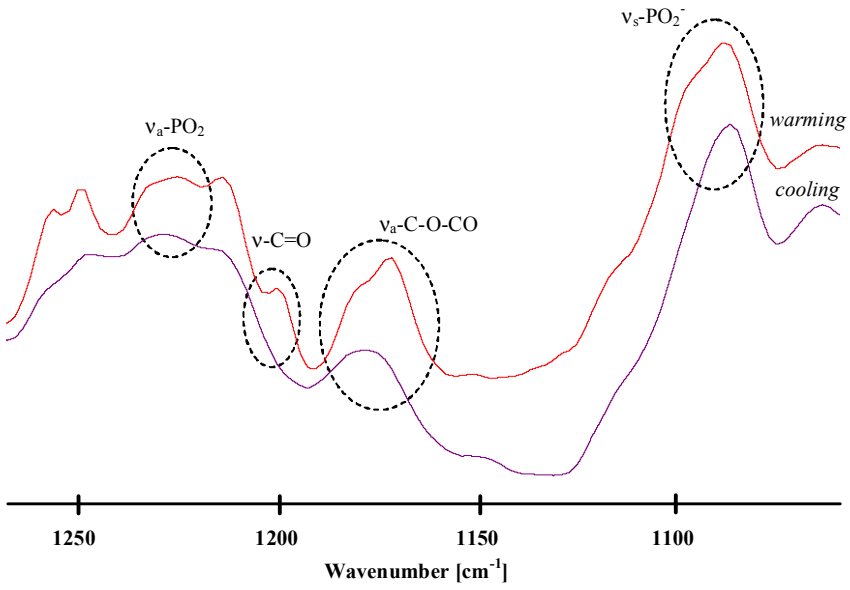

Figure 2.4 Comparison of the spectra at T = -29°C during cooling and warming of the DOPC liposomes in 4M NaCl

wavenumbers) were signs of excessive dehydration [202]. The changes in the spectral characteristics of these peaks were very significant in the control and 4 M NaCl groups both during cooling and heating but only during heating in the 0.5 M NaCl group. In general, the ν_a-C-O-CO peak was more asymmetric as compared to its pre-freeze shape. A significant increase in the ν_s-PO_2^- peak intensity of the samples that contained 4M NaCl (Figure 2.4) also demonstrated that the lipid head groups underwent significant dehydration [203].

The data above indicates that with increasing amounts of NaCl in the system, less lipids transition into the L_c state during cooling (hence the higher ν-CH_2 at -80 °C. There is an increase in the population of lipids in the L_c phase with the formation of the $NaCl{\cdot}2H_2O$ phase which appears to pull more liquid water away from the lipid headgroups. This

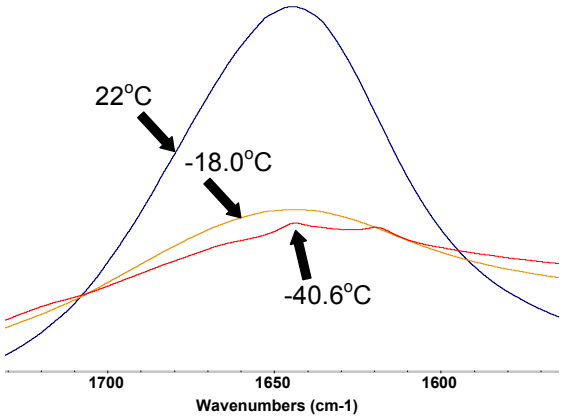

Figure 2.5 Changes in the δ-OH peak of water in 0.5M NaCl solution with temperature. *Note the spectral changes during supercooling, freezing and NaCl·2H$_2$O formation.*

newly detected dehydration phenomenon due to NaCl·2H$_2$O formation may play a role in the increased damage that is observed when cells are in contact with a eutectic phase during freezing [146].

In the presence of NaCl, $T_{M2,o}$ (corresponding to the onset of the L_α/L_c to L_α transition) shifted to higher temperatures (-21.3 ± 1.3 °C for 0.5M and -22.7 ± 0.8 °C for 4M, respectively). Moreover, this temperature corresponded to the melting/dissolution of the NaCl·2H$_2$O crystals and the formation of brine as evidenced by the disappearance of the two sharp peaks near 1650 cm^{-1} in the δ-OH band of water (Figure 2.5). However, the lipid phase transition completion temperatures ($T_{M2,e}$) remained relatively insensitive to the presence of NaCl in the solution (Table 2.1). The correlation between dissolution/melting and the lipid transition is interesting particularly in light of the fact that the freezing point of water in the 4 M NaCl sample (T_F = -27.7 °C) is below the onset of the lipid transition ($T_{M1,o}$ = -20.1 °C). This reinforces the idea that in these systems, the

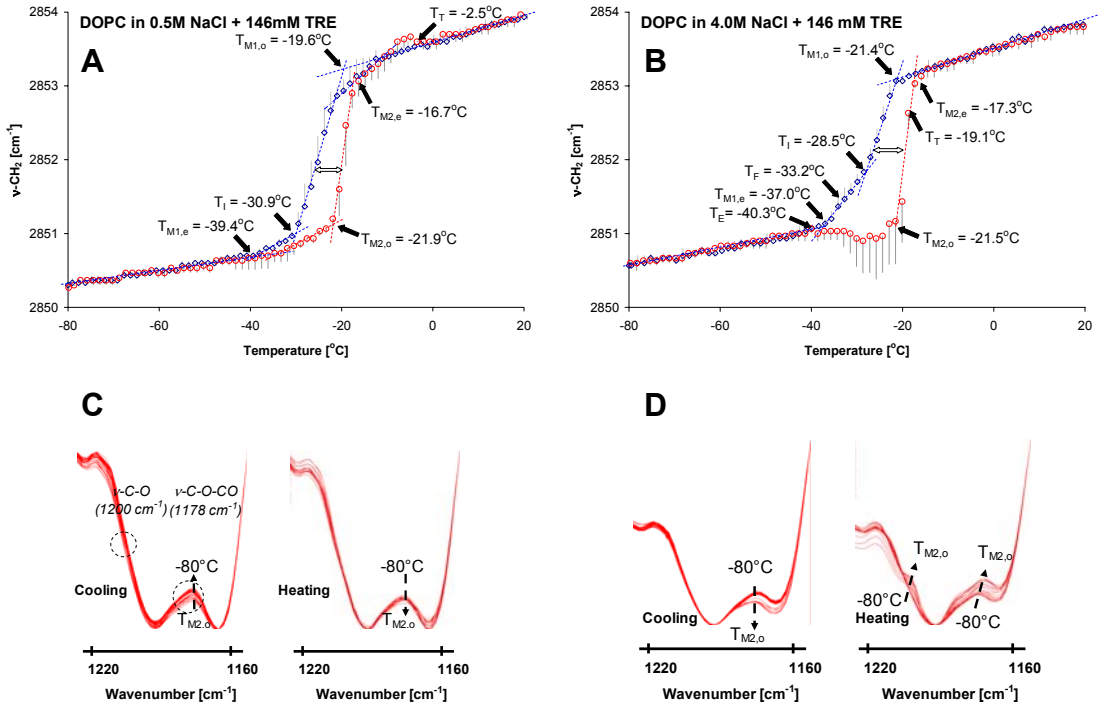

Figure 2.6 Variation of ν-CH_2 peak with temperature in, ***A)*** 0.5M NaCl + 5% TRE, and ***B)*** 4M NaCl + 5% TRE solutions during a freeze/thaw cycle (T = 20→ -80→ 20°C at 1°C/min) (◇ - cooling, ○ - heating). ***C)*** Spectral changes in the 1160 – 1220 cm^{-1} spectral range with temperature (dashed arrows indicate direction of temperature change; dashed circles indicate ν-C=O and ν_a-C-O-CO bands) for 0.5M NaCl + 5% TRE D***)*** Spectral changes in the 1160 – 1220 cm^{-1} spectral range with temperature for 4M NaCl + 5% TRE.(n=3).

lipid transition occurs largely independent of water of hydration during the cooling process for $a_w \geq 0.87$.

Finally, the values of ν-CH_2 measured at room temperature after completion of the freeze/thaw cycle differed for the two salt concentrations. In the 0.5 M NaCl sample, a drop in frequency occurred at -2.9 °C (1.9 °C lower than that in the buffer). In the 4 M NaCl sample, ν-CH_2 values were lower than those measured in the buffer at $T_{M2,e}$ and

remained lower through the completion of heating, following a parallel course to that obtained during cooling (Figure 2.3:B).

For liposomes in buffer and in NaCl solutions, there was a drop in the ν-CH_2 at T_T, which indicated that a permanent change in the liposome structure occurred. For these samples, the formation of lipid aggregates could also be observed using phase contrast microscopy. We propose that the observed drop at T_T arise from the changes in liposome structure due to fusion events. Fusion may occur due to compression of the liposomes in the narrow channels containing freeze-concentrated liquid. Such fusion events have been previously observed for egg lecithin liposomes undergoing freeze/ thaw [204].

Effect of Trehalose:

It has been previously observed that the addition of trehalose can reduce the degree of damage sustained by DPPC liposomes frozen in the presence of NaCl [205]. In order to investigate the effect of trehalose on the freeze/thaw response of DOPC liposomes in the presence of NaCl, we first added 146 mM trehalose to the samples containing 0.5 and 4 M NaCl, and the spectral changes during freeze/thaw were determined. Trehalose did not affect the lipid phase transition behavior or change the ν-CH_2 values observed during cooling (Figure 2.6A and B). However, during heating ν-CH_2 values progressively increased with temperature in the range of $T_{M1,e} < T < T_{M2,o}$ for liposomes in buffer with 0.5 M NaCl and 146 mM TRE. This is in contrast to the modest decrease seen in DOPC in buffer (Figure 2.1A), and the significant decrease seen in the samples containing NaCl (Figure 2.3:A and B). This suggests that there was no further conversion of the L_α state to

Table 2.2 Hysteresis area (see inset in Figure 2.1) for DOPC liposomes in buffer and in buffer with NaCl and trehalose (n = 3 experiments)

Sample	TRE/ NaCl Ratio [mole/mole]	Hysteresis area [cm^{-1}°C] (Average ± S.D.)	Dehydration observed during heating
buffer	-	25.8 ± 9.8	Yes
+ 15 mM TRE	0.3	12.9 ± 5.1	No
+ 0.5M NaCl	-	20.2 ± 3.1	Yes
+ 0.5 M NaCl + 73 mM TRE	0.13	13.8 ± 1.1	No
+ 0.5 M NaCl + 146 mM TRE	0.27	12.5 ± 2.5	No
+ 2M NaCl	-	24.4 ± 5.4	Yes
+ 2M NaCl + 146 mM TRE	0.07	16.5 ± 8.0	Slight dehydration in some samples
+ 4M NaCl	-	21.6 ± 7.7	Yes
+ 4M NaCl + 146 mM TRE	0.04	15.7 ± 2.7	Dehydration in some samples

the L_c state in this temperature region. Moreover, the effect of NaCl on the L_α/L_c to L_c transition (i.e. the further conversion of L_α to L_c) during heating was abolished. It was also observed that for liposomes in buffer with 0.5 M NaCl and 146 mM TRE no lipid aggregates could be observed using phase contrast microscopy. However, for liposomes in 4 M NaCl + 146 mM trehalose, there was a modest decrease in ν-CH_2 values during heating from $T_{M1,e}$ to $T_{M2,o}$ (Figure 2.6B) and the presence of small aggregates.

Another effect of trehalose was that post freeze/thaw ν-CH_2 values returned back to the pre-freeze values both in the 0.5 M NaCl and the 4 M NaCl solutions. Furthermore, no

detectable amount of $NaCl{\cdot}2H_2O$ was formed during the freeze/thaw cycle in the 0.5 M NaCl solution (spectra not shown). However, in the 4 M NaCl + 146 mM trehalose solution, $NaCl{\cdot}2H_2O$ formation was observed.

Liposomes in 0.5 M NaCl that underwent freeze/thaw in the presence of 146 mM trehalose did not exhibit dehydration-induced changed to the ν-C=O and ν_a-C-O-CO peaks (Figure 2.6C). However, for liposomes in 4 M NaCl + 146 mM trehalose the appearance of a significant ν-C=O peak only during heating ($T_{M1,e} < T < T_{M2,o}$) and the formation of asymmetry in the ν_a-C-O-CO (Figure 2.6D) indicate that the lipids did undergo further dehydration during heating. This result also indicates that trehalose did not completely abrogate the effect of the $NaCl{\cdot}2H_2O$ crystals on the lipid phase behavior.

In order to further investigate the relative effects of NaCl and trehalose on the observed hysteresis behavior and the dehydration phenomena observed during heating in the region $T_{M1,e} < T < T_{M2,o}$, we measured the area of the hysteresis loop (hatched area in Figure 2.1:A) for samples containing various amounts of NaCl and trehalose (Table 2). It was observed that the hysteresis was more pronounced for liposomes in buffer (which contains 50 mM NaCl) and liposomes in buffer with added NaCl. Addition of trehalose reduced the hysteresis at each concentration of NaCl (Table 2.2). With higher ratios of trehalose to NaCl, the hysteresis was further reduced (Table 2.2). For all samples containing trehalose, there was a return to pre-freeze ν-CH_2 values, despite some samples still exhibiting dehydration, albeit reduced, in the region $T_{M1,e} < T < T_{M2,o}$ (Table 2).

These results suggest that the presence of trehalose not only reduced the magnitude of the dehydration during heating but also prevented changes in liposome structure.

It was observed that trehalose reduced the hysteresis for liposomes in buffer (Table 2.2). This result suggests that the hysteresis for liposomes in buffer may have been partly due to the formation of $NaCl{\cdot}2H_2O$ crystals, similar to samples where NaCl was added (although these crystals were not in sufficient quantity to be detected for the liposome in buffer sample.

DOPC phase transition behavior during freeze/thaw is significantly altered in the presence of trehalose. One direct effect of trehalose was to alter the solution properties resulting in the elimination of the $NaCl{\cdot}2H_2O$ phase at sufficiently high trehalose/NaCl concentrations. Elimination of eutectic crystallization by trehalose (and other cryoprotectants) was shown in DSC and NMR studies [206]. However, trehalose had an additional effect on the freeze/thaw response of DOPC liposomes where there was a recovery of the pre-freeze ν-CH_2 values. The reason behind the recovery of the pre-freeze ν-CH_2 values in the presence of trehalose is unclear. It is probably due to a combination of factors: One factor could be the reduction of severe dehydration in the $T_{M1,e} < T < T_{M2,o}$ region, which would alleviate the formation of membrane defects [75] and the resulting fusion between liposomes due to the presence of defects [126]; A second factor could be due to reduction in fusion events due to direct trehalose-lipid headgroup interactions. Direct trehalose-lipid headgroup interactions have been observed from molecular dynamics simulations [165, 207]. This reduction in fusion events due to direct

trehalose-lipid headgroup interactions was suggested by Kristiansen [205] who observed a reduction in leakage of multilamellar DPPC liposomes in the presence of NaCl during freeze/thaw with the addition of trehalose.

2.4 CONCLUSION

The IR analysis affirms and adds to results obtained with X-ray diffraction and DSC on the freeze/thaw response of DOPC liposomes and to previous freeze/thaw studies of DPPC liposomes. More importantly, it was demonstrated that the induction of the condensed (L_c) phase during heating was highly dependent on the state of water. It was observed that addition of trehalose maintained membrane structure during freeze/thaw. Finally, it was shown that trehalose alters the phase transition behavior of NaCl solutions thereby modulating the hydration of the lipid bilayer to prevent further conversion of the lipid bilayer to the condensed phase during heating.

CHAPTER 3: ROLES OF MEMBRANE STRUCTURE AND PHASE TRANSITION ON THE HYPEROSMOTIC STRESS SURVIVAL OF *GEOBACTER SULFURREDUCENS*[1]

3.1 SUMMARY AND INTRODUCTION

Geobacter sulfurreducens is a δ-proteobacterium bacteria that has biotechnological applications in bioremediation and as biofuel cells. Development of these applications requires stabilization and preservation of the bacteria in thin porous coatings on electrode surfaces and in flow-through bioreactors. During the manufacturing of these coatings the bacteria are exposed to hyperosmotic stresses due to dehydration and the presence of carbohydrates in the medium. In this study we focused on quantifying the response of *G. sulfurreducens* to hyperosmotic shock and slow dehydration to understand the hyperosmotic damage mechanisms and to develop the methodology to maximize the survival of the bacteria. We employed FTIR spectroscopy to determine the changes in the structure and the phase transition behavior of the cell membrane. Hyperosmotic shock resulted in greatly decreased membrane lipid order in the gel phase and a less cooperative membrane phase transition. On the other hand, slow dehydration resulted in increased membrane phase transition temperature, less cooperative membrane phase transition and a small decrease in the gel phase lipid order. Both hyperosmotic shock and slow

[1] *Reprinted* from *Biophysica Acta (BBA)-Biomembranes 1778*, *V. Ragooonanan, M. J., D.R. Bond, A. Aksan Roles of Membrane Structure and Phase Transition on the Hyperosmotic Stress Survival of Geobacter sulfurreducens*, *2283-2290, copyright (2008), with permission from Elsevier*

dehydration were accompanied by a decrease in viability. However, we identified that in each case the membrane damage mechanism was different. We have also shown that the post-rehydration viability could be maximized if the lyotropic phase change of the cell membrane was eliminated during dehydration. On the other hand, lyotropic phase change during re-hydration did not affect the viability of *G. sulfurreducens*. This study conclusively shows that the cell membrane is the primary site of injury during hyperosmotic stress, and by detailed analysis of the membrane structure as well as its thermodynamic transitions it is indeed possible to develop methods in a rational fashion to maximize the survival of the bacteria during hyperosmotic stress.

Geobacter sulfurreducens, *Rhodoferax ferrireducens,* and *Shewanella oneidensis* are *capable of transferring electrons across the cell membrane* [208-212]. In particular, G. sulfurreducens *can oxidize organic compounds and transfer electrons directly to metal surfaces even in the absence of soluble mediators* [208]. This makes *G. sulfurreducens* a valuable bioremediative agent *for* oxidation of contaminants and reduction of toxic metals [213-215]. *G. sulfurreducens* can also be used to generate electricity from waste organic matter in remote biosensors or as biofuel cells [208, 216, 217]. Such biotechnological applications require successful encapsulation and stabilization of the catalytically reactive bacteria in thin protective coatings on electrode surfaces [218] and in flow-through bioreactors. It is also of utmost importance to develop effective preservation methods for the storage of the coatings that contain the encapsulated bacteria.

Latex coatings can be used to form hyperporous biocatalytic matrices to encapsulate reactive bacteria [219, 220]. The hyperporous matrix enables rapid diffusion of chemicals while mechanically protecting and isolating the bacteria from the solution environment [214]. The reaction rates in biocatalytic coatings are dependent on the porosity of the matrix [221]. To adjust the porosity, carbohydrates (such as sucrose, sorbitol or trehalose) are incorporated in the latex formulation during the encapsulation process [221]. The pore-forming ability of the carbohydrates is attributed to their high water affinity, which generates a "water buffer" in the matrix [214]. An added benefit of the carbohydrates is their protective capability against dehydration. It is known that carbohydrates can protect liposomes [176], isolated biological membranes [134], isolated organelles [135], bacteria [136, 137] and mammalian cells [5, 138] against dehydration stress. It is generally accepted that carbohydrates stabilize the biological structures and protect the organisms during dehydration by replacing the water surrounding the biomolecules and the membranes [46, 47, 222] and by dampening the molecular motions [115].

Inevitably, osmotic, mechanical, and thermal stresses are formed during the encapsulation process due to polymerization of the coating material, and the presence of carbohydrates in the surrounding medium. These stresses reduce the viability and the reactivity of the encapsulated bacteria. Since the cell membrane is the primary site for hyperosmotic injury [39, 49] the structural changes it undergoes and its integrity are of primary interest. It is proposed that the de-/rehydration kinetics as well as the environmental temperature determine the structure and the integrity of the cell membrane

and therefore directly affect the survival of the bacteria during exposure to hyperosmotic stress [31, 52, 53].

Cell membrane lipids are highly hydrated. Therefore, individual lipid mobility and collective lipid dynamics (i.e., the packing structure and organization) depend on the activity of the surrounding water [28]. When the cell membrane is fully hydrated it is dominantly in the liquid crystalline (l.c.) phase. However, it transitions into the gel phase with reduction in temperature (thermotropic transition) or water activity (lyotropic transition). The liquid crystalline state is characterized by increased lipid head group spacing, increased disorder in the lipid acyl chains, and a small bilayer thickness [81, 82]. In the gel phase the lipid head groups are very tightly packed, the lipid acyl chains become straighter and ordered, and the bilayer thickness increases [81, 82]. The direct influence of the osmotic stress on the cell membrane is documented in bacteria with the observation of endocytotic vesiculation and membrane fluidity change in osmotically stressed *Escherichia coli* [31, 52], increased membrane fluidity in osmotically stressed *Bradyrhizobium japonicum* [53], and increased membrane phase transition temperature in air-dried *Lactobacillus bulgaricus* [137]. Membrane phase transition is believed to initiate lipid phase separation [223], and membrane fusion [223], directly affecting the viability of the dehydrated organism. Also due to co-existence of the different phases during a phase transition, membrane permeability increases and cells become leaky [88]. Leaking of the cellular contents during rehydration has been identified as the major reason for reduction in viability [223].

The structure of the membrane, and its lyotropic and thermotropic phase transitions can be monitored using fluorescence microscopy [185], Differential Scanning Calorimetry [186], and Fourier Transform Infrared (FTIR) spectroscopy [187]. FTIR spectroscopy has been successfully used to measure the lipid phase transition temperatures of liposomes [176], pollen [192], yeast [224] sperm [225] and bacteria [49, 137]. IR spectra, in addition to supplying information on the membrane state and transition kinetics, also contains information on the secondary structures of the cellular proteins [226, 227]. The ability to nondestructively and simultaneously quantify the changes in different cellular structures makes FTIR the method of choice in our experiments.

Lyophilization and cryopreservation are the preferred methods for the preservation of bacteria [228]. However, lyophilization and cryopreservation require processing at cryogenic temperatures. To reduce the processing and storage costs, alternative preservation methods such as air, foam, spray and fluidized bed drying have been proposed (see Morgan et al., 2006 [228] for a review of the last three methods). Of all the drying methods listed, air drying is the most feasible and advantageous one for the preservation of the latex-encapsulated *G. sulfurreducens*. The costs associated with cryopreservation can be eliminated if *G. sulfurreducens* can be successfully encapsulated, preserved in a dehydrated state, and stored at room temperature. Therefore, development of methods to increase the resistance of the cells to dehydration stress is crucial not only for encapsulation in coatings but also from preservation point of view.

In this study, we explored the mechanisms of hyperosmotic stress-induced viability loss in *G. sulfurreducens* in order to maximize its survival during encapsulation and

preservation in a desiccated state. We employed FTIR spectroscopy to investigate the structure and the thermodynamic phase transitions of the cell membrane. We have determined the changes in the membrane phase transition temperature (T_m), membrane phase transition cooperativity (ξ), and lipid order as a function of the magnitude and the rate of the extracellular osmotic stress, and dehydration/re-hydration temperatures. The values chosen for these parameters mimicked the conditions encountered during encapsulation in latex coatings [214].

3.2 MATERIALS AND METHODS

3.2.1 BACTERIAL CULTURE

G. sulfurreducens strain PCA (ATCC #51573) was sub-cultured in our laboratory at 30 °C using a vitamin-free anaerobic medium containing (per l liter of solution): 0.38 g KCl, 0.2 g NH_4Cl, 0.069 g $NaH_2PO_4.H_2O$, 0.04 g $CaCl_2.2H_2O$, 0.2 g $MgSO_4.7H_2O$, and 10 ml of a mineral mix (containing per 1 liter of solution : 0.1 g $MnCl_2.4H_2O$, 0.3 g $FeSO_4.7H_2O$, 0.17 g $CoCl_2.6H_2O$, 0.1 g $ZnCl_2$, 0.04 g $CuSO_4.5H_2O$, 0.005 g $AlK(SO4)_2.12H_2O$, 0.005 g H_3BO_3, 0.09 g Na_2MoO_4, 0.12 g $NiCl_2$, 0.02 g $NaWO_4.2H_2O$, and 0.10 g Na_2SeO_4). Acetate (as electron donor) was added to the solution at a concentration of 20 mM. The pH of the culture media was adjusted to 6.8, 2 g/l $NaHCO_3$ was added, and the media was flushed with oxygen-free N_2/CO_2 (80/20 v/v) prior to sealing with butyl rubber stoppers and autoclaving. Within 3 h of reaching maximum optical density (OD^{600}>0.6), 10 ml aliquots of the cell suspension were centrifuged for 5 min at 5,000 g. The cells were then pelleted and re-suspended in either 20 µl of fresh

culture medium, or culture medium containing sucrose (see below). Solid media (used in measuring viability by colony forming units) was prepared by adding 1.5 % agar (Difco Corp., Lawrence, KS) to the culture media, and pouring into petri plates inside an anaerobic chamber.

3.2.2 Application of hyperosmotic shock and slow dehydration

In order to investigate the effects of hyperosmotic shock on *G. sulfurreducens* viability, pelleted bacteria were re-suspended in growth medium that contained 0% (as the control group), 6.75, 13.5, or 27% w/w sucrose. In order to investigate the effects of slow dehydration, 20 µl solutions containing *G. sulfurreducens* were air-dried up to 45 minutes in growth medium that contained 0, 6.75 or 13.5% w/w sucrose. The drying temperature (T_d) was 30 ºC and the environmental relative humidity (RH) was kept constant at 65%. Dried samples were re-hydrated at a re-hydration temperature (T_r) of 30 or 40ºC. In order to investigate the effects of drying temperatures, 20 µl solutions containing *G. sulfurreducens* were dried in growth medium that contained 0% (as the control group) or 6.75% w/w sucrose at T_d = 5ºC and RH = 11%, and were re-hydrated either at T_r = 5ºC or 30ºC. The environmental RH was adjusted to 11% for the T_d = 5ºC case so that the partial pressure of water in the environment was the same as in T_d=30ºC, 65% RH case. This ensured that the drying kinetics and the water content at the final state were identical in both drying temperatures. Drying times at each temperature were also varied (0, 15, 30, 45 or 60 minutes) to achieve samples of different final state water content and activity.

3.2.3 G. SULFURREDUCENS VIABILITY MEASUREMENTS

G. sulfurreducens viability experiments were performed in an anaerobic box (flushed with H_2:CO_2:N_2 5:20:75) after the dried samples were re-hydrated with growth medium at different temperatures (T_r = 5°C, 30°C or 40°C) by adding 1 ml of growth medium. Re-hydrated bacteria were then incubated for 30 minutes at either 5°C, 30°C or 40°C. A fluorescence-based viability assay (Baclight L7012; Molecular Probes, Portland, OR) was used to determine cell viability. The viability assay utilized the change in the permeability of *G. sulfurreducens* membrane to specific dyes as a measure of viability. The assay consisted of two dyes: Propidium Iodide and SYTO 9, which were mixed at a 1:1 molar ratio. Fluorescence from the live *G. sulfurreducens* population was measured at an excitation wavelength of 430 nm and an emission wavelength of 530 nm using a fluorescent plate reader (Spectra Max, M2, Molecular Devices Company, Sunnyvale, CA). Fluorescence from the dead/permeable *G. sulfurreducens* population was measured at an excitation wavelength of 430 nm and an emission wavelength of 630 nm. Measurements were calibrated during each experiment by using hydrated control cells (100% live) and cells exposed to 70% ethanol (100% dead). T-test (two-sample test, assuming unequal variances) was applied to determine the statistical significance (P) of the experimental results. Comparison of the viability determined by the fluorescent live/dead assay to that measured by regular plate counts (based on cell growth on agar plates) demonstrated a linear, one-to-one correlation between the two methods (data not shown) showing the validity of the fluorescence viability assay.

3.2.4 DETERMINATION OF THE PHASE, LIPID ORDER AND THERMODYNAMIC TRANSITIONS OF THE MEMBRANE

Temperature ramp Fourier Transform Infrared Spectroscopy (FTIR) measurements were performed on osmotically shocked or slowly dehydrated *G. sulfurreducens* to monitor the changes in the structure and the phase transition behavior of the cell membrane. 20 µl of the experimental solutions containing *G. sulfurreducens* were deposited on CaF_2 windows and dried under specified RH and temperature conditions for different lengths of time matching the conditions in the viability experiments. After drying, the samples were sandwiched between two CaF_2 windows and placed in a controlled temperature cell. FTIR spectra were collected in the 930-8000 cm^{-1} range using a Thermo-Nicollet 6700 spectrometer, equipped with a DTGS detector (Thermo-Nicolet, Madison, WI, USA). The temperature of the sample was recorded using a thermocouple that was located in the controlled temperature cell. FTIR spectra was recorded at 1 minute increments while the sample was initially cooled from ambient temperature (22°C) down to 0°C, and then heated at a constant rate of 2°C/min to 100°C. At each temperature data point an IR spectrum was obtained by averaging 32 scans.

G. sulfurreducens membrane lipid order which refers to the order/ straightness of the lipid acyl chains, was quantified by measuring the location of the νCH_2 symmetric stretching band maximum [187], which was located approximately at 2850 cm^{-1} in the control sample. Higher νCH_2 wavenumber/ frequency indicates decreased lipid acyl chain order [197]. The change in the temperature dependence of the νCH_2 peak wavenumber was used to determine the membrane phase transition temperature (T_m). Cooperativity of

the membrane phase transition (ξ) was determined by measuring the slope of the νCH_2 wavenumber change at T_m. A more cooperative phase transition was indicated by a larger slope at the membrane phase transition temperature.

3.2.5 WATER CONTENT ANALYSIS

Water contents of the dehydrated samples were determined gravimetrically and spectroscopically. Gravimetric analysis was performed by measuring the weight of the samples before and immediately after drying and also after baking for 2 hours at 110°C (to remove all the water in the sample). The average water contents reported were the averages of three independent gravimetric experiments. In addition, spectroscopic analysis was used to obtain a measure of the ratio of water per cell by ratio of the combination water band area (1900-2300 cm^{-1}) to the peak intensity of νCH_2 peak. The peak intensity of the νCH_2 peak was calculated from the second derivative peak intensity [229].

3.3 RESULTS

3.3.1 EFFECT OF HYPEROSMOTIC SHOCK ON G. SULFURREDUCENS VIABILITY AND MEMBRANE PHASE TRANSITION BEHAVIOR

Experiments were first conducted to evaluate the effects of rapid hyperosmotic shock on the viability of *G. sulfurreducens*. Cells were exposed to growth medium solutions

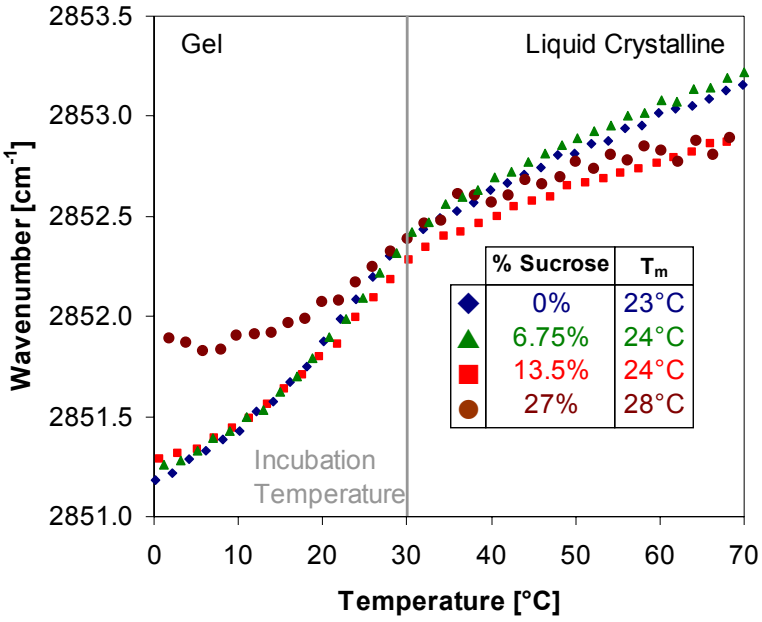

Figure 3.1 Change in νCH_2 band maxima with temperature for *G. sulfurreducens* in growth medium (◆),growth medium + 6.75% w/w sucrose (▲), growth medium + 13.5% w/w sucrose (■), and growth medium + 27% w/w sucrose (●). (Representative data set)

containing sucrose concentrations up to 27%. Based on live/dead fluorescence analysis, viability of *G. sulfurreducens* was not significantly affected by the presence of up to 6.75% extracellular sucrose (Viability = 95 ± 9%), showing that *G. sulfurreducens* could tolerate mild hyperosmotic shock. However *G. sulfurreducens* viability decreased significantly with further increase in the extracellular sucrose concentration (Table 3.1).

FTIR spectroscopy was used to quantify the membrane response to hyperosmotic shock. Control cells suspended in growth medium had cooperative membrane phase transition (ξ = 0.058 ± 0.001 cm^{-1}/°C) at T_m = 23 ± 1°C (Figure 3.1). As *G. sulfurreducens* do not have membrane bound organelles, the temperature-induced transition in the CH_2 peak

Table 3.1 Effect of Hyperosmotic Shock on G. sulfurreducens Viability (n: number of samples in each group).

Extracellular Sucrose Concentration [% w/w]	Extracellular Osmolality [mOsm]	Viability [%]	Significance
0 (n=4)	300	100 ± 0	-
6.75 (n=4)	500	95 ± 8.9	0.163
13.5 (n=4)	700	63 ± 4.7	0.0003
27 (n=3)	1100	41 ± 6.5	0.002

wavenumber is associated exclusively with the gel to l.c. phase transition of the cellular membrane. A membrane phase transition located at 23°C for the unstressed cells indicated that, as expected, the cell membrane was almost completely in the l.c. phase at the growth temperature (30°C).

There was no significant difference in the T_m values for *G. sulfurreducens* suspended in growth medium containing 0, 6.75 or 13.5% sucrose (Figure 3.1). However, membrane lipids were less ordered in the l.c. phase for the control cells (0% sucrose) compared to the cells suspended in 13.5 and 27% sucrose solutions (as indicated by the high νCH_2 wavenumbers [230]) . In the gel phase however, there was no significant difference in terms of lipid order between the cells suspended in 0, 6.75 and 13.5% sucrose solutions. There was no significant difference in the ξ values for *G. sulfurreducens* suspended in growth medium containing 0 and 6.75% sucrose. Exposure to 13.5% extracellular sucrose decreased the cooperativity of the membrane phase transition ($\xi = 0.053 \pm 0.001$ $cm^{-1}/°C$) compared to the control cells ($\xi = 0.058 \pm 0.001$ $cm^{-1}/°C$). In the presence of 27%

sucrose, membrane phase behavior was drastically different with a higher membrane phase transition temperature (T_m = 28°C ± 1°C), significantly reduced lipid order in the gel phase and reduced cooperativity (ξ = 0.033 ± 0.001 cm^{-1}/°C). These results showed the changes in the properties of *G. sulfurreducens* membranes during hyperosmotic shock and revealed that extracellular sucrose directly affected the membrane structure and its thermodynamic phase transitions.

3.3.2 Effect of dehydration on G. sulfurreducens viability and membrane phase transition behavior

In order to determine the effects of gradually increased osmotic stress, and to test for possible protection capability of sucrose during dehydration, *G. sulfurreducens* suspended in growth medium (0% sucrose) and growth medium containing 13.5% sucrose were dried at T_d = 30°C, and 65% RH for different time periods up to 1 hour. Viability of the dried bacteria was determined after re-hydration at T_r = 30 ºC. In both experimental groups viability decreased with increased drying time (Figure 3.2A). At all timepoints the viability of the growth medium group was higher even though the difference between the two groups started to diminish after 45 minutes of drying.

Gravimetric analysis of bacteria revealed that growth medium samples dried for 1 hour had 0.55 ± 0.14 $g_{water}/g_{drymatter}$. It is reported that 0.3 $g_{water}/g_{drymatter}$ is the critical water content below which a significant reduction in viability is observed for *E. coli* and *Serratia marcescens* [7, 46]. The continuous decrease in viability at all drying times beyond 15 minutes demonstrate that *G. sulfurreducens* was sensitive to osmotic stress via slow dehydration.

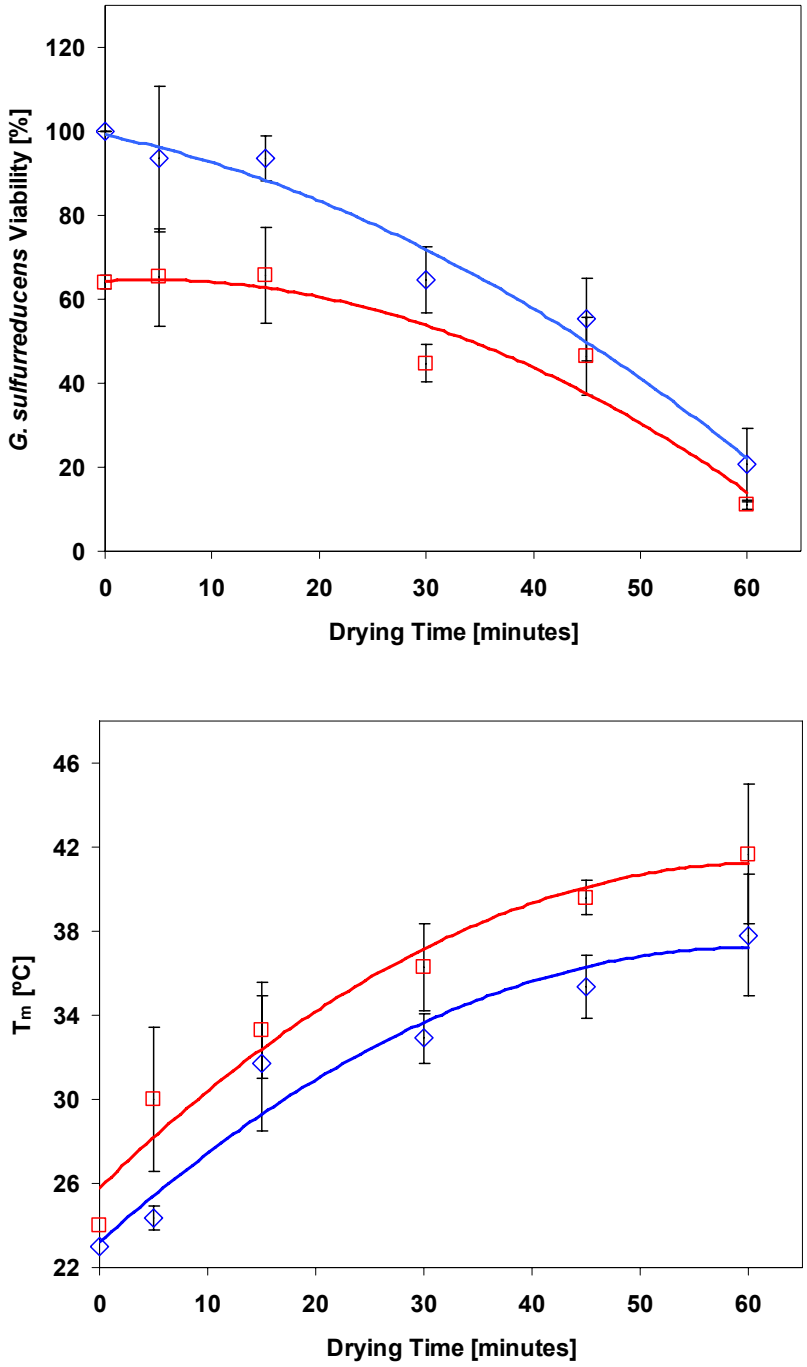

Figure 3.2 Change in *G. sulfurreducens* **A)** viability, and **B)** T_m with drying time for samples dried at 30°C and 65% RH for up to 60 minutes in growth medium (◇) and growth medium containing 13.5% w/w sucrose (□) (n=3 in all data points. Lines are guides for the eye).

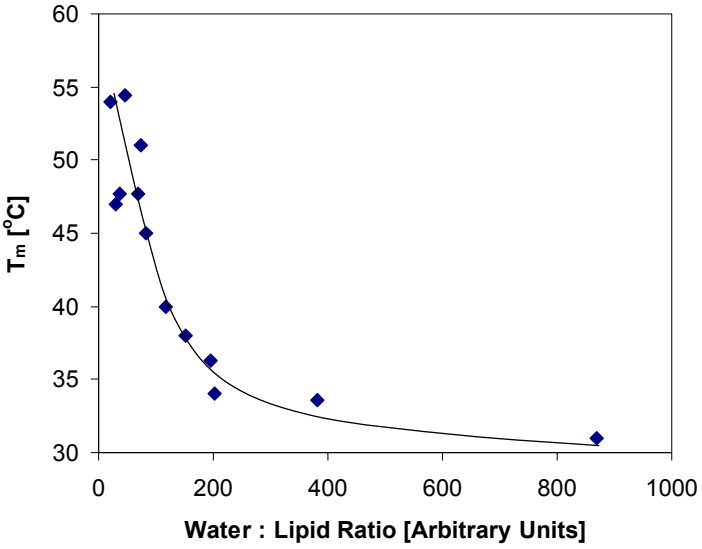

Figure 3.3 Membrane phase transition temperature versus water content as measured by the ratio of the amount of water to CH (see methods)

Temperature ramp FTIR analysis was also performed on the *G. sulfurreducens* samples dried (65% RH, T_d = 30°C) in growth medium and growth medium + 13.5% sucrose solutions. For both treatments, drying increased membrane T_m values (Figure 3.2B). At all drying times, average T_m values for *G. sulfurreducens* dried in growth medium + 13.5% sucrose solution were higher than the cells dried in the absence of sucrose. After 45 minutes of drying, T_m values reached equilibrium *at about 41°*,, possibly due to equilibration of the solution water activity with the surroundings. *Samples that were dried at lower relative humidity (up to 0% RH) demonstrated a continued shift in T_m up to 55°C (Figure 3.3).* The higher T_m values for cells dried in the presence of sucrose revealed that extracellular sucrose posed additional osmotic stress on the membrane, and did not have membrane protection capability when it was present extracellularly.

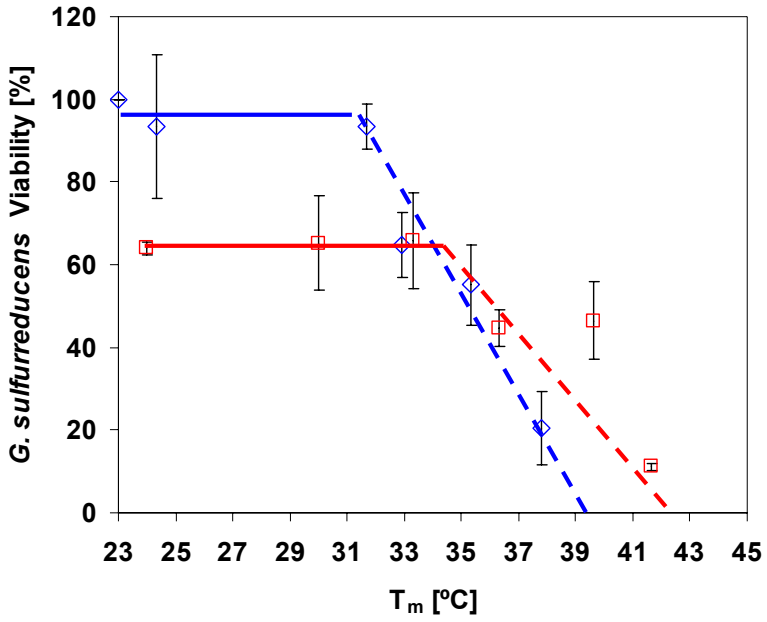

Figure 3.4 Change in Viability with T_m for *G. sulfurreducens* samples dried at 30°C and 65% RH for up to 60 minutes in growth medium (◇) and growth medium + 13.5% w/w sucrose (□) (lines are drawn as guides for eye; error bars for T_m are not shown for clarity; range of error: 1°C – 3.5°C)

Figure 3.4 shows the post re-hydration viability of *G. sulfurreducens* as a function of T_m. When *G. sulfurreducens* was partially dried in growth medium, and the membrane phase transition temperature rose as high as T_m=32°C, viability was not affected (i.e., *G. sulfurreducens* could tolerate mild hyperosmotic stress without loss of viability). Above T_m = 32°C, there was a negative linear correlation between *G. sulfurreducens* viability and the dehydrated state membrane phase transition temperature.

Similar behavior was also observed for *G. sulfurreducens* dried in 13.5% sucrose solution. The absolute viability of these cells differed at T_m = 23°C due to the initial osmotic shock. For T_m values greater than 32°C, cooperativity values for the membrane

phase transition were not significantly different for all the sampled dried in the growth medium ($\xi = 0.053 \pm 0.006$ cm^{-1}/°C) and also for those dried in growth medium + 13.5% sucrose ($\xi = 0.049 \pm 0.006$ cm^{-1}/°C). This graph revealed that while the initial hyperosmotic shock (rapid exposure to 13.5% sucrose) altered the membrane integrity (indicated by the lower initial viability), remaining cells retained the ability to withstand slow dehydration, so long as membrane phase transition temperatures remained below a key threshold.

3.3.3 THERMOTROPIC AND LYOTROPIC PHASE TRANSITIONS

Based on our results on membrane phase transition and lipid order, we investigated the possibility of improving cell viability during dehydration by altering the drying and rehydration conditions. Previous results indicated that during drying at 30°C the cell membrane underwent lyotropic phase change from l.c. to gel phase. Similarly, upon re-hydration, the membrane experienced a lyotropic phase change, this time transitioning from gel to l.c. phase. In order to explore the effect of lyotropic phase change, *G. sulfurreducens* samples were dried at different temperatures (30 or 5°C). The cells dried at 30°C for 45 minutes experienced lyotropic phase transition as indicated by their $T_m >$ 30°C (Figure 3.2B). However, the cells dried at 5°C experienced a thermotropic phase change from l.c. to gel phase during cooling (prior to dehydration). Therefore, when dried, these cells were already in the gel phase and lyotropic phase transition was completely eliminated in the 5°C group.

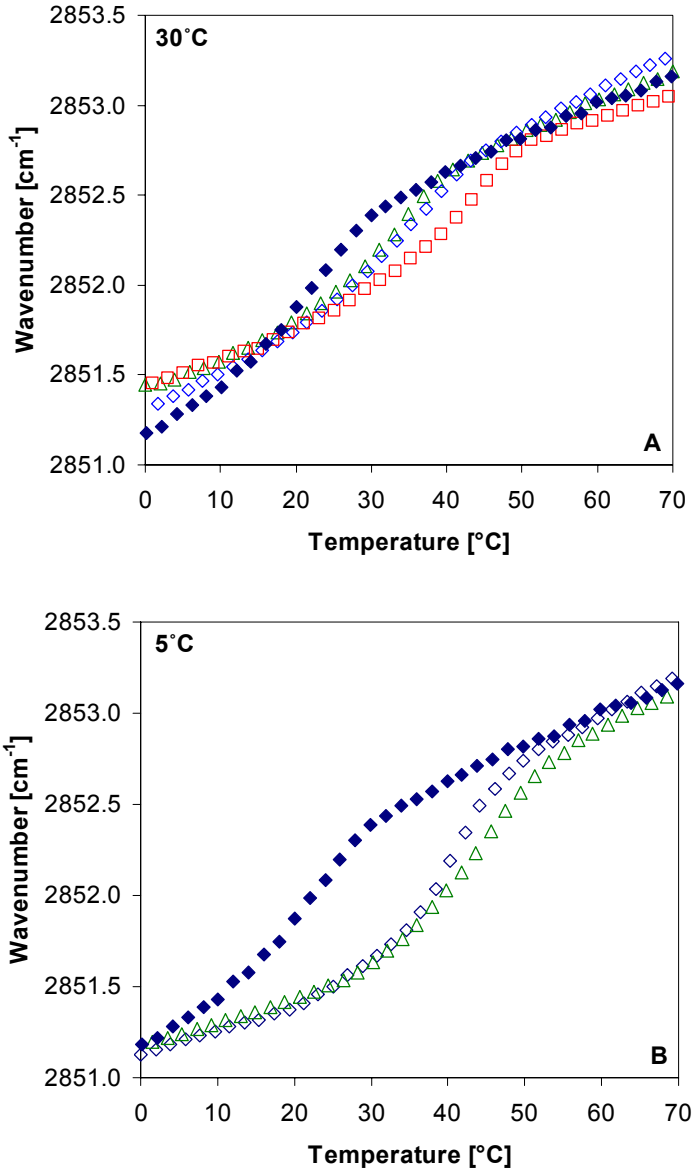

Figure 3.5 Comparison of the membrane phase behavior of *G. sulfurreducens* dried in growth medium containing different concentrations of sucrose. (A) Change in νCH_2 maxima with temperature for *G. sulfurreducens* in growth medium (hydrated control) (◆), dried in growth medium (◇), dried in growth medium + 6.75% w/w sucrose (△) and dried in growth medium + 13.5% w/w sucrose (□) (samples were dried at 30°C for 45 minutes). (B) Change in νCH_2 maxima with temperature for *G. sulfurreducens* in growth medium (hydrated control) (◆), dried in growth medium (◇) and dried in growth medium + 6.75% w/w sucrose (△) (samples were dried at 5°C for 45 minutes). (Representative data sets)

3.3.4 MEMBRANE STRUCTURE CHANGE WITH LYOTROPIC PHASE CHANGE (T_D = 30°C GROUP)

Temperature ramp FTIR spectroscopy analysis revealed that T_m values for the cells dried in the growth medium (0% sucrose) (T_m = 35 ± 1.5 °C) and growth medium + 6.75% sucrose (T_m = 35 ± 4 °C) were similar while those dried in growth medium + 13.5% sucrose were higher (T_m = 40 ± 1 °C) (Figure 3.5). All dried samples had higher wavenumber values at 0°C as compared to the hydrated *G. sulfurreducens* sample, indicating reduced membrane lipid order at this temperature [230], especially for the cells dried in the presence of sucrose, reflecting a change in the membrane structure (see Discussion). A comparison of lipid order at the l.c. state at higher temperatures for growth medium (0% sucrose) and growth medium + 6.75% sucrose was not performed due to increased drying at the higher temperatures. The phase transition cooperativities (ξ) of the dried samples were not significantly different.

3.3.5 MEMBRANE STRUCTURE CHANGE WITH THERMOTROPIC PHASE CHANGE (T_D=5°C GROUP)

When cells were dried at 5°C (preventing a lyotropic phase change during drying), *G. sulfurreducens* samples dried in growth medium and growth medium + 6.75% sucrose solutions also had high average T_m values. T_m values for the cells dried in growth medium (0% sucrose) (T_m = 40 ± 6°C) and growth medium + 6.75% sucrose (T_m = 42 ± 3.5 °C) were similar. Unlike the cells dried at 30°C, wavenumber values at 0°C were similar to hydrated *G. sulfurreducens* cells indicating that membrane lipid order did not

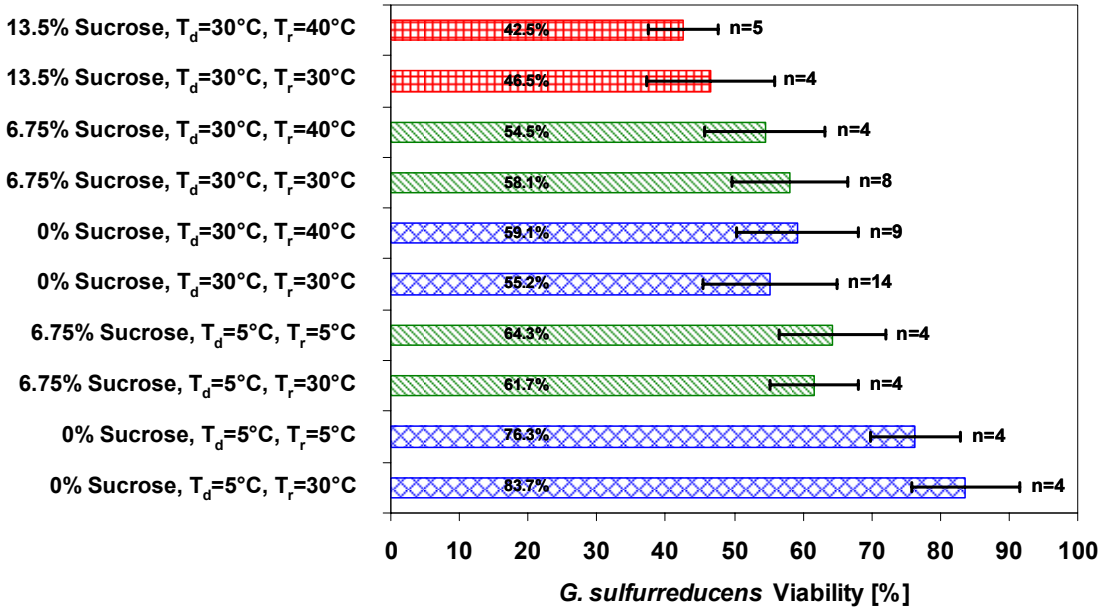

Figure 3.6 Post re-hydration viability of *G. sulfurreducens* dried for 45 min at 65% RH. (T_d: drying temperature, T_r : re-hydration temperature) (n>3)

decrease during dehydration at 5°C. Membrane phase transition cooperativity of *G. sulfurreducens* dried in growth medium ($\xi = 0.077 \pm 0.005$ cm^{-1}/°C) was greater than that of *G. sulfurreducens* dried in growth medium containing 6.75% sucrose ($\xi = 0.059 \pm 0.001$ cm^{-1}/°C) (Table 3.2). Cooperativity of *G. sulfurreducens* dried in growth medium + 6.75% sucrose at 5°C was slightly higher than that of *G. sulfurreducens* dried in growth medium at 30°C (Table 3.2). These results showed that dehydration at 5°C created significantly different conditions in the cell membranes.

3.3.6 Effects of thermotropic and lyotropic membrane phase transitions on post-rehydration viability

Effects of various drying and rehydration conditions on post-rehydration viability of *G. sulfurreducens* were also examined (Figure 3.6). *G. sulfurreducens* suspended in growth medium (containing up to 13.5% sucrose) were dried at 5 or 30°C, and re-hydrated at 5, 30 or 40°C. These conditions were chosen based on FTIR spectroscopy and viability data shown above to investigate the combined effects of sucrose and thermotropic and lyotropic phase transitions on the viability *G. sulfurreducens* following dehydration and rehydration.

3.3.7 Effect of the lyotropic phase change during re-hydration on G. sulfurreducens viability

Viability measurements were performed with *G. sulfurreducens* samples dried for 45 minutes in the growth medium containing 0, 6.75, and 13.5% sucrose at T_d = 30°C and 65% RH. Re-hydration was performed at T_r = 30°C to ensure that *G. sulfurreducens* underwent lyotropic membrane phase transition during re-hydration, or at T_r = 5°C or T_r = 40°C to eliminate lyotropic phase transition. In the preliminary experiments, we

Table 3.2 Effect of Drying Conditions on Membrane Phase Transition Cooperativity (units= $cm^{-1}°C^{-1}$)

Growth Medium (Control Group)	**Growth Medium (Td=30°C group)**	**Growth Medium (Td=5°C group)**	**Growth Medium+6.75% w/w sucrose (Td=5°C group)**
0.058 ± 0.001	0.055 ± 0.002	0.077 ± 0.005	0.059 ± 0.001

verified that *G. sulfurreducens* (which has maximum growth rate at 35°C) could survive incubation at 40°C without loss of viability (data not shown).

Viability of *G. sulfurreducens* dried at T_d = 30°C in the growth medium (0% sucrose) for T_r = 30°C and T_r = 40°C (Figure 3.6) were not significantly different (P = 0.159). Similar results, showing a lack of significant change in viability due to re-hydration at a higher temperature, were obtained for the 6.75% sucrose (P = 0.262) and the 13.5% sucrose (P = 0.242) samples (Figure 3.6). The lack of a significant improvement or protective effect due to re-hydration at temperatures higher than T_m indicated that a lyotropic phase transition during re-hydration did not affect viability and the reduction in viability was actually due to lyotropic phase transition during dehydration. This was also confirmed with low temperature experiments presented below.

For T_r = 30°C, viability of *G. sulfurreducens* dried at T_d = 30°C in the growth medium (0% sucrose) and in the growth medium containing 6.75% sucrose were not significantly different for (P = 0.1540), which was similar to the previous results obtained with rapid hyperosmotic shock (Table 3.1). At T_d = 30°C viability of the cells dried in the growth medium containing 13.5% sucrose was significantly lower (P = 0.0316) than those dried in the growth medium containing 6.75%, also similar to what was observed in hyperosmotic shock experiments. For T_r = 40°C, viability of the cells dried at T_d = 30°C in the growth medium (0% sucrose) and in the growth medium containing 6.75% sucrose were not significantly different (P = 0.356). However, viability at both conditions were significantly higher than that obtained in the growth medium containing 13.5% sucrose (P=0.001 and P=0.029, respectively).

3.3.8 EFFECT OF THE LYOTROPIC PHASE CHANGE DURING DEHYDRATION ON G. SULFURREDUCENS VIABILITY

In order to eliminate lyotropic phase transition during dehydration, cells were initially cooled (without drying) down to 5°C, where they were isothermally dried. Re-hydration was performed either at T_r = 5 or 30°C (Figure 3.6). Viability of *G. sulfurreducens* dried in growth medium at 5°C was significantly higher than all of the other conditions examined ($P \leq 0.001$). This demonstrated the pronounced effect of avoiding lyotropic phase transition during dehydration. However, for T_d = 5°C there was a significant decrease in viability for the growth medium + 6.75% sucrose group ($P \leqq 0.029$) when compared to *G. sulfurreducens* dried in growth medium (Figure 5), showing that higher osmotic stress was detrimental even when the membrane was already in the gel phase. There was no statistically significant difference between the T_r = 5°C and T_r = 30°C groups at T_d = 5°C for either the growth medium ($P = 0.0986$) or growth medium + 6.75% sucrose ($P = 0.309$) solutions, once again proving that membrane phase change was not detrimental for *G. sulfurreducens* during re-hydration.

3.4 DISCUSSION

In certain biotechnological applications bacteria need to be stably encapsulated in a matrix and preserved for transportation and storage. During encapsulation cells are often exposed to high osmotic stresses due to polymerization of the matrix material and the presence of carbohydrates in the surrounding medium. Carbohydrates serve two purposes; they are used to adjust the porosity of the matrix and to protect the bacteria against freezing and dehydration damage. In this study, we performed spectroscopic

analysis to understand the mechanisms of hyperosmotic damage to *G. sulfurreducens* in order to develop methodologies that maximize viability during, *a)* encapsulation in bioreactive coatings, and *b)* preservation of the encapsulated bacteria in a dehydrated state. Knowing that the cell membrane is a primary site of osmotic injury [39, 49], we have focused our attention to the osmotically-induced alterations in the cell membrane. Temperature ramp FTIR spectroscopy analysis was used to provide a measure of the structure, lipid order, and the thermodynamic transitions of the membrane. We have conclusively shown that the information collected through FTIR analysis could be used to design techniques to maximize the viability of the bacteria during encapsulation and preservation.

We have conducted controlled dehydration and hyperosmotic shock experiments with *G. sulfurreducens.* With increasing concentration of sucrose in the extracellular solution, viability of the bacteria decreased. Extracellular sucrose altered the bacteria membrane structure, however, it neither inhibited the increase of T_m nor protected the bacteria against dehydration. It is well known that to protect the membrane structure sugars should be present on both sides of the cell membrane [231]. Hence, the lack of dehydration protection by sucrose was not surprising. In fact, the presence of extracellular sucrose generated additional hyperosmotic stress, which correlated to a decrease in viability.

The high water affinity of sucrose [232] created a competition for water between the sucrose and the membrane lipids. This high affinity of sucrose for water can be seen by comparing the amount of water per cell and the T_m for *G. sulfurreducens* dried in 0% and

13.5% sucrose solutions for 45 minutes (T_d = 30°C, RH = 65%). Using spectroscopic analysis, it was found that the water content in the 13.5% sucrose samples (Viability: 46.5 ± 9.3 %) was on average 80% more than that in the 0% sucrose samples (Viability: 55.2 ± 9.7 %). The higher T_m for the 13.5% sucrose sample demonstrated that the extra water was not available to the membrane. The direct correlation between *G. sulfurreducens* viability and its membrane phase transition temperature (Figure 3) also showed the determining factor is the availability of the water in the sample, not its quantity. This also shows that when comparing samples, thermogravimetric measurement of sample water content (a commonly utilized method) can be misleading since water content does not give an indication of the hydration level of the membrane.

We have quantified the hyperosmotic stress-induced structural changes in the cellular membrane by the change in the νCH_2 band peak location, which corresponds to the order of the lipid acyl chain. For example, due to higher concentration of sucrose in the medium, membrane lipid order in the l.c. phase of *G. sulfurreducens* suspended in 13.5% and 27% sucrose solutions (Figure 3.1) was greater than that in the 0% or 6.75% sucrose solutions. On the other hand, the large decrease in lipid order in the gel phase for *G. sulfurreducens* in the 27% sucrose solution (Figure 3.1) can be attributed to the destabilization of the membrane such as membrane rupture as suggested by Beney et al. [53]. Changes reflected by increased fluidity, which encompasses decreased membrane lipid order, have also been observed in *Bradyrhizobium japonicum* (also a gram-negative bacteria) when it was subjected to increased osmotic pressure [53]. In addition to decreased lipid order of the membrane in the gel phase, decreased cooperativity of the

phase transition and increase in T_m were also observed during hyperosmotic shock and slow dehydration.

In general, the effect of hyperosmotic shock on the membrane was marked by changes in the lipid order and phase transition cooperativity (Figure 3.1), whereas the effect of slow dehydration was reflected by an increase in T_m and decrease in cooperativity (Figure 3.2b). The direct correlation between T_m and viability (Figure 3.4) obtained during slow dehydration shows that decreasing water activity is directly responsible for the damage to the cell. The viability of *G. sulfurreducens* dried in the 13.5% sucrose solution (T_d = 30°C; RH = 65%) is the same as that in the 27% sucrose solution. However, the pronounced difference in the membrane structure and phase behavior between the two samples illustrates the difference between hyperosmotic shock and slow dehydration. The loss of phase transition cooperativity and low gel phase lipid order in *G. sulfurreducens* in the 27% sucrose sample may indicate the lack of stabilizing interactions among neighboring lipids. These characteristics may be attributed to membrane dissolution and disruption during hyperosmotic shock, whereas the small changes in cooperativity and lipid order observed in the slow dehydrated samples may indicate more subtle structural changes such as membrane fusion and vesiculation. These results point to the existence of two different mechanisms of membrane damage for hyperosmotic shock and slow dehydration.

Exposing *G. sulfurreducens* to slow dehydration stress in the absence of sucrose at temperatures (T_d = 5°C) lower than the membrane phase transition temperature (i.e. eliminating lyotropic phase transition during dehydration) had a significant beneficial

effect on the post-rehydration viability (Figure 3.6). It also revealed a direct correlation between the membrane structure (indicated by lipid order and cooperativity) and viability. *G. sulfurreducens* dried under these conditions had gel phase membrane lipid order similar to that of the hydrated control sample (Figure 3.5B) and also had significantly increased phase transition cooperativity as compared to the hydrated control sample (Table 3.2) (P=0.016).

The higher phase transition cooperativity of growth medium samples dried at T_d = 5°C (Figure 3.5B, Table 3.2) can be explained by stabilization of the gel phase due to higher gel-gel lipid interaction energies [200]. Cooperativity of a thermotropic gel to l.c. phase transition for a lipid bilayer is dependent on the magnitude of nearest neighbor interaction energy, ε, [200] between the lipid molecules in the gel and l.c. phases given by:

$$\varepsilon = \left| 2\varepsilon_{l.c.-gel} - \varepsilon_{gel-gel} - \varepsilon_{l.c.-l.c.} \right|. \qquad (3.1)$$

An increase in the absolute magnitude of ε corresponds to an increase in cooperativity of a thermotropic gel to l.c. phase transition [200]. An increase in ε, and therefore cooperativity, results from an increase in the stability of the gel-gel region interactions as might be expected in the dried state. Therefore, with increasing dehydration, i.e. higher T_m values, an increase in cooperativity is expected for a membrane that retained its original overall structure and organization. Therefore, the higher cooperativity values measured for growth medium samples (T_d = 5°C) indicated that the cell membranes experienced minimal destructive changes when dried under these conditions. The reduction of destructive changes, such as fusion and vesiculation, may be due to the

membrane bilayer being energetically less susceptible to fusion events in the gel phase [233].

Even though the damage associated with lyotropic phase change during dehydration could be minimized by drying *G. sulfurreducens* at $T_d = 5^oC$, the additional stress due to presence of extracellular sucrose can still be detrimental. Even the presence of 6.75% sucrose caused a significant decrease in viability (Figure 3.6). This was reflected by the significantly lower cooperativity of 6.75% sucrose samples (T_d = 5°C) (P=0.017) as compared to growth medium samples (T_d = 5°C) (Table 3.2). *G. sulfurreducens* samples slowly dehydrated in 0% and 13.5% sucrose (T_d = 30°C) also did not exhibit increased cooperativity with increased T_m (T_m > 32°C) due to already existing membrane damage with progressive dehydration (i.e. the increase in membrane damage with T_m beyond a certain threshold offsets the propensity for increased cooperativity.

The results presented highlight there are two main factors of importance during dehydration of *G. sulfurreducens*. The first factor is the existence of two distinct mechanisms of membrane damage dependent on the rate of osmotic stress (Figure 3.7). The second factor is that the lyotropic phase transition during drying enhances membrane damage. By considering these two factors it may be possible to design an appropriate procedure to produce coatings with a high percentage of viable *G. sulfurreducens* bacteria.

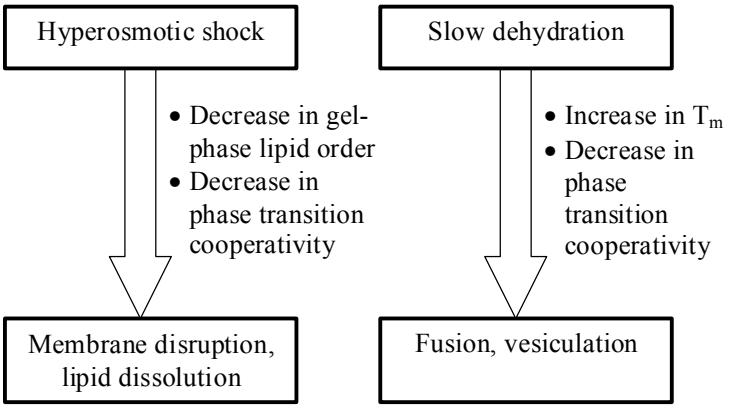

Figure 3.7 Schematic showing the two modes of osmotic stress and the respective suggested mechanisms of membrane damage (associated FTIR spectroscopy measurements are also shown).

3.5 CONCLUSION

We determined that *G. sulfurreducens* viability decreased with increasing sucrose concentration in the medium showing that extracellular sucrose acted only as an osmolyte and did not protect *G. sulfurreducens* against the dehydration stress. Depending on the rate of application of the hyperosmotic stress, we identified two different membrane damage mechanisms to be responsible for viability loss in *G. sulfurreducens*. We have also established that the resistance of *G. sulfurreducens* to hyperosmotic stress could be improved when lyotropic phase transition was avoided during dehydration by desiccating the bacteria at a temperature lower than the membrane phase transition temperature. We have therefore distinguished the effects of the lyotropic and thermotropic phase transitions of the cell membrane on the hyperosmotic stress survival of *G. sulfurreducens*.

CHAPTER 4: HYPEROSMOTIC STRESS OF HUMAN FORESKIN FIBROBLASTS

4.1 SUMMARY

The objective of this study was to investigate how an increase in osmotic pressure affects the cell membrane and the underlying actin cytoskeleton in a model mammalian cell, human foreskin fibroblast (HFF). Cells were subjected to an isothermal osmotic stress cycle going from isotonic conditions to hyperosmotic conditions. In the first part of this study, osmotic stress was imposed on the cell using sorbitol (and NaCl in select experiments). However, observations from these experiments strongly indicated that solute uptake occurred. In order to investigate the effect of hyperosmotic stress without solute uptake, polyethylene glycol (PEG 600) was used in the second part of this chapter.

Transmitted light, Infrared spectroscopy, scanning electron microscopy and fluorescence- and cryo- microscopy were used to investigate the changes in the cell membrane and the actin cytoskeleton. Our data suggest that the cells experienced a decrease in the availability of membrane material (i.e. a decrease in the available membrane reservoir) thereby reducing the cell's ability to expand during return to isotonic conditions. Our data also suggests that solute uptake can occur during hyperosmotic stress, which could further exacerbate the damage due to an insufficient membrane reservoir. We also observed that hyperosmotic stress was responsible for the formation of membrane defects, which increased with osmotic pressure and the time of exposure. Changes in the actin cytoskeleton were also observed with hyperomostic stress. These changes were

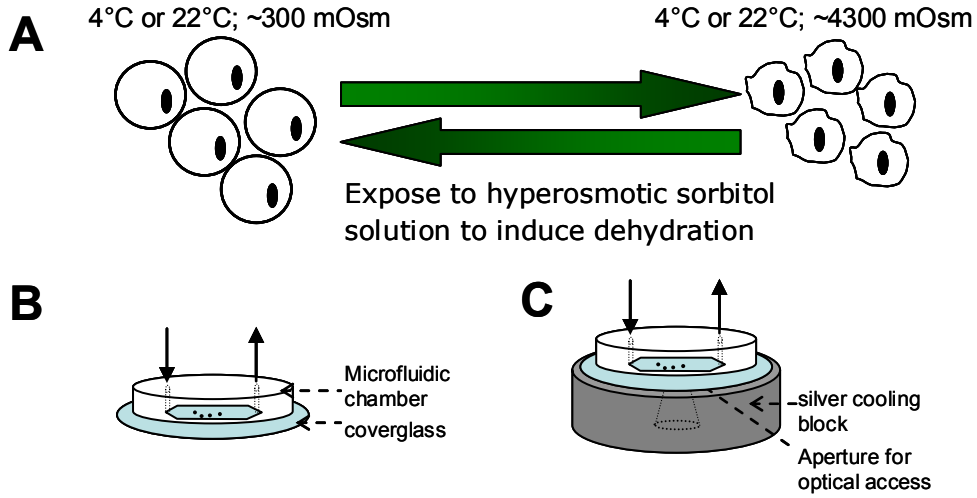

Figure 4.1 Schematic representations of: (a) the osmotic stress experiments conducted; (b) Microfluidic flow-through device used in the osmotic stress experiments. The device was made from poly(dimethylsiloxane) (PDMS) made from an SU-8 mold cast on a silicon wafer. The inner chamber height was 70μm. Solutions were exchanged using a syringe pump;(c) Linkam cryostage block on which samples were cooled

dependent on the temperature at which the hyperosmotic stress was applied. Membrane morphology was altered with the application of hyperosmotic stress and the temperature at which the stress was applied. It was observed that altering the mechanical properties of the cortical cytoskeleton using a Rho kinase inhibitor led to a change in membrane morphology during hyperosmotic conditions and an increae in viability.

4.2 PART I – HYPEROSMOTIC STRESS EXPOSURE WITH SORBITOL OR NACL

In this part of the study, we subjected a mammalian cell, human foreskin fibroblast (HFF), to hyperosmotic stress using up to 4M sorbitol solutions or 4.5M NaCl solutions in select experiments.

Table 4.1 Cell response and measurements

Cell response	***Measurement Method***
Membrane integrity	Propidium iodide uptake
Cell morphology	Phase contrast microscopy
Change in actin cytoskeleton	GFP-actin; Immunofluorescence
Membrane structure	FTIR spectroscopy

4.2.1 MATERIALS AND METHODS

The objective of this study is to elucidate the role of the membrane-cytoskeleton complex on the osmotic response of mammalian cells. To this end, an isothermal osmotic challenge was imposed on the selected model cells (Figure 4.1). Cellular response was determined using the following methods: (1) basic microscopic analysis of the changes in cell morphology (including volume change and blebbing); (2) quantification of the level of actin polymerization (using the two different techniques described below); (3) measurement of the structural changes to the membrane using Fourier Transform Infrared (FTIR) spectroscopy. The methods that were used to quantify the specific cellular parameters are summarized in Table 4.1.

4.2.1.1 Cell culture

Human foreskin fibroblasts, HFFs, (ATCC, Rockville, MD, USA; ATCC catalog #: SCRC-1041) were incubated at 37°C in a 5% CO_2 atmosphere in a growth media

comprised of Dulbecco's Modified Eagle Medium (DMEM) enriched with 15% FBS and 10 ml/l penicillin-streptomycin. Upon reaching 80-90% confluency, cells were trypsinized (0.05% Trypsin + 0.53 mM EDTA) and centrifuged at ~150g for 8 minutes. Depending on the specific experiment to be conducted, the cell pellet was resuspended in the experimental solution (based on either growth media or phosphate buffered saline solution (PBS)).

4.2.1.2 Isothermal osmotic stress experiments

HFFs were incubated on a glass coverslip (not coated) enclosed in a microfluidic PDMS (Polydimethylsiloxane) chamber (Figure 4.1b) for 30 minutes at 37°C to promote cell attachment without spreading. The extracellular solution around the cells was altered by replacing the isotonic solution (~300 mOsm) with different hypertonic solutions containing sorbitol up to 4 M in concentration (Figure 4.1a). Sorbitol was chosen as the osmotic agent due to its high solubility in water (70% wt.) and its established use in dehydration studies [133, 168]. The range of osmotic conditions tested mimics those encountered during freezing (equivalent osmotic stress to extracellular medium freezing at a temperature in the range of -0.5°C to -8°C). After exposure to hyperosmotic stress, HFFs were returned back to the isotonic environment for subsequent analysis (Figure 4.1a). Viability was assessed using propidium iodide (PI) uptake 10 minutes after return to isotonic conditions.

In order to determine whether stiffness of the membrane-cytoskeleton system, henceforth referred to as 'cortical tension', had any role in the cells' response to osmotic stress, the cortical tension was decreased by depolymerizing actin or inhibiting myosin activity [59].

‘Cortical tension’ specifically refers to the contractile force/ tension (due to the myosin motor proteins) in the cell cortex that increases the pressure inside a cell [234]. Actin depolymerization was accomplished using CD [235] (CD at a concentration of 10 μM). Myosin activity was inhibited either directly using blebbistatin [236] (50 μM) or indirectly using a Rho kinase inhibitor, Y27632 (10 μM) [237] (all chemicals were obtained from Sigma-Aldrich). As with the previous studies, cells were allowed to attach to the glass cover slip by incubation for 30 minutes (without spreading) at 37°C. Subsequently, they were incubated for 30 minutes at room temperature in either CD (10 μM) or blebbistatin (50 μM) or Y27632 (10 μM). After incubation, the cells were subjected to osmotic stresses as described previously.

4.2.1.3 Measuring changes in actin cytoskeleton

Two methods were used to monitor changes in the actin cytoskeleton with osmotic incursions: (1) HFFs were transfected with green fluorescent protein (GFP) actin plasmid and the actin cytoskeleton was visualized via using conventional fluorescence microscopy; (2) Direct measurements of the amount of polymerized actin were also made by fluorescent staining.

(1) In experiments investigating changes in the actin cytoskeleton of rounded cells GFP-transfected cells were imaged before and after the treatment. For osmotic stress experiments, GFP-transfected cells were imaged (exposure time of 3.5 s) using a Nikon TE 200 microscope equipped with a Spot Diagnostic camera (Diagnostic Instruments Inc., MI).

(2) For fluorescent staining of polymerized actin, rhodamine-phalloidin (Invitrogen Corporation) was used to stain actin filaments. In these experiments, cells were attached to polylysine coated glass. Prior to staining, cells were fixed using 3.75% formaldehyde for 10 minutes, permeabilized by exposure to 0.1% TritonX-100 for 5 minutes and later incubated with 1% BSA for 15 minutes (cells were washed twice with 1X PBS between steps). Actin filaments were then stained by incubation with 1μg/ml rhodamine phalloidin for 20 minutes at room temperature. The microscope slide was washed with 1X PBS and then dried and mounted for imaging. Images were collected on a Nikon TE 200 (Nikon Corporation, Tokyo, Japan) inverted microscope and the amount of polymerized actin was quantified by fluorescence intensity using the ImageJ software (NIH, USA).

4.2.1.4 Characterization of the membrane structure using FTIR

Conformation of membrane lipids was characterized using FTIR spectroscopy. HFFs sandwiched between two CaF_2 windows that were separated by a 6-μm Mylar spacer (Thermo Electron North America Inc., Madison, WI, USA). The periphery of the sample was sealed using vacuum grease applied to both sides of the spacer. Solutions were exchanged using a syringe pump. IR spectrum was obtained using a Thermo-Nicollet Continuμm IR microscope equipped with a MCT detector connected to a Thermo-Nicollet 6700 FTIR Spectroscope (Thermo Electron Corporation LLC, Waltham, MA). An average of 128 scans were taken per spectrum. Spectral analysis was carried out using Omnic software (Thermo-Nicolet, Madison, WI, USA). Lipid conformational order was

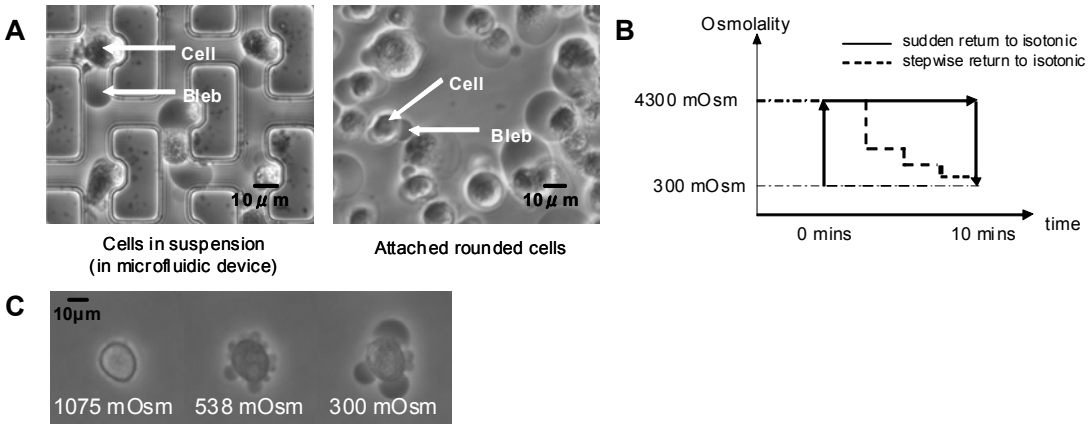

Figure 4.2 Phase contrast microscopy images of (a) cells in suspension using a microfluidic device [238], and attached rounded cells that were exposed to rapid hyperosmotic shock. (b) The osmotic stress history for the cells in (a) and (c) (dashed line). (c) Attached, rounded cells that experienced stepwise decrease in osmolality back to isotonic.

monitored by measuring the peak location of the υ-CH_2 (symmetric stretching) band located at approximately 2850 cm^{-1}.

4.3 RESULTS

The first phase of the experimentation conducted involved exposing cells to a step change in the osmotic environment from isotonic (~300 mOsm 1X PBS) to hyperosmotic (~4300 mOsm 1X PBS + 4M sorbitol) for 10 minutes, and then back to isotonic. This particular change in extracellular osmolality represents the step change that would be experienced by the cell during extracellular ice nucleation at -8°C. These tests were performed isothermally at room temperature using attached rounded HFFs and also with HFFs in suspension.

It was observed that during the 10 minutes at hyperosmotic conditions cells would exhibit a small but significant ($p > 0.05$) increase in volume from 32% of the original cell volume at 0 minutes to 44% of the original volume at 10 minutes. For both attached rounded cells and suspended cells, the return to isotonic conditions resulted in the formation of very large blebs (Figure 4.2a). The presence of blebs indicated that there was either detachment of the membrane from the underlying cytoskeleton or rupture of the cytoskeleton [56]. The fact that the cells in both types of experiments resulted in similar bleb formation demonstrated that the attachment to the glass substrate did not affect the blebbing behavior

In the case of attached rounded cells 73 ± 23% (n=4 experiments) of cells formed blebs. Since an osmotic intervention such as the one outlined here was expected to result in loss of viability, the membrane integrity of the cells was measured (post-stress) using propidium iodine (PI). Cells that stained negative for PI (PI-) were considered alive and cells that stained positive for PI (PI+) were considered dead. It was observed that the blebbing cells fell into both PI- and PI+ populations. Cells whose blebs did not burst during return to isotonic conditions were generally PI-. It is noteworthy that blebbing was observed irrespective of whether the cells were returned back to isotonic conditions in a stepwise manner or rapidly in a single step. Cells that were returned back to isotonic conditions in a stepwise manner (4300→2150→1075→538→300 mOsm with ~2 minutes of hold time between steps) developed small blebs at 538 mOsm, which increased in size upon further decrease in the osmotic stress down to 300 mOsm (isotonic conditions) (Figure 4.2c). Interestingly, hyperosmotic stressing to 2150 mOsm or lower

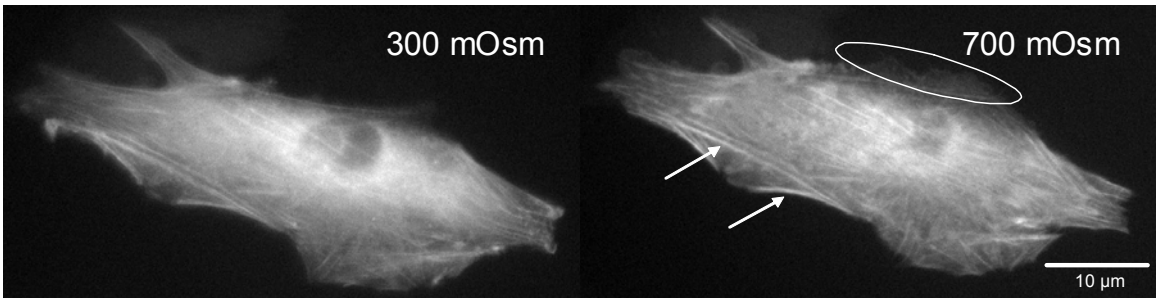

Figure 4.3 GFP-actin fluorescence microscopy with attached spread cells exposed to hyperosmotic stress. Arrows indicate the increased definition of the stress fibers. The increase in lamllelipodia is indicated by the circle.

did not result in the formation of blebs. This suggested that the lower threshold for a change in the cytoskeleton-membrane interaction that resulted in blebbing lay between 2150 mOsm and 4300 mOsm. It was observed that cells exposed to lower hyperosmotic stresses (2150 mOsm or lower) did not exhibit any observable volume recovery unlike the cells that were exposed to 4300 mOsm for 10 minutes.

Bleb growth is driven by intracellular pressure that can be either hydrostatic [234] or osmotic [239] pressure. Increase in hydrostatic pressure can be induced by an increase in the cortical tension thereby favoring bleb formation and growth [59, 234]. Following up on these findings, the next phase of experimentation involved assessing the influence of the decrease in cortical tension on the osmotic response of the cells. HFFs were incubated in CD (10 μM), blebbistatin (50 μM) or Y27632 (10 μM) to reduce cortical tension. The treated cells were subjected to the same osmotic stress history described above (b solid line) and the bleb formation was measured. With all three cortical actin modification treatments the formation of blebs upon return to isotonic conditions was observed in over 90% of the population. These results showed that bleb growth was not due to an increase

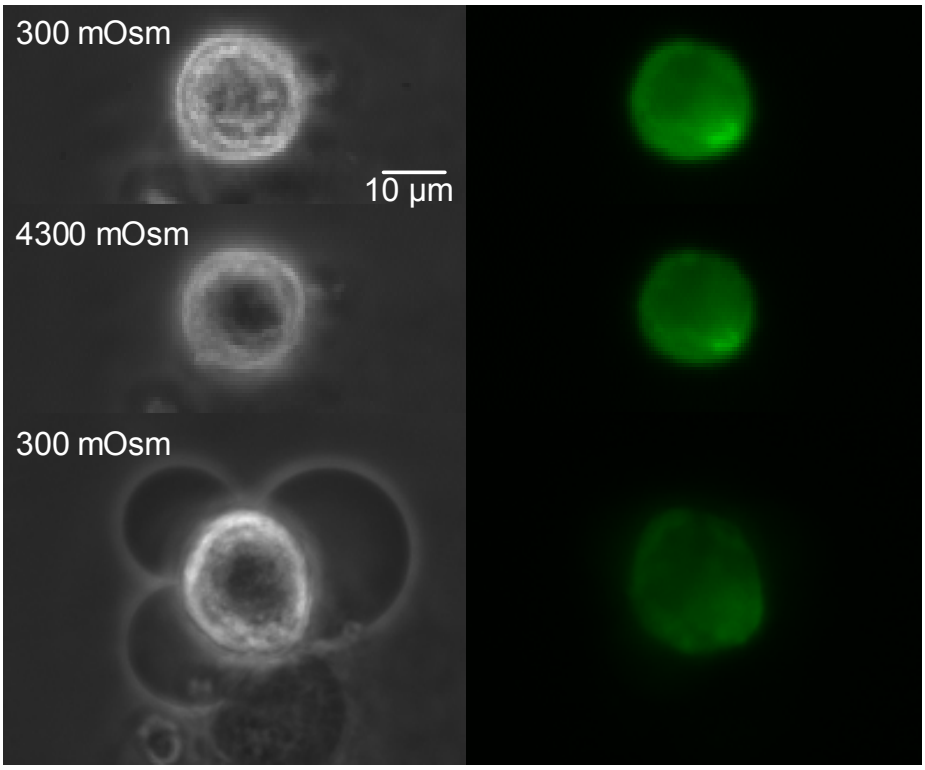

Figure 4.4 Transmitted light (left column) and GFP-actin fluorescence (right column) microscopy with attached spherical cells exposed to stepwise hyperosmotic stress (the cell was exposed to 4300 mOsm for 10 minutes).

in tension in cell cortex since reducing this tension did not affect blebbing. This result points towards an increase in intracellular osmotic pressure being responsible for bleb growth.

Bleb formation was, however, markedly influenced by temperature such that a reduced incidence of blebbing was observed when the same experiments were repeated at a lower temperature. Specifically, no cell exhibited blebbing when the cells were exposed to the same osmotic stress history (Figure 4.2b) at 4°C (300 mOsm followed by exposure to 4300 mOsm and return to 300 mOsm) in contrast to 73 ± 23% at room temperature. At 4°C the percentage of PI^+ cells was greater (69 ± 4%; n=4 experiments) than that at room

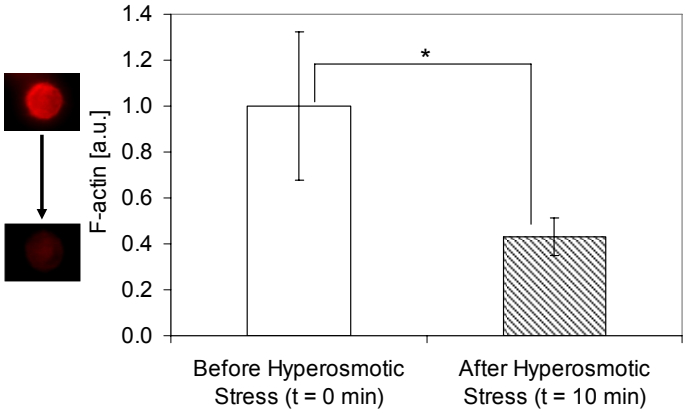

Figure 4.5 F-actin content at isotonic conditions as determined by rhodamine-phalloidin fluorescence intensity for attached spherical cells before and after stepwise hyperosmotic stress exposure. Fixation was performed ~5 minutes after start of rehydration. Cells were on poly-lysine coated glass. Statistical differences ($p < 0.05$) are marked with *. $n > 30$ cells

temperature (35 ± 13%). It was also observed that some of the cells that were subjected to hyperosmotic shock at 4°C were darkened after return to isotonic conditions. These dark cells typically belonged to the PI^+ population.

Experiments with HFFs expressing GFP-actin revealed that remodeling of the cytoskeleton in attached spread cells depended on the level of osmotic stress. With an increase in the osmotic stress from 300 mOsm (isotonic media) to 500 mOsm (media + 0.2M sorbitol), fibroblasts demonstrated an increase in 'ruffling' or projection of lamellipodia (Figure 4.3). Increase in osmotic stress was also accompanied by cytoskeletal remodeling, which resulted in the formation of more defined actin stress fibers (Figure 4.3). The increase in lamellipodial rate is likely due to the decrease in membrane tension [240] demonstrating the interdependency of the actin cytoskeleton and the membrane responses. It is thought that a decrease in membrane tension allows

addition of actin monomers to filaments thereby increasing lamellipodial extension rate [240]. However, at higher osmotic stresses (> 700 mOsm: media + 0.4 M sorbitol) this behavior diminished and there was almost no 'ruffling' activity.

Hyperosmotic shock (following the osmotic stress course shown in Figure 4.2b indicated by the solid line) was also applied to rounded, attached GFP-actin transfected cells in order to observe the membrane in relation to the underlying cytoskeleton. Comparison of the brightfield and fluorescence images of GFP-transfected cells revealed that the membrane dissociated from the underlying cytoskeleton as the blebs did not contain an underlying actin cytoskeleton (Figure 4.4). Changes in the actin cytoskeleton in response to hyperosmotic shock at room temperature was measured by F-actin staining (with rhodamine-phalloidin dye) of the attached, rounded cells. Analysis of rhodamine-phalloidin stained cells (non GFP-transfected) that underwent the same osmotic stress revealed that there was significant reduction in the amount of filamentous actin after a return to isotonic conditions (Figure 4.5). This is likely due to the resulting lower concentration of actin monomers due to cell expansion.

In order to see if the observed blebbing effect was limited to sorbitol only, a limited set

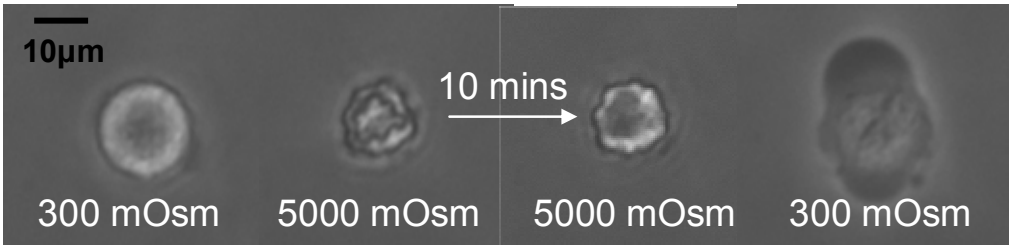

Figure 4.6 Transmitted light microscopy of a cell subject to an osmotic stress cycle using 2.5 M NaCl

of experiments were also conducted using NaCl as a water activity suppressor. 2.5M NaCl (5000 mOsm $\rightarrow \Pi$ = 12.3 MPa) was used following the same osmotic general path at in (Figure 4.2b). It was observed that during the 10 minutes exposure to the sodium chloride that cells lost their crenated appearance indicating possible solute uptake (Figure 4.6). As with sorbitol, upon returning to isotonic conditions nearly all cells blebbed due to osmotically increased hydrostatic pressure in the cell. Almost all cells (93.1 ± 0.9 %; n = 3) were PI^- upon return to isotonic conditions at room temperature. At 4°C the population of PI^- cells decreased significantly (62 ± 9 %; n = 3), again demonstrating that osmotic stress at low temperatures is detrimental to HFFs. The distinct difference between NaCl and sorbitol osmotic stress experiments in terms of viability at room temperature (93% versus 65% respectively) despite the sorbitol experiments having a slight lower osmolality may be due to a solute specific effect. NaCl is known to interact directly with the lipid headgroups [241, 242] which causes an increase in the mechanical stability of both artificial and real membranes [243]. This increase in mechanical stability may be responsible for the observed difference in viability between NaCl and sorbitol experiments. The high viability observed for cells in 2.5M NaCl solutions after 10 minutes has also been observed with human prostatic adenocarcinoma cells which did not show any significant drop in viability under similar conditions [55].

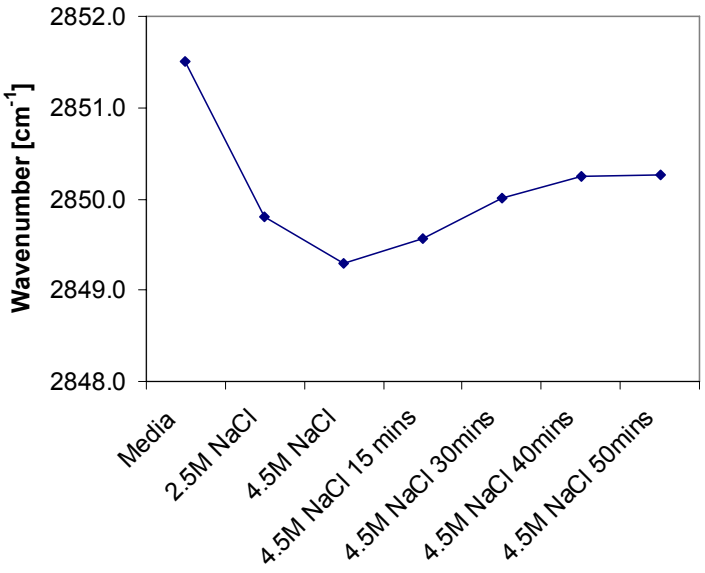

Figure 4.7 Change in νCH_2 band maxima for cells undergoing osmotic stress with exposure to NaCl solutions (n=1 experiment).

Change in the cell membrane state during osmotic stress with NaCl was investigated using FTIR spectroscopy. Changes in the membrane lipid conformational disorder were determined by monitoring the change in the location of the lipid acyl chain νCH_2 stretching band located at approximately 2850 cm^{-1}. Due to the location of the band a similar analysis could not be performed with sorbitol solutions. FTIR spectroscopy measurements were made of cells in 2.5M NaCl and compared to those in media. It was found that there was a decrease in νCH_2 values from 2851.25 ± 0.14 cm^{-1} (n=3) to 2849.82 ± 0.03 cm^{-1} (n=2). The decrease in wavenumber reflects an increased packing of membrane lipids (resulting from a cell volume decrease). It was found that upon further increase in NaCl concentration that there was a further increase in packing of membrane lipids as indicated by a decrease in νCH_2 wavenumber values (Figure 4.7). However, prolonged exposure led to a partial recovery in νCH_2 wavenumber values/ decrease in

lipid packing. This partial recovery was likely due to the volume recovery observed (Figure 4.6) when cells are exposed to concentrated NaCl solutions [55]. This volume recovery has been associated with loss of semi-permeability of the membrane in human prostatic adenocarcinoma cells [55].

4.4 PART II – HYPEROSMOTIC STRESS EXPOSURE WITH PEG 600

In this part of the study, we subjected HFFs, to hyperosmotic stress using up to 67 % w/w PEG 600 (Π = 30 MPa) solutions. PEG 600 was used in order to simplify the analysis of the cell response to hyperosmotic stress which can be complicated by the volume recovery response observed in Part I of this chapter. PEG 600 is not permeable to the cell membrane due to its large size (~600 Da) [244]. In order to investigate the effect of temperature in select experiments, the osmotic stress was applied at 22 °C and at 4 °C.

4.4.1 MATERIALS AND METHODS

The objective of this study is to investigate the response of the cell membrane to hyperosmotic stress and the role of the cortical cytoskeleton in modulating the response of the membrane. To this end, an isothermal osmotic challenge was imposed on the selected model cells (Figure 4.1). Cellular response was determined using the following methods: (1) Basic microscopic analysis of the changes in cell morphology; (2) Quantification of the level of actin polymerization; (3) Measurement of changes to the membrane using two different dyes as described below; (4) Scanning electron microscopy imaging of the cells before and after hyperosmotic stress. Cell culture was performed using the same methods outlined in section 4.2.1.1.

4.4.1.1 Isothermal osmotic stress experiments

HFFs were incubated on a glass coverslip (not coated) enclosed in a polydimethylsiloxane (PDMS) microfluidic chamber (Figure 4.1) for 30 minutes at 37°C to promote cell attachment without spreading. The extracellular solution around the cells was altered by replacing the isotonic solution (~300 mOsm) with different hypertonic solutions containing PEG 600 up to 67 %w/w. PEG 600 was chosen due its use in previous dehydration studies of yeast [245] and due to its large size (~600 Da) which makes it highly non-permeant to the plasma membrane [244]. The range of osmotic conditions tested mimics those encountered during freezing (equivalent osmotic stress to extracellular medium freezing at a temperature in the range of -0.5°C to -20°C).

In order to determine whether stiffness of the membrane-cytoskeleton system, had any role in the cells' response to osmotic stress, the stiffness of the cytoskeleton was decreased by inhibiting myosin activity [59] indirectly using a Rho kinase inhibitor, Y27632 (20 μM) [237] (Sigma-Aldrich). As with the previous studies, cells were allowed to attach to the glass cover slip (without spreading) by incubation for 30 minutes at 37°C. Subsequently, they were incubated for 30 minutes at room temperature Y27632 (20 μM). After incubation, the cells were subjected to hyperosmotic stress as described previously. Viability was assessed using PI uptake 10 minutes after rehydration.

4.4.1.2 Measuring changes in actin cytoskeleton

Changes in the actin cytoskeleton were quantified using fluorescent staining with rhodamine-phalloidin as described in section 4.2.1.3.

4.4.1.3 Monitoring changes in cell membrane

Two methods were used to monitor the changes in the cell membrane with exposure to hyperosmotic stress: (1) HFFs were hyperosmotically stressed using varying concentrations of PEG 600 for up to 10 minutes. The insertion of the fluorescent styryl dye, FM1-43 was used to measure the formation of "surface defects" in the cell membrane; (2) HFFs were hyperomotically stressed using varying concentrations of PEG 600. The desorption of the lipophilic membrane dye, CellMask™ was used to investigate the effect of osmotic stress on desorption of lipid-like molecules from the cell membrane.

(1) The fluorescent styryl dye, FM1-43, was used to measure the formation of "surface defects" in the cell membrane during hyperosmotic stress. FM1-43 is similar to merocyanine 540 (MC540) [246], which has been used to monitor the formation of "surface defects" in liposomes exposed to hyperosmotic stress [247, 248]. MC540 was not used in our studies because it stained the PDMS chamber, which resulted in a high background fluorescence. Quantum yield of FM1-43 increases by two orders of magnitude when it partitions into the cell membrane [249] making insertion of the dye into the membrane easily detectable. Due to its double cationic charge FM1-43 partitions into the outer leaflet of the bilayer and does not easily transverse the membrane over short timescales (<10 minutes) [249]. One caveat in using FM dyes to monitor changes of the cell membrane during hyperosmotic stress is that FM dyes are sensitive to changes in viscosity [250] and may therefore be sensitive to the increase in membrane viscosity during cell shrinkage. Therefore, measurements were taken after the cell had reached a steady state, i.e. after shrinking to its final volume. After initial attachment onto the glass

coverslip in the PDMS chamber, cells were incubated in PBS in the presence of 4μM FM1-43 for 10 minutes at room temperature. To prepare the stock solution of, FM1-43 was dissolved in DMSO at 4mM and stored at 4 °C. Solutions of varying concentrations of PEG 600 (containing 4μM FM1-43) were then introduced into the chamber using the syringe pump. Fluorescent measurements were started approximately 30s after the cells were visually observed to stop shrinking and then and in 2 minute intervals thereafter.

(2) The CellMask™ orange plasma membrane dye from Invitrogen (C10045) was used to investigate the movement of a lipid-like molecule during the application of hyperosmotic stress. As per Invitrogen literature, "The CellMask™ plasma membrane stains are amphipathic molecules providing a lipophilic moiety for excellent membrane loading, and a negatively charged hydrophilic dye for "anchoring" of the probe in the plasma membrane". The CellMask™ stain was chosen because unlike most other lipophilic fluorescent dyes it is designed to have a very slow rate of internalization, it evenly stains the plasma membrane and the initial fluorescence (before osmotic stress) is high, thereby facilitating subsequent comparisons during the dehydration process. After initial attachment onto the glass coverslip in the PDMS chamber, cells were incubated in PBS containing 5 μg/ml Cell Mask™ for 10 minutes at room temperature. The stock solution of CellMask™ solution (5 mg/ml in DMSO) was stored at -20 °C. Three sets of experiments were performed using the CellMask™ dye. In the first set of experiments, cells were incubated with the dye to upload the dye into the membrane and then they were exposed to hyperosmotic PEG 600 solutions (either of Π = 10 MPa or Π = 30 MPa) (with no dye). The aim of this experiment was to use the dye to mimic membrane

constituents and thereby investigate the effect of hyperosmotic stress on the partitioning of the dye between the membrane and solution. In the second set of experiments, cells were incubated with the dye and the cells were either osmotically stressed by suddenly exposing them to 48.3% w/w (10 MPa) PEG 600 solution or slowly stressing in a stepwise manner from isotonic to 10 MPa (0.7 MPa $\rightarrow$ 2 MPa $\rightarrow$ 4 MPa $\rightarrow$ 6 MPa $\rightarrow$ 8 MPa $\rightarrow$ 10 MPa) with 2 minutes hold between steps. In the second experiment all solutions contained the same concentration (5 μg/ml) of CellMask™ dye. The total fluorescence of each cell before the start of hyperosmotic stress and 1 minute after the completion of stressing was measured and compared. The aim of this experiment was to assess the effect of rapid versus slow dehydration on the partitioning of membrane constituents. In the third set of experiments, cells were incubated in the solution containing the dye and then osmotically stressed using Π = 10 MPa PEG 600 at 22 °C and 4 °C (with 5 μg/ml Cellmask™ present in the extraceullular solution at all times). The aim of this experiment was to investigate the influence of temperature on desorption of lipid-like molecules from the membrane.

4.4.1.4 Scanning electron microscopy (SEM)

SEM images were taken of samples before and after being subjected to hyperosmotic stressing to Π = 10 MPa. Sample preparation for SEM imaging was as follows:

1. Fixation in 2% glutaraldehyde and 0.1M sodium cacodylate for 5 hours.

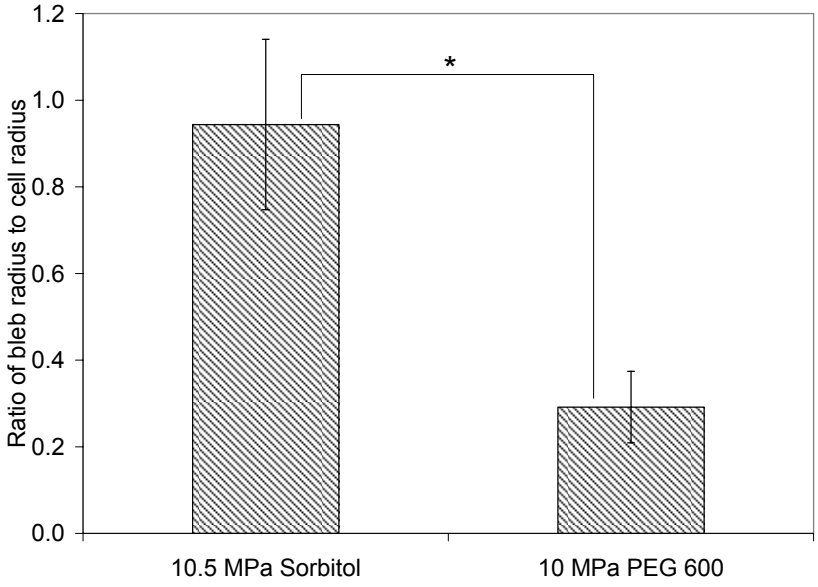

Figure 4.8 Ratio of the radius of the largest bleb to the cell radius for cells that were exposed to osmotic stress using sorbitol and 48% w/w PEG 600 for 10 minutes before returning to isotonic conditions

2. Exposure to 0.1M sodium cacodylate for 45 minutes (buffer was changes every 15 minutes).

3. Exposure to 1% osmium tetroxide and 0.1M sodium cacodylate for 90 minutes.

4. Exposure to 0.1M sodium cacodylate for 45 minutes (buffer was changed every 15 minutes).

5. Serial dehydration using increasing concentrations of ethanol: 50%, 70%, 80%, 95%, 100%.

6. Critical point drying using a Tousimis Model 780A Critical-Point Dryer.

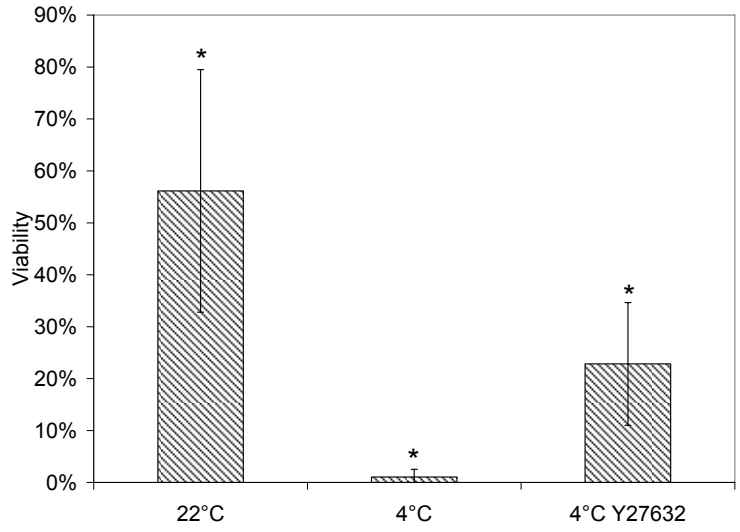

Figure 4.9 Viability upon return to isotonic conditions after stressing with Π = 10 MPa PEG 600 at 22 °C, 4 °C, and at 4 °C in the presence of 20μM Y27632

7. Sample coating using a VCR high resolution indirect ion-beam sputtering system to deposit a platinum coating of about 2 nm.

Imaging was performed using a Hitachi S-900 scanning electron microscope at an accelerating voltage of 3kV. For experiments where PEG was used as an osmotic agent, samples were first fixed for 10 minutes at the temperature at which the experiment was conducted with 2% glutaraldehyde in the PEG solution.

4.4.2 RESULTS

The first stage of our experiments involved using Π = 10 MPa PEG to osmotically stress cells at 22 °C and 4 °C. Using a PEG solution of Π = 10 MPa enabled comparison of results to that of the 4M sorbitol solution (Π = 10.5 MPa) used in Part I of this chapter. In

these experiments, there was no observable increase in cell size during the 10 minute incubation with PEG, a strong indication that there was little or no solute uptake. However, small blebs did form upon return to isotonic conditions for experiments performed at 22 °C. A comparison of bleb sizes using the ratio of the radius of the largest bleb to the same cell radius (Figure 4.8) revealed that the size of blebs formed with Π = 10 MPa PEG 600 were significantly smaller than those observed with Π = 10.5 MPa sorbitol. Cells also exhibited blebs even when they were pre-treated (prior to hyperosmotic stress with Π = 10 MPa PEG 600) with 20 μM Y27632 in order to reduce the cortical tension of the membrane. Taken together these results suggest that there was some uptake of PEG during hyperosmotic stress albeit limited when compared to sorbitol. Cells that were osmotically stressed at 4 °C using Π = 10 MPa PEG 600 did not demonstrate any blebs upon return to isotonic conditions. This result was similar to that obtained in Part I of this chapter using Π = 10.5 MPa sorbitol. Also similar to results in Part I of this chapter, cells that were stressed at 22 °C had a higher viability than those at 4 °C. It was further observed that addition of 20 μM Y27632 at 4 °C improved the post-rehydration viability (Figure 4.9).

The amount of intracellular F-actin before and after hyperosmotic stress was measure using fluorescent staining. In cells at 22 °C there was a significant increase in F-actin content upon return to isotonic conditions (Figure 4.10). However, in cells stressed at 4 °C there was no increase in the amount of intracellular F-actin. It was also observed that after 10 minutes hyperosmotic stress with Π = 10 MPa PEG 600, cells at 22 °C had a

A

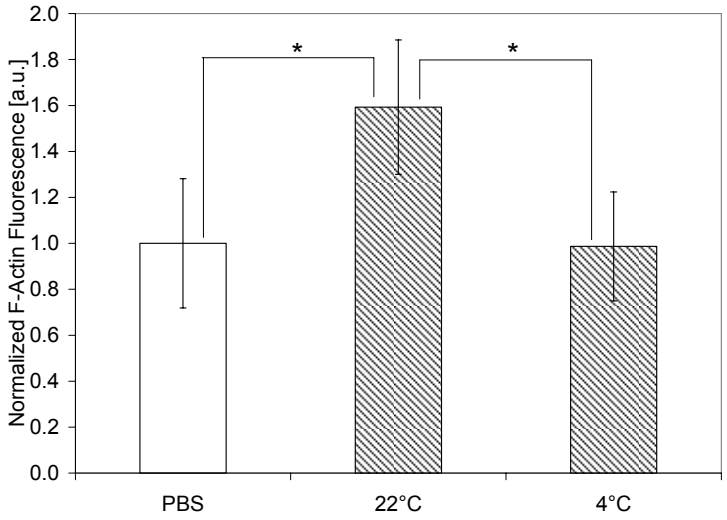

B

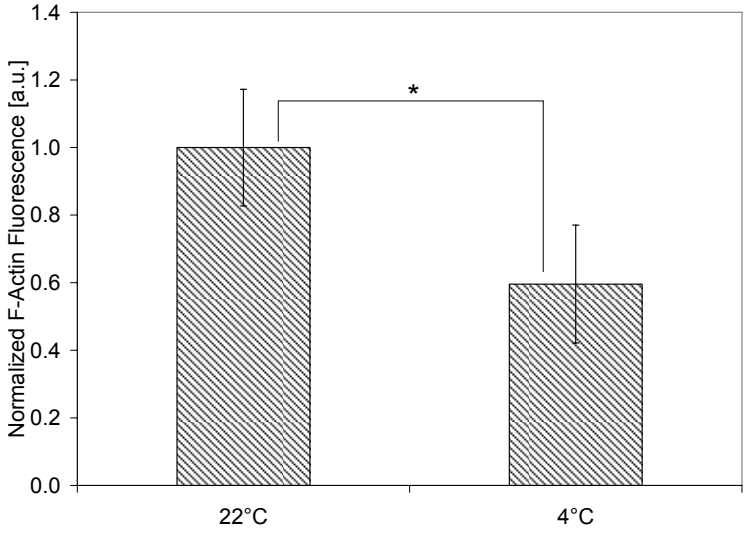

Figure 4.10 F-actin content determined by rhodamine-phalloidin fluorescence intensity at (a) isotonic conditions before and 10 minutes after hyperosmotic stress with 48% w/w (Π = 10 MPa) PEG 600 (hatched), and at (b) 10 minutes exposure to the same hyperosmotic stress

significantly higher amount of F-actin than the cells at 4 °C (Figure 4.10b). This indicated that actin polymerization was inhibited at lower temperatures.

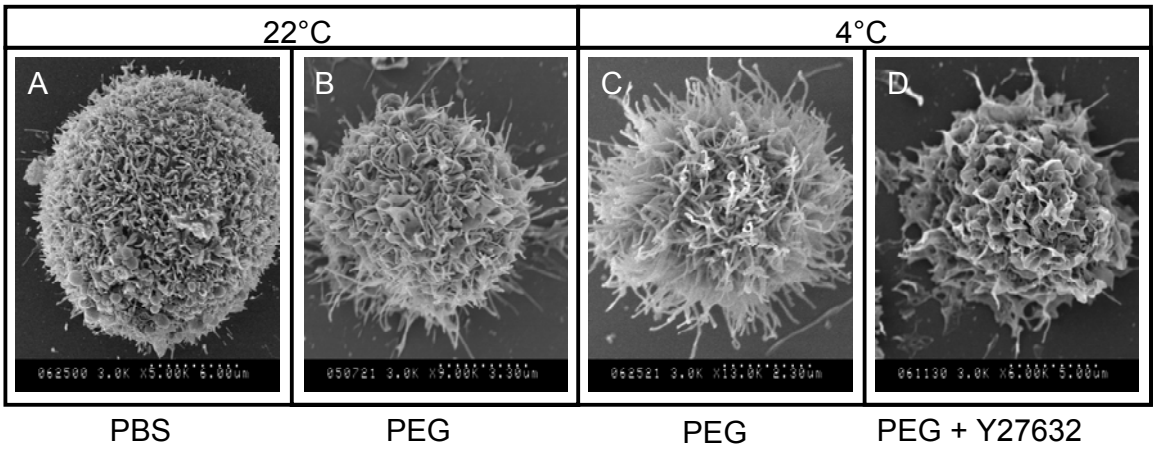

Figure 4.11 SEM images (a) before and (b,c,d) after dehydration with 48% w/w (Π = 10 MPa) PEG 600 at 22 °C and at 4 °C and with Y27632

Scanning electron microscopy was used to investigate the differences in the morphology of cells that were experienced hyperosmotic stress at 4 °C versus 22 °C. It was found that cells stressed at 4 °C cells extensively formed microvilli (Figure 4.11b) whereas those stressed at 22 °C had a "mixed" morphology with microvilli, bleb-like and lamellae-like projections (Figure 4.11a). Interestingly, cells that were pre-treated with 20 μM Y27632 (in order to reduce the stiffness of the cytoskeleton) and subsequently stressed at 4 °C did not form microvilli, but exhibited lamellae-like projections (Figure 4.11d). Upon return to isotonic conditions, cells stressed at 4 °C had a mixed population with some cells having a more smooth appearance with few microvilli (Figure 4.12c) and others having more membrane protrusions (either microvilli or very small bleb-like protrusions) (Figure 4.12d) than control cells. Cells that were osmotically stressed at 22 °C had small blebs and ruffles upon rehydration (Figure 4.12a,b). These results demonstrate that the difference in temperature alters a particular property of the cell such that very different

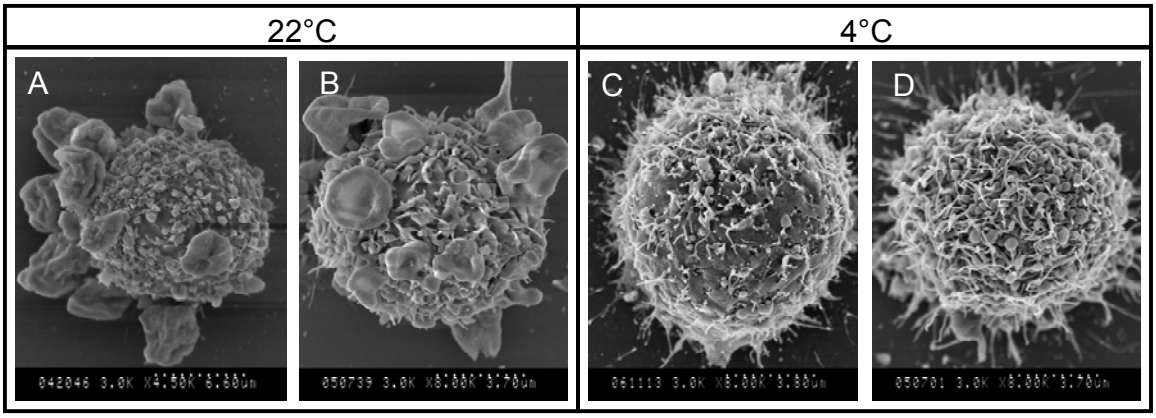

Figure 4.12 SEM images after return to isotonic conditions after dehydration with 48% w/w (Π = 10 MPa) PEG 600 at (a,b) 22 °C and at (c,d) 4 °C .

membrane morphologies are obtained at the same osmotic pressure. The results from the Y27632 treat cells hint that this property may be the stiffness of the cytoskeleton which is expected to increase at lower temperatures [251]. This hypothesis is discussed in further detail in Chapter 6.

In order to investigate the effect of increasing hyperosmotic stress (10 MPa to 30 MPa) on formation surface defects in the cell membrane, the cationic styryl dye, FM1-43, was used (see Section 4.4.1.3). Confocal microscopy showed that the dye was primarily localized in the cell membrane for cells exposed to the highest osmotic pressure in these

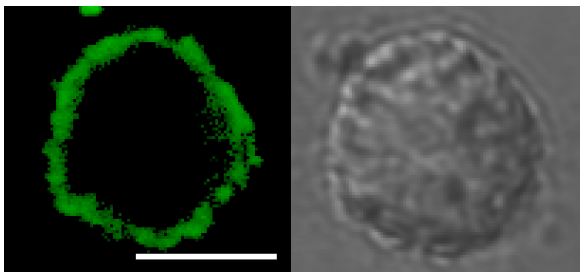

Figure 4.13 (a) Fluorescence and (b) Transmitted light confocal microscopy images of HFF after 10 minutes exposure to Π = 30 MPa (67 % w/w) PEG 600 showing FM1-43 dye location in cell membrane. Scale bar represents 10μm.

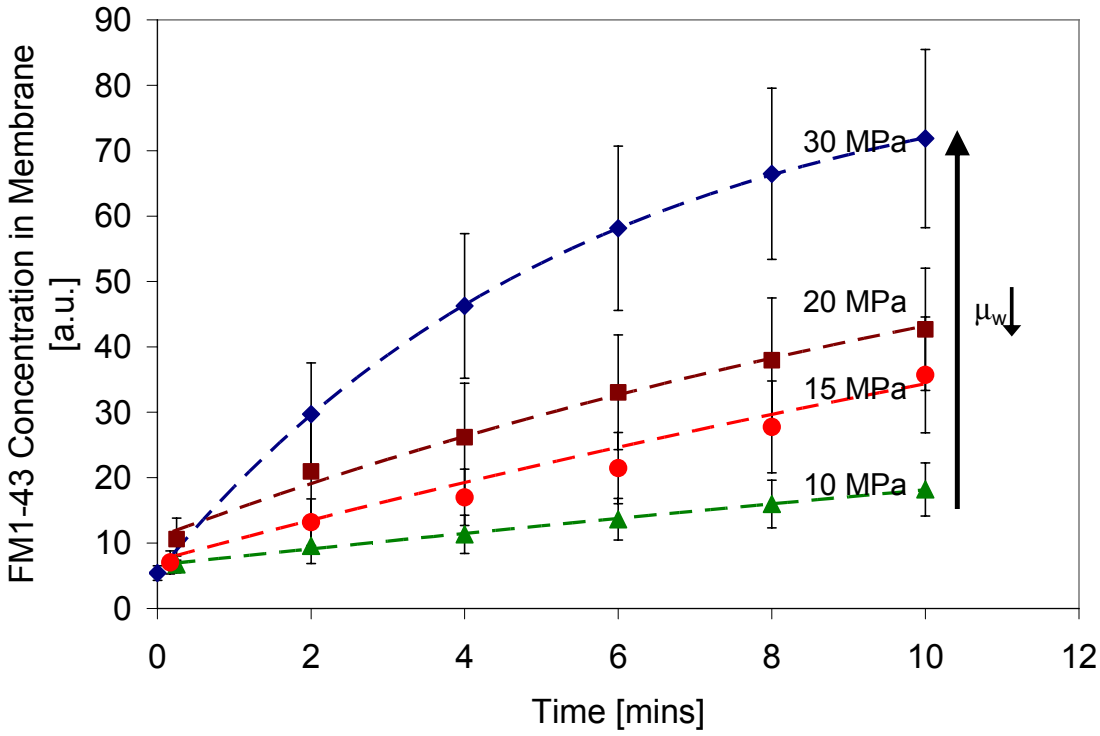

Figure 4.14 FM1-43 uptake for cells subject to osmotic stress using 48.3% w/w (▲),54.7% w/w (●) , 59.6% w/w (■), 67% w/w (◆) PEG 600 at 22 °C. n ≥ 60 cells. Lines are drawn as guides for eyes.

experiments, Π = 30 MPa (Figure 4.13). Using conventional fluorescence microcopy, it was found that with increasing osmotic stress there was an increase in the amount of the dye partitioning into the membrane (Figure 4.13). It was also observed that the initial rate at which the dye partitioned into the membrane increased with osmotic stress. This suggests that at higher osmotic pressures there was an increase in "surface defects" in the membrane.

Lipid desorption from the cell membrane during osmotic stress was investigated using the Cellmask™ dye by using the dye to mimic a lipid molecule (see Section 4.4.1.3). Initial

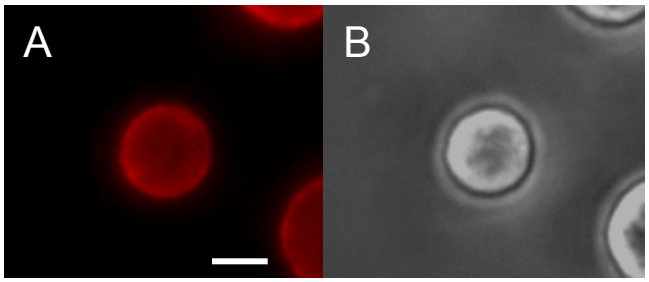

Figure 4.16 (a) Fluorescence and (b) Transmitted light images of HFF at isotonic conditions in PBS after loading with Cellmask dye (exposure time = 1s). Scale bar represent 10μm

(isotonic conditions) staining using the Cellmask™ dye clearly showed that the cell membrane was stained (Figure 4.16). Upon increasing the osmotic stress, the intensity of the dye increased dramatically and saturated such that the camera exposure time had to be decreased. It was observed that "downstream" of the cells of dye exiting the cell were present (Figure 4.15).

Continuous measurement of the dye intensity (exposure time = 100 ms) in cells stressed to (Π = 10 MPa showed that after cell shrinkage for t ≥ 2 min fluorescence continued to decrease. However, for the cells stressed to Π = 30 MPa, no decrease in fluorescence for t

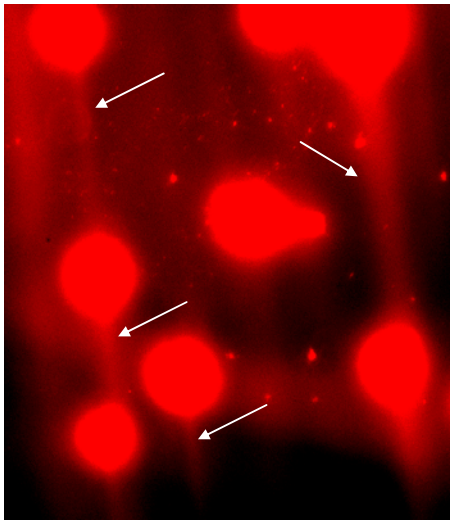

Figure 4.15 Cellmask dye exiting cell soon after start of osmotic stress using 67% w/w (Π=30MPa) PEG 600. Arrows indicate streaklines of dye coming from cells.

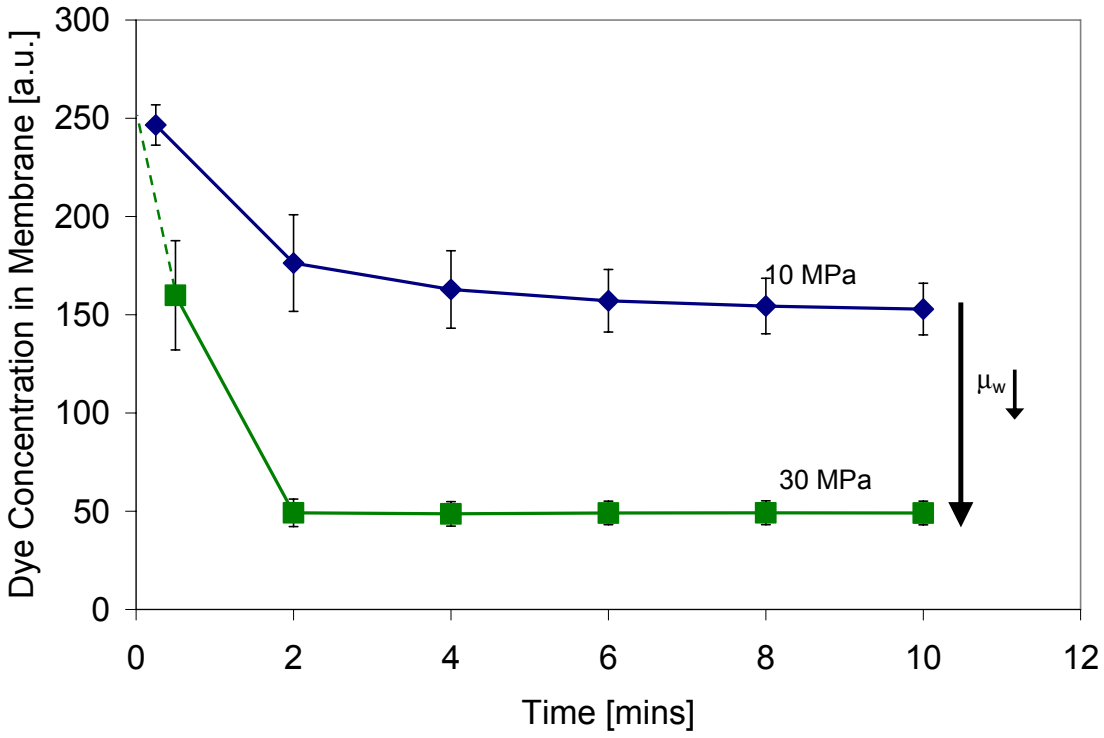

Figure 4.17 Decrease in Cellmask concentration in membrane after osmotic stress with (◆) 48% w/w (Π=10MPa) and (■) 67% w/w (Π=30MPa) PEG 600. n ≥ 60 cells. Lines are drawn as guides for eyes. Both conditions start at the same point.

≥ 2 min was observed (Figure 4.17). These results firstly show that when exposed to hyperosmotic stress, lipid-like molecules leave the cell membrane into the extracellular solution. Secondly, similar to observations made in the FM1-43 experiments, the rate of dye transfer increases with increasing osmotic pressure such that for Π = 30 MPa equilibrium was attained by 2 minutes unlike Π = 10 MPa (Figure 4.7).

In order to determine the difference between effects of absolute osmotic stress and the transmembrane stress difference on the cell, expose to hyperosmotic stress, cells were exposed to osmotic pressures a stepwise manner from isotonic to 10 MPa (with Cellmask

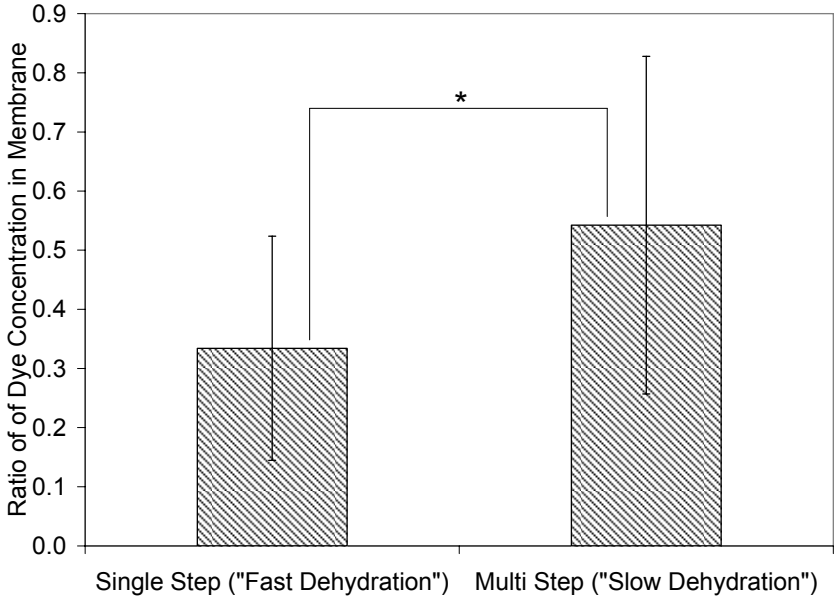

Figure 4.18 Ratio of Cellmask dye intensity 1 minute after (using 100 ms exposure) the end of the applied osmotic stress (Π=10MPa), to the dye intensity before (using 1000 ms exposure) at isotonic conditions. n ≥ 100 cells

present in the extraceullular solution at all times). It was found that the total fluorescence was slightly but significantly greater in cells that were dehydrated in a multi-step fashion versus those that were dehydrated in a single step (Figure 4.18). This indicated that the differential effects of transmembrane osmotic gradient as well as the absolute stress the cell is exposed to affects the extent of lipid desorption from the membrane .

In order to investigate the influence of temperature on Cellmask™ desorption from the membrane, cells were subjected to Π = 10 MPa at 22 °C and 4 °C. Prior to the application of osmotic stress the cells exhibited a significant initial increase (58 ± 13%) in Cellmask fluorescence intensity. This increase in fluorescence intensity suggests that at lower temperatures there was an increase in the partitioning of dye into the membrane.

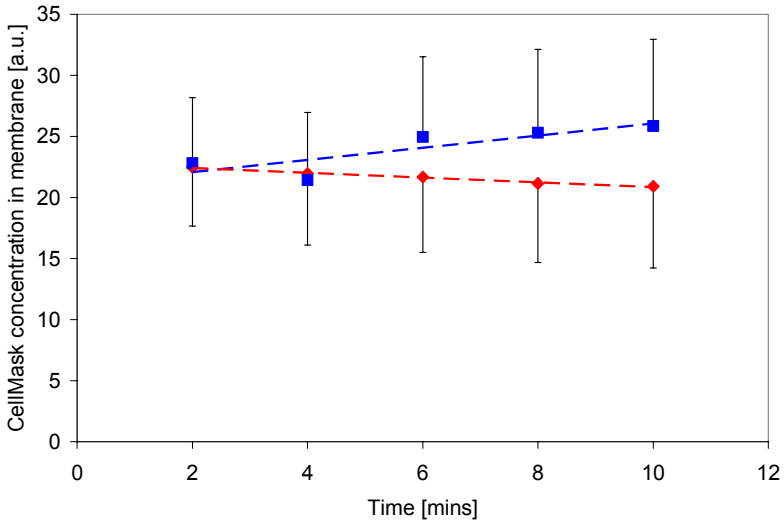

Figure 4.19 Cellmask concentration in membrane in dehydrated state after dehydration at (◆) 22 °C and (■) 4 °C using 48% w/w (Π=10MPa) PEG 600. n ≥ 60 cells. Lines are drawn as guides for eyes.

When cells were osmotically stressed at 22 °C (with Cellmask present in the extraceullular solution at all times) there was a decrease in fluorescence (t ≥ 2 min). For cells stressed at 4 °C there was an increase in fluorescence (t ≥ 2 min) (Figure 4.19) following the initial decrease with the application of osmotic stress. The rate of increase (t ≥ 2 min) was statistically different from that at 22 °C using linear regression analysis with a 95% confidence interval. This result indicates that the temperature at which the osmotic stress is applied affect the partitioning of the dye between the membrane and the solution.

4.5 DISCUSSION

Cells experience a wide range of osmotic, mechanical and thermal stresses during cryopreservation often leading to cell injury and death [252]. Osmotic stress is also encountered by cells that are preserved by drying. One of the primary sites of damage is the cell membrane [5]. In eukaryotic cells the cell membrane is directly and indirectly connected to the cytoskeleton [106, 107, 109] and the actin cytoskeleton has been show to actively re-organize in response to osmotic stress [150, 158]. Other investigators have observed that cryoprotectants, such as DMSO, alter membrane structure and permeability [253], and also affect the cytoskeleton structure and organization [254, 255]. Given the physical connection between the membrane and the cytoskeleton and the fact that cryoprotectants have been shown to affect both the membrane and the cytoskeleton, it is plausible that the freeze/thaw response of the membrane-cytoskeleton complex (not of the membrane alone) plays a role in cell survival during cryopreservation. Therefore, in this study we investigated the changes in the actin cytoskeleton and the cell membrane in response to isothermal exposure to osmotic stress (without freezing).

In part I of this study we observed that the cells exposed to hyperosmotic sorbitol solutions exhibited a slight but significant increase in volume during the 10-minute incubation in 4M sorbitol. The increase in volume was dependent on the magnitude of hyperosmotic stress as well as the incubation time. One possible explanation for this phenomenon is solute uptake, which could be due to the formation of membrane defects, regulatory volume increase, inadequate active transport of ions or damage to the transport proteins in the membrane. Similar osmotic stress studies performed with human prostatic

adenocarcinoma cells using NaCl as an osmolyte have also suggested that the observed volume recovery during hyperosmotic stress exposure was due to solute uptake [55, 252]. Another potential mechanism for an increase in cell volume is a decrease in cortical tension caused by damage to the cytoskeleton. A decrease in cortical tension would reduce the intracellular hydrostatic pressure, thereby causing an influx of water and the corresponding increase in cell volume. However, it is unlikely that a decrease in cortical tension is responsible for the observed increase in cell volume as a decrease in cortical tension at isotonic conditions (induced by 30 minutes incubation with Y 27632) did not result in a significant increase in cell volume.

We also observed extensive blebbing when the cells experienced a stepwise change in osmotic stress (to a minimum of 2150 mOsm) at room temperature, when sorbitol was used as the osmolyte. However, when a larger solute (polyethylene glycol 600) was used as an osmolyte, extensive blebbing was not observed (Figure 4.8). Blebbing is thought to be due to the dissociation of the membrane from the underlying cytoskeleton [256] induced by rupture of regions in the cytoskeleton or a reduction in the adhesion between the actin cytoskeleton and the membrane [56]. Blebbing can also result from damage to the organelles e.g. lysosomes, which can release proteases into the cytosol [257]. However, osmolyte specificity of the blebbing response (Figure 4.8) rules out the latter possibility. Another phenomenon that can induce blebbing is solute uptake (which would also explain the volume increase response as discussed above): Increase in intracellular solute concentration, upon return to isotonic conditions would cause an influx of water, which would increase the hydrostatic pressure within the cell causing blebbing. We

showed that blebbing did not depend on cortical tension: When cortical tension was reduced (using Y27632, blebbistatin or CD), blebbing behavior of the stressed cells was still observed. These observations reinforce the hypothesis that there is solute uptake by the cells during hyperosmotic challenge.

There was a marked difference in terms of the amount of polymerized actin upon return to isotonic conditions for cells which were osmotically stress using 48.3% PEG 600 versus 4M sorbitol. Cells stressed using sorbitol showed a significant decrease in F-actin upon return to isotonic conditions whereas cell stressed with PEG showed a significant increase. One possible reason this difference is the reduced solute uptake with PEG 600 when compared to sorbitol and the resulting variations in cell size during and after hyperosmotic stress. In experiment with PEG 600 cells remain shrunk during the hyperosmotic stress thereby increasing G-actin concentration and favoring the G-actin to F-actin conversion. Upon return to isotonic conditions, the cell volume for PEG treated cells does not increase as greatly as with sorbitol treated cells (Figure 4.8) which would again favor the presence of F-actin over G-actin.

The increase in FM1-43 partitioning into the membrane from the solution phase with increase in osmotic stress may be a result of changes to the membrane surface due to osmotic stress. Arroyo et al [75] have shown that hyperosmotic stress causes changes at the interface (solution-lipid headgroup) region of lipid bilayers. These changes, termed "surface defects" allowed increased partitioning of the styryl dye, merocyanine 540, into the membrane. In our experiments, we observed uptake of FM1-43, a dye similar to MC540 [246]. The formation of these "defects" at the membrane surface may be

responsible of uptake of PEG 600 despite its large size. This is supported by the work done by Disalvo [258] who showed that the permeability of a lipid bilayer to solutes increases with increasing osmotic stress.

Cellmask™ experiments showed that hyperosmotic stress can cause desorption of lipid-like molecules from the membrane. A similar observation was made by Arnold et al [259] who showed that a hydrophobic dye, pyrene, was extracted from the cell membrane with increasing osmotic stress using PEG 6000. This desorption lipids or lipid-like molecules from the membrane is one of the mechanisms of damage that occurs during dehydration of cells. It was also discovered that a faster rate of dehydration increased the amount of CellMask dye that desorbed from the membrane. This result suggests that a faster rate of dehydration may result in more membrane damage than a slower rate. This result is supported by numerous studies which show that rapid dehydration is more injurious to cells than slow dehydration [7, 114, 132]. The effect of temperature on CellMask partitioning before osmotic stress and desorption during osmotic stress (Figure 4.19) suggests that at low temperatures, partitioning of the dye into the membrane is favored such that even though the dye molecules initially desorb, they reinsert after some time. This mechanism is discussed in detail in Chapter 6. Alternatively, there may be some time dependent alteration in the membrane that occurs at one temperature versus the other that allows the dye to reinsert.

The decrease in viability in osmotically stressed cells at 4°C may be due in part to a decrease in the membrane area. SEM images of osmotically stressed cells at 4°C showed pronounced formation of microvilli which the cells either retained or shed during return

to isotonic conditions. Either case may present a problem for a cell that is returning to isotonic conditions. If the microvilli are not retracted there is a decrease in available membrane material to "cover" the cells as it expands. If the microvilli are shed then there is definitely a lack of membrane material to accommodate cell expansion.

The decrease in viability at 4^{o}C temperatures may also be due in part to a decrease in the membrane reservoir (i.e., loss of invaginations and surface folds) during hyperosmotic stress exposure at low temperature: Takamatsu et al [252] exposed prostatic adenocarcinoma cells to hyperosmotic NaCl solutions at different temperatures, and observed that cells osmotically stressed at 0^{o}C appeared smoother (when compared to those at 23°C, which appeared wrinkled). This suggests a temperature-induced reduction in cell's membrane area (combined with hyperosmotic exposure) which would reduce the cell's capacity to expand during return to isotonic conditions. Loss of membrane material has been observed for yeast subjected to hyperosmotic shock [260] and also when *Escherichia Coli* is desiccated [194]. To our knowledge loss of membrane material during hyperosmotic stress has not been demonstrated for mammalian cells but the converse, i.e., increase in membrane area with hypoosmotic stress has been shown [261].

Hyperosmotic stress experiments at lower temperatures (i.e. 4°C) demonstrated a lower cell viability, which was accompanied by a lower incidence of blebbing. The drop in viability may be related to the lack of available membrane material which may also be responsible for the lower incidence of blebbing. The higher incidence of membrane damage at lower temperatures is analogous to the outcome observed by Stroetz et al. [251] when subjecting cells to mechanical strain. Specifically, membrane damage due to

mechanical strain in alveolar epithelial cells increased at lower temperatures. The increase in membrane damage was attributed to reduced lipid trafficking to the plasma membrane at lower temperatures (i.e. reduction in the size of the membrane reservoir). Reduced trafficking of membrane material at low temperatures has also been observed during hypotonic exposure of cells [262]. Since bleb formation is dependent on the membrane reservoir [56] it is therefore not surprising that bleb formation is inhibited at lower temperatures.

4.6 CONCLUSION

It was observed that with increasing osmotic stress there was an increase in the number of "surface defects" formed in the membrane. It was also observed that desorption of lipid-like molecules occur during hyperosmotic stress and that the degree of desorption is dependent on osmotic pressure and osmotic gradient. Our data suggest that solute uptake can occur during hyperosmotic stress. This solute uptake may be related to the formation of "surface defects" due to hyperosmotic stress which increases the permeability of the membrane to solutes. As a result of solute uptake during osmotic stress cell, the membrane tears away from the cytoskeleton in the form of blebs upon return to isotonic conditions. Altering the cortical tension does not alter the formation of blebs which suggests that bleb growth is osmotically driven. The increase is filamentous actin during hyperosmotic stress is favored at higher temperatures. In cells that exhibited pronounced blebbing there was a net depolymerization of actin which is likely due to a reduction in

G-actin concentration. Reducing the stiffness of the cytoskeleton alters the membrane morphology during hyperosmotic stress and increases the viability upon return to isotonic conditions.

CHAPTER 5: SLOW FREEZING OF HUMAN FORESKIN FIBROBLASTS

5.1 SUMMARY

The objective of this study was to understand how freeze/ thaw stresses affect the cell membrane and what is the role of the underlying cytoskeleton in modulating these stresses. In this study, we subjected a model mammalian cell, human foreskin fibroblast (HFF), to freeze/thaw. Transmitted light, Infrared spectroscopy, scanning electron microscopy, fluorescence- and cryo- microscopy were used to investigate the changes in the cell membrane and the actin cytoskeleton.

In the first part of this chapter, cells were frozen in media/ PBS or media/ PBS with cryoprotectants. Our data suggest that the cells experienced a loss of membrane material thereby reducing the cell's ability to expand during thawing. Our results also suggest that interaction with ice can cause significant damage to cells during a freeze/ thaw cycle. Our results indicated that the actin cytoskeleton stabilizes the cell membrane and that damage to the cell membrane is accompanied by damage to the cytoskeleton.

In the second part of this chapter, cells were frozen in isotonic solutions of polyethylene glycol in order to minimize the effects of ice interaction and avoid sodium chloride eutectic effects observed in Chapter 2. Two different molecular weights polyethylene glycol were used, PEG 200 (M_w = 200) and PEG 600 (M_w = 600). For cells frozen to moderate freezing temperatures (-20 °C) with PEG 600 there was a significant increase in viability. This was attributed to decreased ice interaction due to the large unfrozen

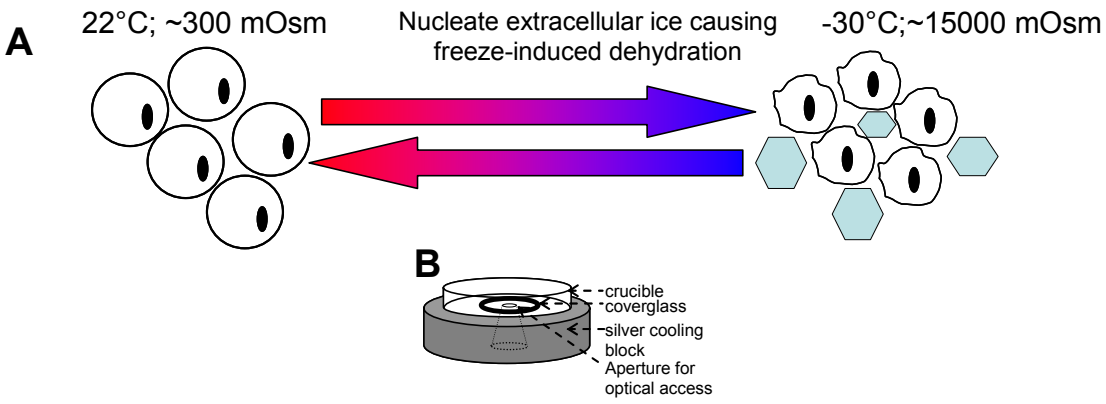

Figure 5.1 Schematic representations of (a) experiments conducted (freeze/thaw), (b) Linkam cryostage block on which samples were frozen/thawed. Samples were either manually nucleated using a chilled needle or using *Pseudomonas syringae*,

fraction of the sample (16 w/w%). For cells frozen to -80 °C the viability was not significantly different from cells frozen in PBS. However, a significantly higher viability was obtained using 300 mOsm PEG 200, which was attributed to its ability to enter the cell thereby reducing the extent of cell shrinkage. Viability was further improved using Y27632 and wheat germ agglutinin (WGA). The increase in viability with Y27632 and WGA was attributed to change in membrane morphology during shrinking and increased membrane strength, respectively.

5.2 PART I – FREEZE/ THAW IN MEDIA

In this part of the study, we subjected a mammalian cell, human foreskin fibroblast (HFF), to freeze/thaw stresses and monitored changes in the cell membrane and actin cytoskeleton. Also, polyvinyl alcohol was used to modify the structure of the surrounding ice to investigate if ice crystal morphology would have an effect post-thaw viability.

Table 5.1 Cell response and measurements

Cell response	**Measurement Method**
Membrane integrity	Propidium iodide uptake
Cell morphology	Phase contrast microscopy
Change in actin cytoskeleton	GFP-actin; Immunofluorescence
Membrane structure	FTIR spectroscopy

5.2.1 MATERIALS AND METHODS

The objective of this study is to elucidate the role of the membrane-cytoskeleton complex on the freeze/thaw response of mammalian cells. Cellular response was determined using the following methods: (1) basic microscopic analysis of the changes in cell morphology (including volume change and blebbing); (2) quantification of the level of actin polymerization (using the three different techniques described below); (3) dynamic measurement of the structural changes to the membrane using Fourier Transform Infrared (FTIR) spectroscopy. The methods that were used to quantify the specific cellular parameters are summarized in Table 1. HFFs were cultured and harvested as outlined in Chapter 4.

5.2.1.1 Freeze/thaw experiments

HFFs were subjected to freeze/thaw conditions using two different temperature-controlled cryostages. A commercial stage (FDCS 196, Linkam Scientific Instruments Ltd., UK) with a liquid nitrogen cooled silver block (Figure 5.1b) was used for the transmitted light and fluorescence microscopy experiments. A custom-made cryostage was used for the FTIR spectroscopy studies. Cells that underwent the freeze/thaw cycle were suspended either in media, media + 10% DMSO, media + 10% glycerol or 1xPBS. The cooling rate for all experiments was the same at 2°C/min. Cells were cooled down to -30°C and warmed back up to 23°C at 2°C/min (unless otherwise stated). In FTIR and viability experiments where the freeze/thaw response of cells in media with and without cryoprotectants were compared, *Pseudomonas syringae* (ATCC, Rockville, MD, USA) was used as a natural ice nucleator to control the nucleation temperature (NT) [263]. Viability was assessed immediately after freeze/thaw by propidium iodide (PI) uptake (PI was present in the extracellular solution at all times). NTs for solutions with cryoprotectants were different than solutions without cryoprotectants due to freezing point depression (using *Pseudomonas syringae*, ice nucleation occurred at -4°C in media, -7.3°C in media + 10% glycerol and -8.5°C for media + 10% DMSO). In all other freeze/thaw experiments with cells in PBS without cryoprotectants, samples were manually nucleated using a chilled needle at -2°C. The results (images, FTIR spectroscopy and viability) shown for cells suspended in media or PBS were the same for either nucleation temperature (NT = -2°C or -4°C).

5.2.1.2 Change in ice structure

Previous studies have implicated the presence of ice as being a major form of damage [143, 252, 264]. In order to investigate if ice morphology had any effect on the post-thaw viability polyvinyl alcohol (PVA) was used to modify the structure of ice. Polyvinyl alcohol is thought to change the structure of ice in a similar manner to anti-freeze proteins by adsorbing onto the prism faces of hexagonal ice crystals [265-267]. It has previously been shown that using high concentrations (20 mg/ml) of anti-freeze proteins can modify the structure of ice so as to maximize destruction of cells [143]. In these experiments 5 mg/ml of polyvinyl alcohol (PVA) (M_w=13000 – 23000 from Sigma-Aldrich) in PBS was used. This concentration of PVA had minimal effect on the osmolality of the solution and as such, did not alter the temperature at which the solution was nucleated or thawed. Cells were cooled down to -30 °C at 2°C/min and warmed back up to 22 °C at 130 °C/min.

5.2.1.3 Measurement of the degree of actin polymerization

Three different methods were used to characterize the structure of the intracellular actin (polymerized F-actin versus G-actin monomers) after freeze/thaw and osmotic incursions: (1) HFFs were transfected with enhanced green fluorescent protein (EGFP) actin plasmid and the actin cytoskeleton was visualized via using conventional fluorescence microscopy; (2) Direct measurements of the amount of polymerized actin were also made by fluorescent staining; (3) The extent of intracellular actin polymerization was quantified indirectly through the measurement of cytoplasmic crowding using a fluorescent molecular rotor. See details below:

(1) In experiments investigating changes in the actin cytoskeleton, GFP-transfected cells were imaged before and after freeze/thaw or osmotic stress. GFP-transfected cells were imaged (exposure time of 3.5 s) using an Olympus BX50 fluorescent microscope (Tokyo, Japan) equipped with a Spot Diagnostic camera (Diagnostic Instruments Inc., MI). GFP fluorescence was normalized with respect to its initial value, i.e. before freeze/thaw. The overall fluorescence intensity of the cell was calculated using ImageJ software (NIH, USA).

(2) For fluorescent staining of polymerized actin, rhodamine-phalloidin (Invitrogen Corporation) was used to stain actin filaments. See Chapter 4 for detail method.

(3) Cytoplasmic crowding was quantified using the 9-(2-carboxy-2-cyanovinyl) julolidine (CCVJ, Santa Cruz Biotechnology, Santa Cruz, CA) fluorescence probe. CCVJ is a molecular rotor whose fluorescence depends on the viscosity of the medium [268]. Similar probes (i.e. molecular rotors) have been previously used to monitor actin polymerization [269]. Note that since CCVJ, the molecular rotor used to measure intracellular viscosity, is a relatively large molecule (256 Da) when compared to the estimated free-space between structures in the cytoplasm [270], we envisage that rather than measuring the fluid-phase viscosity of the cytoplasm, the rotor is measuring a characteristic of the intracellular space, which is a function of fluid-phase viscosity and the entanglement with the surrounding molecules (we term this characteristic, crowding). It is further assumed that the contribution to the entanglement from polymerized filamentous actin would be much more significant than that from the monomer actin. HFFs were incubated with 95 μM CCVJ for 30 minutes at 37°C prior to freeze/thaw to -

30 °C. Measurements of the CCVJ fluorescence intensity in selected cells were conducted before and after freeze/thaw using conventional fluorescent microscopy. Images were collected (exposure time of 3.5 s) on the Nikon TE 200 microscope. The CCVJ fluorescence (average fluorescence intensity of several cells) measured was normalized using the pre-freeze initial value. The fluorescence intensity was measured and averaged using ImageJ software.

5.2.1.4 Characterization of the membrane structure using FTIR spectroscopy

Conformation of membrane lipids was characterized using FTIR spectroscopy. HFFs sandwiched between two CaF_2 windows that were separated by a 6-μm Mylar spacer (Thermo Electron North America Inc., Madison, WI, USA) and mounted onto a temperature-controlled stage. Ice nucleation was induced using *Pseudomonas syringae*. FTIR spectra were collected in the 930-8000 cm^{-1} range using a Thermo-Nicollet 6700 spectrometer, equipped with a DTGS detector (Thermo-Nicolet, Madison, WI, USA). FTIR spectra were recorded at 1 minute increments while the sample was cooled from ambient temperature (22°C) down to -30°C at a constant rate of 2°C/min and then immediately warmed at a constant rate of 2°C/min back to 22°C. At each temperature data point an IR spectrum was obtained by averaging 32 scans. Spectral analysis was carried out using Omnic software (Thermo-Nicolet, Madison, WI, USA). Lipid conformational order was monitored by measuring the peak location of the υ-CH_2 (symmetric stretching) band located at approximately 2850 cm^{-1}.

5.2.1.5 Characterization of the membrane viscosity using DCVJ fluorescence

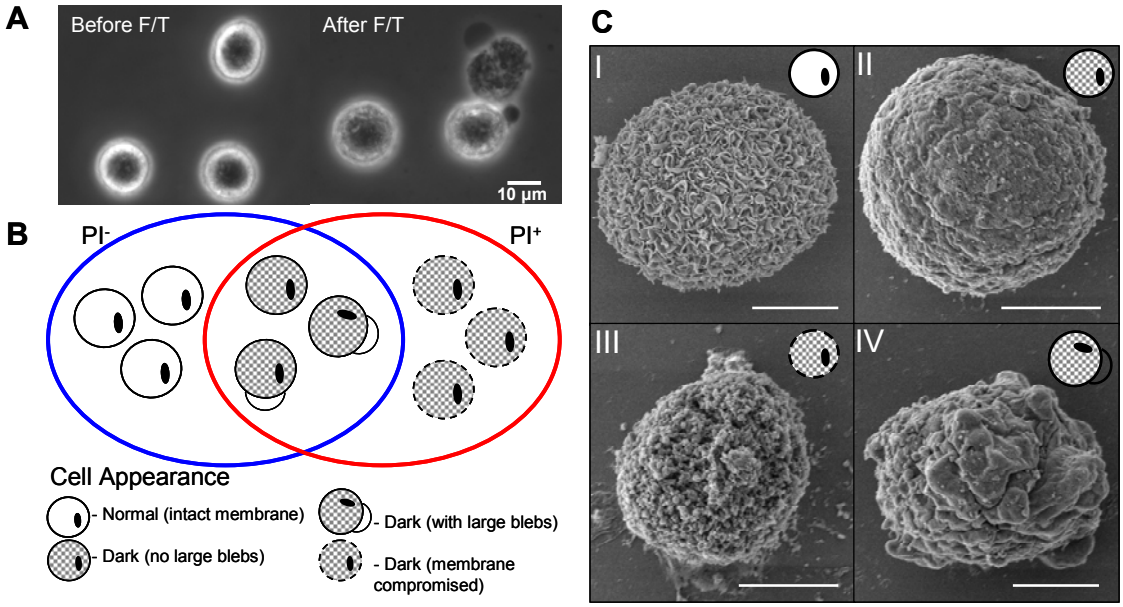

Figure 5.2 (a) Phase contrast microscopy with HFF cells suspended in (a) 1xPBS at room temperature; and after exposure to a freeze/thaw cycle while suspended in PBS. Ice was nucleated at -2°C. (b) Schematic showing the different cell populations observed after freeze/thaw. Some of the darkened blebbing cells were PI^- and some were PI^+. (c) SEM images of cells taken (I) before freeze/thaw and (II), (III), (IV) after freeze/thaw. Scale bars represent 5 µm. Illustrations of cells in upper right corners depict the cell population which the cell is likely to belong to based on its appearance.

Change in membrane viscosity was monitored during freezing by using 9-dicyanovinyl julolidine (DCVJ) (Sigma-Aldrich). DCVJ is a molecular rotor that partitions into the membrane and its quantum yield is sensitive to membrane viscosity [271]. A 10 mM DCVJ stock solution in methanol was prepared and stored at -20°C. HFFs were incubated with 83 µM DCVJ for 30 minutes as 37°C. Images were collected on the Olympus BX50 fluorescent microscope every 1 °C during cooling and freezing.

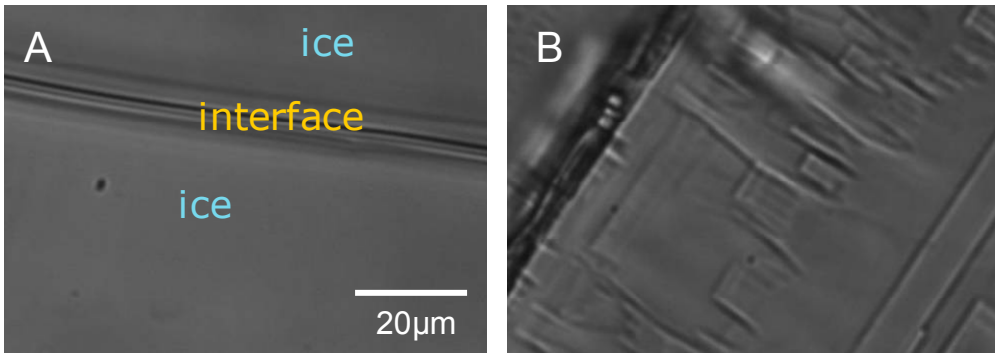

Figure 5.3: Ice crystal morphology at -30 °C in: a) PBS, and b) PBS + 5 w/w% PVA. Solutions were nucleated at -2 °C and cooled at 2 °C/min.

5.2.1.6 Statistical analysis

Statistical significance between data sets was determined at 5% significance level using the Student's t-test (two-sample test, assuming unequal variances). Statistical differences are marked with a *.

5.2.2 Results

Phase contrast microscopy conducted with HFFs suspended in media or 1xPBS solutions showed that after a slow freeze/thaw (2°C/min), most of the cells (96 ± 4%; n=3) had a darkened appearance under the microscope (Figure 5.2a). The number of darkened cells was greatest at slow thawing rates (96 ± 4% at 2°C/min versus 70 ± 1% at 130°C/min; n=3). Cells that experienced freeze/thaw in the presence of either DMSP or glycerol did not exhibit darkening but retained their pre-freeze appearance. A small population of the darkened cells frozen in media also showed distinct membrane blebs. Fluorescence analysis (using Hoechst and PI dyes) revealed that the blebbing behavior was observed in cells independent of whether they were PI^- or PI^+ (Figure 5.2b). The darkened cells that

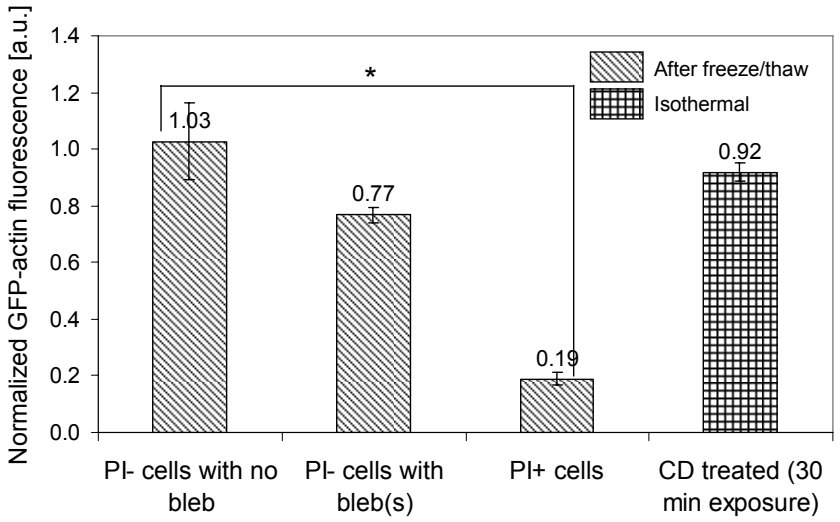

Figure 5.4 GFP-actin fluorescence intensity of cells before and 15 minutes after freeze-thaw to -8°C (n=2 for blebbing cells; n=3 for other conditions) and of cells treated with 10 μM CD for 30 minutes (n=3). Fluorescence is normalized with respect to initial value.

did not exhibit distinct blebs typically belonged to the PI^+ population. SEM (scanning electron microscopy) images of cells after freeze-thaw showed that while pre-freeze/thaw cells exhibited many ruffles or small villi on the surface of the cell (Figure 5.2c(I)), after freeze/thaw these ruffles were not present (Figure 5.2 c(II), c(III), c(IV)). In some cases, cells showed a very smooth exterior (Figure 5.2 c(II)), while some clearly showed disruption of the membrane (Figure 5.2c(III)) and some showed deformation of the membrane (Figure 5.2 c(IV)). SEM analysis suggested that the reason for the darkening of certain cells after freeze/thaw (Figure 5.2 c) could be a change in the membrane structure mainly, loss of fine membrane ruffles and formation of deformities on the membrane surface.

For freeze-thaw experiments where PVA was used to modify the structure of ice, the number of darkened cells increased from 70 ± 1 % to 83 ± 4 % (thaw rate = 130°C/min).

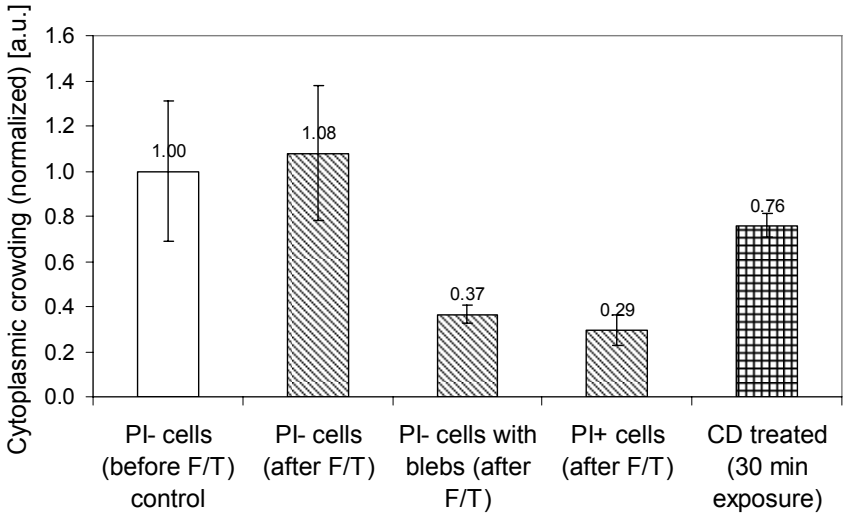

Figure 5.5 Cytoplasmic crowding as measured by CCVJ fluorescence readings taken at 22°C for cells before and immediately after freeze/thaw and of cells treated with 10 μM CD for 30 minutes. Sample was cooled at 2°C/min to -30°C and thawed 130°C/min to 22°C. Values of CCVJ fluorescence were normalized to pre-freeze values. Statistical differences ($p < 0.05$) are marked with *.

The increase in the number of darkened cells was accompanied by a dramatic decrease in viability with 91 ± 4 % of cells being PI^+ as compared to 43 ± 4 % for cells that were frozen and thawed in PBS. It should be noted that PVA did not cause any drop in viability of cells prior to freeze/ thaw. In PVA experiments, ice crystals initially formed in the large planar sheets observed in control experiments but at temperatures lower than -10 °C the appearance of smaller crystals with straight edges were observed (Figure 5.3). This result clearly indicates that PVA significantly altered that the ice crystal morphology.

Freeze/thaw experiments were performed using GFP-actin transfected cells in order to determine the effects of freeze/thaw on the actin cytoskeleton. GFP fluorescence from each cell was collected at room temperature right before freeze/thaw and at 0, 5, 10 and 15 minutes after the freeze/thaw. Freeze/thaw experiments were first carried out down to -8°C (NT = -0.5°C) in order to compare the results to the osmotic stress experiments. Additional experiments were carried out with cells that were frozen down to lower temperatures (-30°C) to further analyze the PI^+ cells (PI^+ cells increase in number at lower freezing temperatures). *In PI^- cells with no blebs*, GFP-actin fluorescence remained approximately unchanged with respect to the pre-freeze values (Figure 5.4). *In PI^- cells with blebs* a small decrease in the GFP-actin fluorescence was measured, which was attributed to a decrease in the intracellular filamentous actin content. The decrease in GFP fluorescence in PI^- cells with blebs was gradual with time post-thaw. The immediate post freeze/thaw fluorescence was comparable to pre-freeze values indicating that the cytoskeleton continued to depolymerize after thawing. The decrease of fluorescence in PI^- cells with blebs was greater than what was measured in cells whose actin cytoskeleton was partially depolymerized by exposure to CD for 30 minutes (Figure 5.4). *PI^+ cells* had the lowest levels of post-thaw GFP fluorescence. Note that the initial GFP fluorescence of the PI^+ cells immediately after freeze-thaw was approximately 0.5 but it decreased steadily with time to 0.19. This observation could be attributed to the loss of membrane integrity, which would cause release of intracellular monomeric actin and subsequently cause further depolymerization of the intracellular F-actin. Note that monomeric GFP

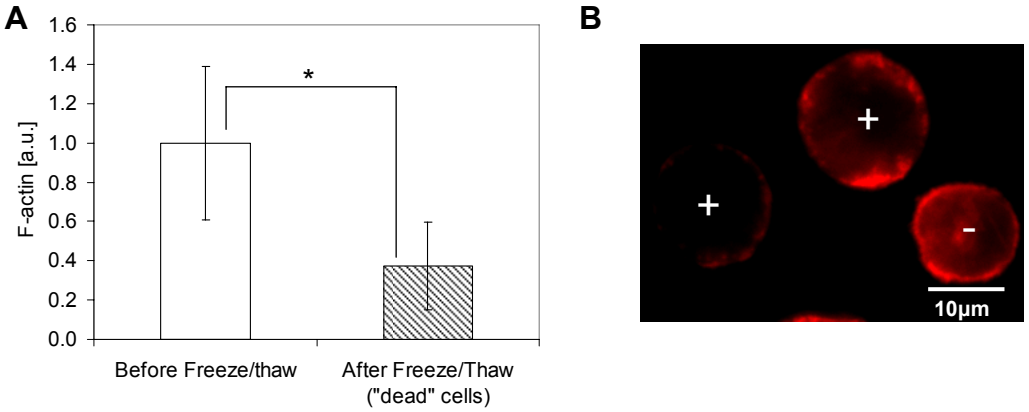

Figure 5.6 (a) Comparison of F-actin content for live cells (before freeze/thaw) and dead cells (after freeze/thaw) at room temperature as determined by rhodamine-phalloidin fluorescence intensity. A statistical difference ($p < 0.05$) is marked with *. n = 20 cells. Sample was cooled and thawed at 2°C/min to from 22°C to -30°C; (b) Typical morphology of actin cytoskeleton for membrane-compromised (+) cells and intact (-) cells. Membrane compromised cells were determined using the LIVE⁄DEAD® Fixable Blue Dead Cell Stain Kit from Invitrogen Corporation.

actin also fluoresces [272]. This may explain why the CD treated cells exhibit much higher GFP fluorescence than the *PI^+ cells.*

GFP-actin measurements (Figure 5.4) were also paralleled by the cytoplasmic crowding measurements in frozen/thawed cells conducted at lower temperatures (-30°C). These measurements (Figure 5.5) revealed a significant decrease in cytoplasmic crowding after freeze/thaw in *PI- cells with blebs* and in PI^+ cells. Similar to the results obtained from the GFP experiments, CCVJ fluorescence results showed that CD treatment caused a significant decrease ($p < 0.05$) in fluorescence intensity (Figure 5.5). However, the values for CD treated cells were still higher than those obtained from the *PI- cells with blebs* (Figure 5.5). The advantage of using a molecular rotor to monitor the degree of actin polymerization over GFP-actin fluorescence is that monomeric or very small filaments of actin are not expected to contribute significantly to crowding whereas they will still have

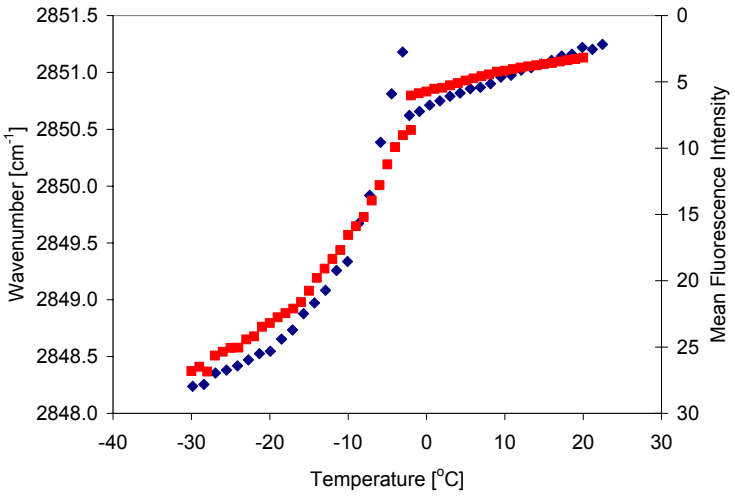

Figure 5.7 Change in DCVJ fluorescence (■) (n=150 cells) and νCH_2 band maxima (◆) (n=3 experimentss) with temperature for cells under going freezing

a high contribution to GFP fluorescence (Figure 5.4). In terms of specific structural breakdown of the actin cytoskeleton after freeze/thaw, fluorescent staining of actin filaments further revealed that membrane-compromised cells exhibited a decrease in the amount of actin filaments and a "spotted" actin ring versus the continuous cortical ring seen in "live" cells (Figure 5.6). This result again suggests that actin depolymerization is correlated with membrane damage (loss of semi-permeability).

5.2.2.1 The cell membrane response to freeze/thaw

Change in the cell membrane state during freeze/thaw was investigated using FTIR spectroscopy and during freezing using DCVJ fluorescence. Changes in the membrane lipid conformational disorder were determined by monitoring the change in the location of the lipid acyl chain νCH_2 stretching band located at approximately 2850 cm^{-1}. With a

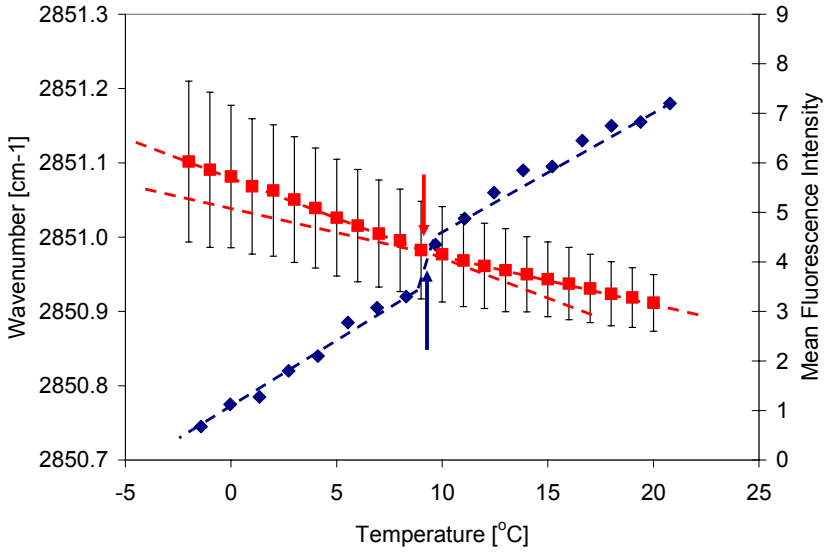

Figure 5.8 DCVJ fluorescence (■) (n=67 cells) and FTIR νCH_2 band maxima (◆) with temperature for during cooling. Both DCVJ and FTIR data show a small thermotropic phase transition indicated by arrows

decrease in temperature there was a decrease in lipid conformational order as measured by the decrease in the νCH_2 stretching band. The decrease in lipid order was matched by an increase in membrane viscosity as measured by DCVJ fluorescence (Figure 5.7). It was also observed that near 9 °C there was a breakpoint in both the FTIR and DCVJ data which indicates a small membrane phase transition (Figure 5.8).

The change in lipid order of cells exposed to freeze/thaw either in the presence or absence of a cryoprotectant (10% glycerol or 10% DMSO) was also quantified. Cells treated with glycerol had lower νCH_2 values than the cells treated with Me_2SO at both supra- and sub-NT regions (Figure 5.9). In the sub-NT region, the cells frozen in the absence of any cryoprotectant had the lowest νCH_2 values. A low νCH_2 wavenumber indicates an increase in the packing of the membrane lipids (with a resulting cell volume

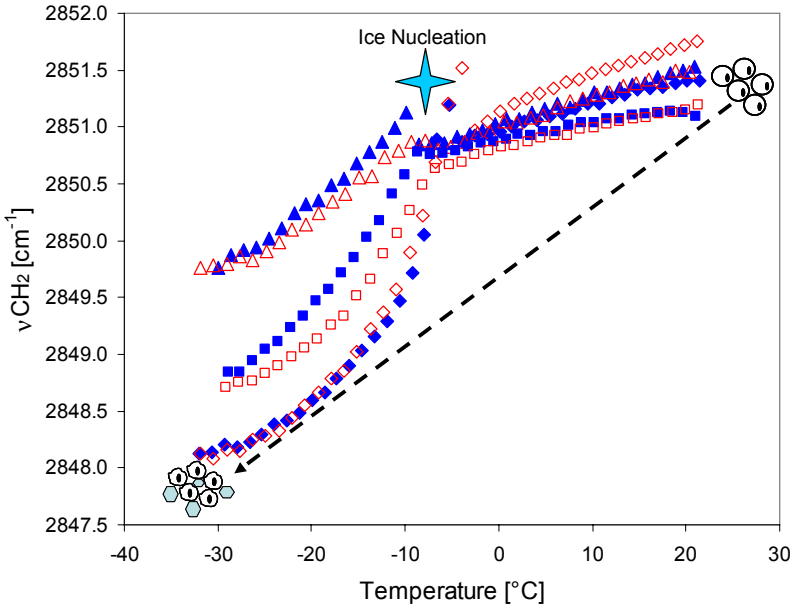

Figure 5.9 Change in νCH_2 band maxima with temperature for cells under going freeze-thaw with cryoprotectant (▲,△10% DMSO; ■,□10% glycerol) and without cryoprotectant (◆,◇ media). Filled symbols represent cooling while open symbols represent warming

decrease). These results meant that the cells frozen in the absence of a permeating cryoprotectant experienced the largest decrease in volume during freezing (Figure 5.9).

Comparison of pre- and post-thaw FTIR measurements demonstrated an increase in the νCH_2 band location ($\Delta\nu CH_2 = 0.3 \pm 0.02$ cm^{-1}) corresponding to a decrease in lipid order in the absence of DMSO or glycerol (Figure 5.10). DMSO treated cells that underwent freeze-induced dehydration exhibited a very different behavior by returning back to a similar lipid conformational state/membrane structure as before freeze/thaw (Figure 5.10). This behavior was also observed in glycerol treated cells despite the fact that these cells at room temperature had different νCH_2 values from the DMSO treated cells. Post-thaw viability (determined by dead/live fluorescence using Hoechst and PI) was 98 ± 1% and 99 ± 2% for DMSO and glycerol samples, respectively, whereas cells without

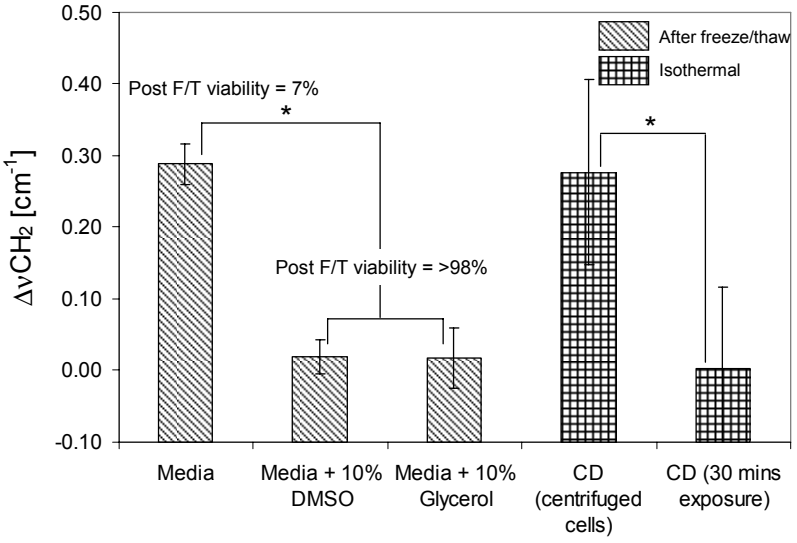

Figure 5.10 Difference in νCH_2 band maxima at room temperature for cells under going freeze-thaw with and without cryoprotectant and for cells treated with CD that did not undergo freeze/thaw. n=3 for each experimental condition.

cryoprotectant had a viability of 7 ± 1%. These results showed that little or no change in the membrane lipid order with freeze/thaw corresponded to high post-thaw viability. The change in νCH_2 values for media samples can be attributed to partial disruption of the cell membrane leading to a highly fluid bilayer.

Two sets of experiments were conducted to analyze the membrane structure of cells with partially depolymerized actin cytoskeleton. In the first set of experiments, 10 μM CD treated cells were centrifuged at room temperature and their IR spectra were compared to untreated centrifuged cells. In the CD treated sample, there was a decrease in the lipid conformational order ($\Delta\nu CH_2 = 0.3 \pm 0.1$ cm^{-1}) with centrifugation, similar to what was seen in cells that experienced freeze/thaw in the absence of any cryoprotectant. In the second set of experiments, untreated centrifuged cells in 1xPBS were sandwiched between two CaF_2 windows and the extracellular solution was gradually changed to

1xPBS + 10 μM CD while IR data were collected. In this experiment there was no significant decrease in the lipid conformational order during the incubation period with CD ($\Delta\nu CH_2 = 0.0 \pm 0.1$ cm^{-1}). The difference in response observed between the two sets of experiments show that the cell membrane is more susceptible to destabilization/structural changes due to mechanical forces (such as those generated during centrifugation) when the cytoskeleton is partially depolymerized. The propensity for destabilization may also be responsible for the slightly higher incidence (8% versus 2% of cell population) of IIF (data not shown) and comparatively higher νCH_2 values at lower temperatures ($\Delta\nu CH_2$ at -30°C = ~0.5 cm^{-1}) for cells treated with CD that underwent freezing. The similarity in the $\Delta\nu CH_2$ values obtained from the cells that underwent freeze/thaw in the absence of a cryoprotectant ($\Delta\nu CH_2 = 0.3 \pm 0.02$ cm^{-1}) and the centrifuged C treated cells ($\Delta\nu CH_2 = 0.3 \pm 0.1$ cm^{-1}) (note that these cells were not exposed to freeze/thaw) may indicate that damage to the cytoskeleton during freeze/thaw directly impacts the membrane structure and its susceptibility and therefore causes irreversible membrane damage

5.3 PART II – FREEZE/THAW IN PEG SOLUTIONS

In this part of the study, we subjected a mammalian cell, human foreskin fibroblast (HFF), to freeze/thaw stresses using PEG 600 and PEG 200. PEG 600 was chosen in order to reduce solute uptake and also compare results to those obtained from osmotic stress experiments in Chapter 4. In order to investigate the role of the cytoskeleton, cells

were treated with Y27632 in order to decrease the cytoskeletal stiffness and also with WGA which increases the stiffness of the membrane.

5.3.1 Materials and methods

The objective of this study is to elucidate the role of the membrane-cytoskeleton complex on the freeze/thaw response of mammalian cells. Cellular response was determined using by: (1) basic microscopic analysis of the changes in cell morphology (including volume change and blebbing); (2) Viability using PI stain; (3) Scanning electron microscopy. Cell culture was performed using the same method as outlined in Chapter 4.

5.3.1.1 Freeze/thaw experiments

HFFs were subjected to freeze/thaw conditions using the Linkam cooling stage (Figure 5.1b). Cells that underwent the freeze/thaw cycle were suspended either in media, 11% (300 mOsm) PEG 600 or 5.5% (300 mOsm) PEG 200. The cooling rate for all experiments was the same at 2°C/min. Cells were either cooled to -20 °C or -80 °C and then warmed back up to 23°C at 130 °C/min. Ice was nucleated at -2 °C and then the solution was warmed until most of ice had disappeared and then the sample was cooled to its end temperature. Viability was assessed immediately after freeze/thaw by propidium iodide (PI) uptake (PI was present in the extracellular solution at all times).

5.3.1.2 Increase in membrane stiffness using wheat germ agglutinin

In order to increase the mechanical stability of the cell membrane WGA (1 μg/ml) was added to the cell suspension at least 10 minutes prior to freeze/thaw. WGA has been shown to increase the stiffness of red blood cell membranes [273]. Some researchers have

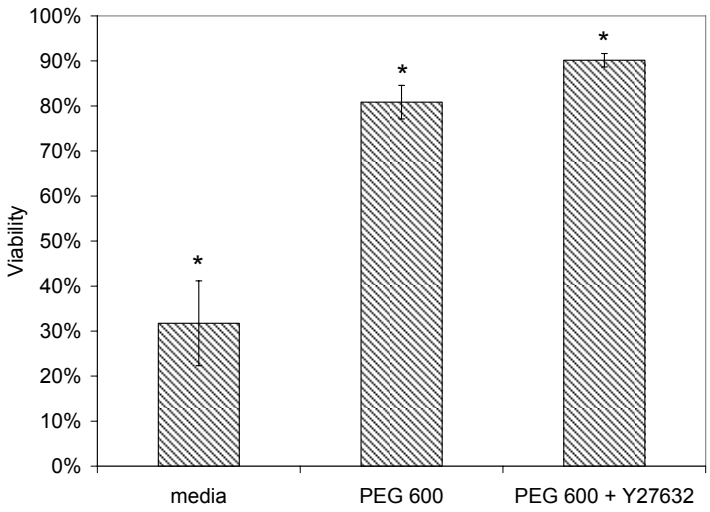

Figure 5.11 Post-thaw cell viability for cells that were cooled and thawed at 2°C/min to from 22°C to -20°C. n=3

attributed the action of WGA in red blood cells to increased cytoskeleton-membrane adhesion [274] while others have argued that it is due to WGA cross-linking of glycoproteins and glycolipids in cell surface [275].

5.3.1.3 Decreasing the cytoskeleton stiffness

In select freeze/ thaw experiments the stiffness of the cytoskeleton was decreased using 20 μM Y27632. The cells were incubated with Y27632 at room temperature for 30 minutes prior to the freeze/ thaw experiment.

5.3.1.4 Scanning electron microscopy

Cells were suspended in either 300 mOsm PEG 200 or 300 mOsm PEG 600. A small amount of glutaraldehyde (0.15 w/w % and 0.09 w/w% for PEG 600 and PEG 200 solutions respectively) was added to the cell suspension such that upon reaching -20 °C the concentration would be approximately 1% in the freeze concentrated solution. The

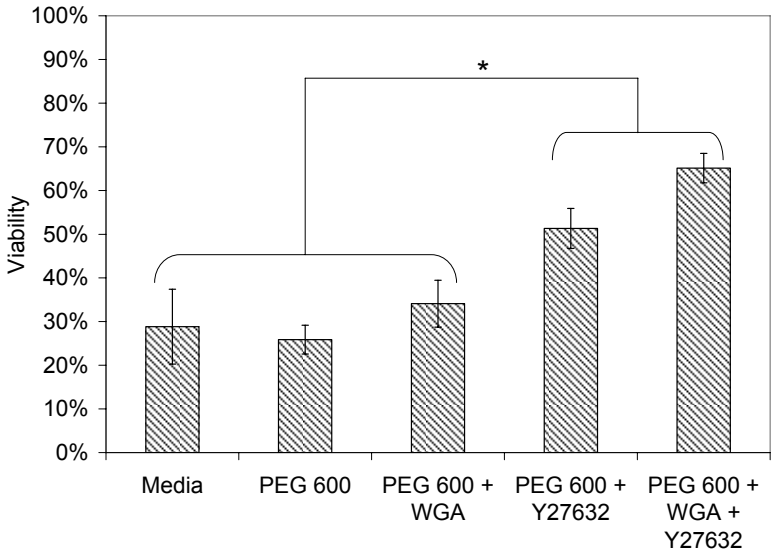

Figure 5.12 Post-thaw cell viability for cells in media and various 300 mOsm PEG 600 solutions that were cooled at 2°C/min to from 22°C to -20°C and thawed at 130°C/min. n≥3

sample was held at -20 °C for 10 minutes to ensure fixation. The sample was then returned to room temperature at 130 °C/min and the normal SEM fixation procedure was followed (see Chapter 4).

5.3.1.5 Statistical analysis

Statistical significance between data sets was determined at 5% significance level using the Student's t-test (two-sample test, assuming unequal variances). Statistical differences are marked with *.

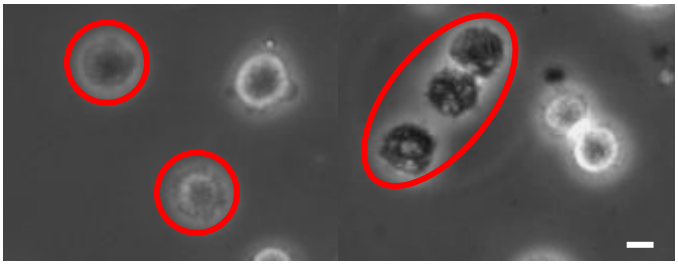

Figure 5.13 Appearance of PI^+ cells in PEG 600 (left) versus media (right). PI^+ cells are outlined in red. The scale bar represents 10 μm.

5.3.2 RESULTS

Cells were first frozen in 300 mOsm PEG 600 in order to investigate if increasing the unfrozen fraction would have an effect on post-thaw viability. It was found that when freezing to moderate temperatures (-20 °C) there was a large (significant) increase in viability when compared to cells in media (Figure 5.11). This viability increased slightly (but significantly) upon the addition of Y27632. However, when cells were frozen to -80 °C there was no significant difference in viability for the cells in media and the cells in

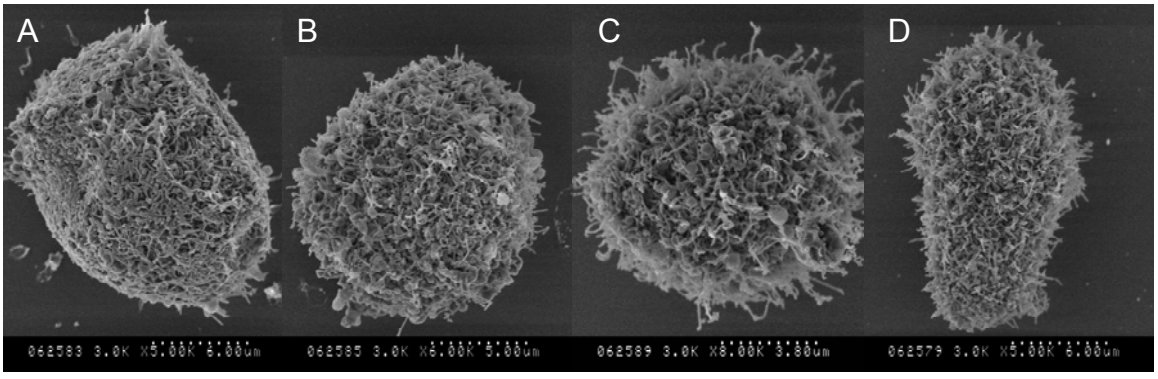

Figure 5.14 SEM images of HFFs frozen to -20 °C in 300 mOsm PEG 600

PEG (Figure 5.12). In terms of appearance, there were very few darkened cells in the PEG sample, even for samples frozen to -80 °C. Instead, they were mostly gray (Figure 5.13) and many (27 ± 6 %) cells (both PI^- and PI^+) exhibited blebs. It was also observed that PI fluorescence was not as pronounced in the cells from PEG samples as compared to the cells in media samples. This may indicate that the cells from PEG samples experienced a lesser degree of damage to the membrane during freeze/thaw. It was also observed that the cell size decreased for cells frozen in PEG 600 solutions with both dead ($p=0.08$) and alive ($p=0.02$) cells being smaller (10% and 14% smaller respectively) than cells before freeze/ thaw. The addition of Y27632 yielded a significant increase in viability (Figure 5.12) indicating that changes in the cytoskeleton structure affects post-thaw viability. Analysis of the PEG 600 + Y27632 samples showed that there was a significant decrease in the number of blebbing cells (9 ± 2 %) after freeze/thaw. While 1μg/ml WGA had no effect on post-thaw viability it was observed that the combination of WGA and Y27632 yielded a significant increase in viability (Figure 5.12).

SEM images of cells frozen in PEG 600 to -20 °C showed that cells were very distorted in shape (Figure 5.14:A & D) and that there were many membrane projections in the form of very small blebs and microvilli (Figure 5.14) (similar to the membrane morphology observed for osmotically stressed HFFs at low temperatures in Chapter 4).

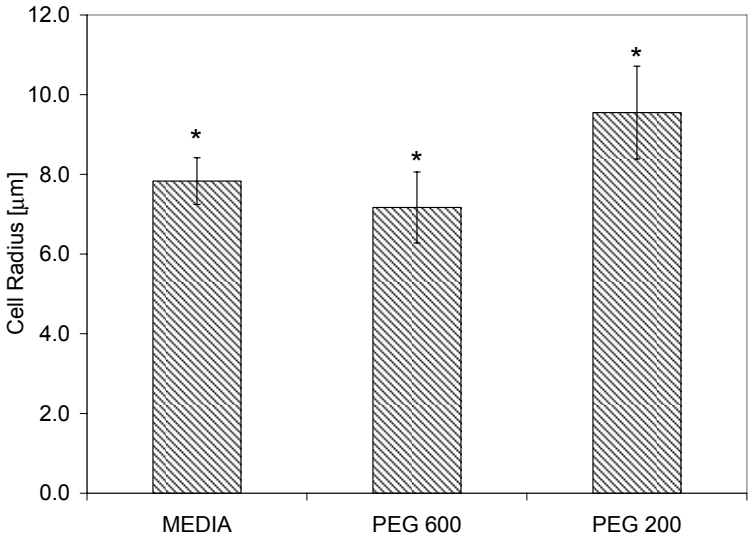

Figure 5.15 Comparison of cell radii for cells in media, 300 mOsm PEG 600 and 300 mOsm PEG 200.

When cells were placed in 300 mOsm PEG 200 there was a significant increase in size (Figure 5.15). This is likely due to uptake of PEG 200 which has also been shown for Jurkat lymphocytes [244]. The viability of cells frozen in 300 mOsm PEG 200 to -80 °C was greater than that of samples in 300 mOsm PEG 600. Addition of Y27632 did not significant affect post-thaw viability (Figure 5.17). Addition of 1µg/ml WGA yielded a significant increase in viability (Figure 5.17). Cells frozen in PEG 200 had a 25% (n=50 cells) larger diameter (making the cells almost twice as large) than those frozen in PEG 600 when measured at-20°C. This is likely a result of the uptake of PEG 200, which would not be transported out of the cell during freeze-induced dehydration. The appearance of dead cells in PEG 200 was reminiscent of those in media samples where darkened cells corresponded to dead cells. It was also observed that the cell size for dead cells did not vary from before freeze/ thaw cells sizes. However, live cells after freeze/

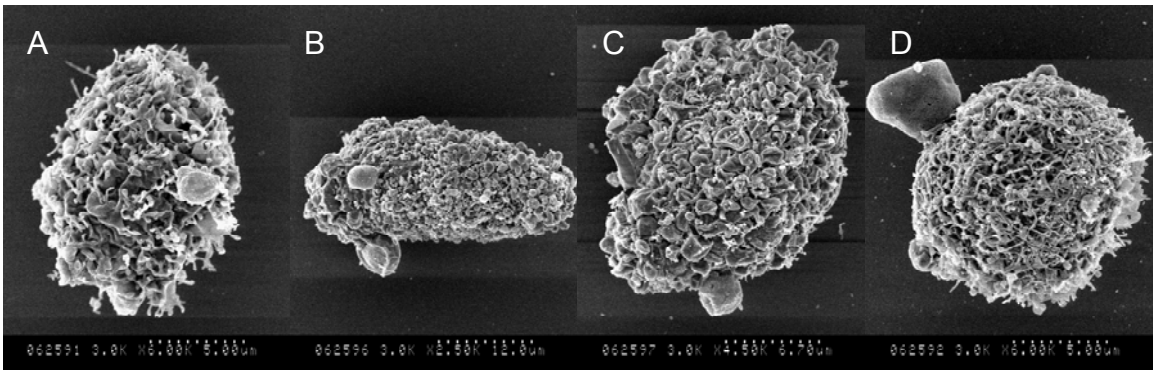

Figure 5.16 SEM images of HFFs frozen to -20 °C in 300 mOsm PEG 200

thaw had a 38% reduction in size ($p < 0.05$). Interestingly, cells in PEG 200 did not bleb upon thawing in contrast to PEG 600 samples.

SEM images of cells frozen in PEG 200 to -20 °C again showed that cells were distorted during freezing (Figure 5.16). Similar to the PEG 600 sample cells also had membrane projections in the form of small blebs but not as many microvilli. Addition of WGA increased viability from 66% to 77% (Figure 5.17). Addition of Y27632 did not have a significant effect on post-thaw viability but when combined with WGA post-thaw viability increased to 84% (Figure 5.17).

It was observed that WGA affected dissociation of the membrane from the underlying cytoskeleton. This was done by exposing cells to water, with and without WGA and quantifying the amount of blebbing after 1 minute. It was observed that the population of blebbing cells in water with WGA (33%) was significantly smaller ($n=3$; $p<0.05$) than control cells in water (76%).

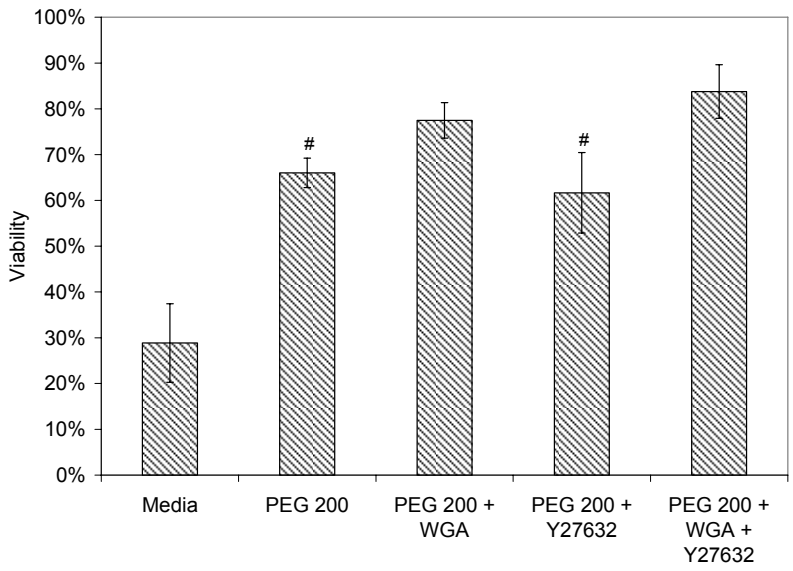

Figure 5.17 Post-thaw cell viability for cells in media and various 300 mOsm PEG 200 solutions that were cooled at 2°C/min to from 22°C to -20°C and thawed at 130°C/min . Groups marked with # are not statistically different. All other groups are statistically different ($p<0.05$).

5.4 DISCUSSION

The formation of blebs is just one manifestation of cell membrane/cytoskeleton response to osmotic stresses (See Chapter 4). Other more subtle changes were observed when cells were exposed to freeze/thaw stresses. For example, membrane ruffles disappeared (Figure 5.2c(II)) after freeze/thaw suggesting that some membrane material might be lost or not reincorporated into the membrane during a freeze/thaw cycle (observed previously in non-acclimated protoplasts [168]). Any loss of membrane material would inhibit volumetric expansion of the cell during thawing.

The increase in the number of darkened cells at slow thawing rates may indicate the interaction with growing ice crystals is partly responsible for damage to the cell

membrane. At slow thawing rates it is expected that there will be ice recrystallization which will allow for changes in the ice morphology and therefore changes in ice-cell interaction. The absence of darkened cells in experiments where cells were frozen to -80 °C in 300 mOsm PEG 600 suggest that PEG was able to minimize direct ice crystal interaction with the membrane. This is further supported by experiments with 300 mOsm PEG 200 which show that a lower amount of PEG (5.5 % w/w for PEG 200 versus 11 % w/w for PEG 600) resulted in PI^+ cells having the same darkened appearance as seen for cells with slow thawing rates. Two possible reasons for a reduction in ice-membrane interaction are: 1) an increase in the unfrozen fraction [264]; or 2) some specific interaction between PEG 600 and ice such as adsorption of PEG onto the ice surface. There is evidence both for PEG interaction with ice [276] and against it [265].

The increase the number of darkened and PI^+ for cells frozen in the presence of PVA also suggest that the ice crystal morphology may have a role to play in the cell damage that occurs during freezing. This destruction of cells during freezing has also been observed for anti-freeze proteins, which like PVA, also adsorbs to the prism faces of ice crystals. The presence of anti-freeze proteins has been found to promote cell injury during freezing of erythrocyte glycerol solutions [277] and hydroxyl ethyl starch solutions [278]. The mechanism behind the anti-freeze protein-ice mediated injury in these studies was attributed to enhanced ice-cell interaction due to either mechanical damage by smaller spicular ice crystal formations [277] or preferential ice growth around the cells [278]. In our experiments, we observed the formation of small ice crystals which would increase the area available for ice-cell interaction and possibly promote mechanical

damage of the cell membrane. Alternatively, PVA may have an unknown cryotoxicity effect on cells. However, this alternative seems less likely as PVA is used as a biocompatible material [279] and exposure to PVA did not show any effect on viability of cells prior to freeze/thaw.

Another form of damage that may have occurred during freeze/thaw or during an osmotic stress cycle is due to the membrane phase change between gel and liquid crystalline states. It was observed previously that the post-rehydrated viability of dried *Geobacter sulfurreducens* decreased if the membrane underwent a phase change during rehydration [280]. Our FTIR data shows that it is impossible to avoid phase change (indicated by the change in wavenumber values during freezing or thawing) during slow freeze/thaw of HFFs. However, cryoprotectants do reduce the magnitude of phase change. This may be one mechanism by which cryoprotectants alleviate membrane damage during freeze/thaw. It has been shown that increase in lipid order is related to the decrease in cell volume, which is due to water transport out of the cell during slow freezing [281]. Therefore, it would be expected that permeating cryoprotectants would reduce the magnitude

There may be different mechanisms responsible for the observed depolymerization of actin in membrane-compromised (PI^+) cells. One of the reasons mentioned earlier is that actin monomers would be able to exit the cell thereby reducing the favorability of actin filaments. Another reason could be that the damage to the membrane affects the actin polymerization directly due to the actin polymerization promoters (e.g. phosphatidylinositol 4,5-bisphosphate [282]) that exist in the membrane. Actin

depolymerization could also be due to the release of proteases from freeze/thaw damage to intracellular organelles [283, 284]. While this possibility does exist, it seems unlikely as no significant changes to the actin cytoskeleton were seen in PI^- cells for which damage to intracellular organelles should also have occurred.

The increased incidence of blebbing in cells frozen in PEG 600 versus PEG 600 + Y27632 indicates that freezing does have an effect on the cytoskeleton. In Chapter 4 we saw that solute uptake was responsible for bleb growth and that various cytoskeletal drugs were unable to change the outcome. In these experiments, bleb growth is inhibited by Y27632 which indicates that the cytoskeleton is involved. Y27632 reduces bleb growth by reducing the stiffness of the cortical cytoskeleton [59]. These results therefore suggest that cells, which were frozen in PEG 600, did increase in stiffness and this increase was not reversible during thawing. Freezing-induced increase in cell stiffness has been previously observed for mouse oocytes [63]. These results indicate a possible role of cell stiffness in freeze/thaw outcome.

The increase in post-thaw viability for cells frozen in the presence of PEG 200 (Figure 5.17) as compared to cells frozen in the presence of PEG 600 (Figure 5.12) suggest that cell shrinkage is a factor in determining post-thaw viability. It was also observed that while Y27632 had a beneficial effect on post-thaw viability with PEG 600, it did not have a significant effect with PEG 200. This may indicate that both the Y27632 and the PEG 200 act to reduce the same mechanism of damage. In Chapter 4 it was observed that membrane morphology was drastically altered by Y27632 when the cell was in a osmotically stressed state. Results from this chapter demonstrate that PEG 200 also alters

membrane morphology during freezing. We suggest that the alteration in membrane morphology in both cases is linked to the increase in viability.

5.5 CONCLUSION

Our data showed that freeze/thaw stresses altered the cell membrane morphology resulting in a loss of membrane material for cells frozen in media. We also observed that membrane damage was accompanied by damage to the cytoskeleton during freeze/thaw. Based on our results, we suggest that acute damage to the cell membrane of HFFs during slow freezing is primarily related to two factors:

1. Interaction with ice – this likely results in mechanical forces such as compression and shear which would damage the cell. The interaction with ice can be decreased, by increasing the unfrozen fraction, or enhanced by using PVA to alter the ice crystal morphology.

2. Cell shrinkage and resulting membrane morphology – the greater the cell shrinkage the more membrane material would go into membrane protrusions/ projections. Damage to the cell may ne due to either the protrusions being sensitive to damage by adjacent ice crystals or perhaps the protru are not retracted during cell expansion when thawing.

Damage to HFFs during slow freezing can be reduced by decreasing the stiffness of the cytoskeleton and increasing the stiffness of the cell membrane. In chapter 4, we observed that decreasing the stiffness of the cytoskeleton resulted in a drastic change in the membrane morphology in the dehydrated state. This interaction between the cytoskeleton and the membrane and its relation to damage during freezing (and osmotic stress at low temperatures) is discussed further in the following chapter.

CHAPTER 6: MECHANISMS AND MODELS OF DEHYDRATION- AND SLOW FREEZING-INDUCED DAMAGE

6.1 SUMMARY

In chapter 4, we observed that dehydration-induced damage involved cell shrinkage, the stiffness of the cytoskeleton, formation of surface defects, and lipid desorption from the membrane. One objective of this chapter is to propose a model to explain the formation of surface defects and lipid desorption during dehydration. We also discuss in further detail the possible links between cell shrinkage, cytoskeletal stiffness and membrane morphology and their effect on dehydration- and freeze/thaw-induced damage to the cell membrane.

Based on the results of the fluorescence experiments conducted to measure the formation of surface defects and lipid desorption a thermodynamic model is proposed. In this chapter, it is shown that the rate of partitioning of the FM1-43 dye into the membrane is directly related to the chemical potential of water. Analysis of similar data in the literature for osmotically stressed liposomes [247] using a structurally similar dye, Merocyanine 540, show a similar relationship. These results can be explained by expanding on the transition state model developed by Aniansson et al [166] to describe amphiphile monomer-micelle dissociation. We suggest that formation of the transition state for adsorption/ desorption of membrane constituents is strongly related to the chemical potential of water and that the observed “surface defects” is related to formation

of this transition state. This model along with concepts from irreversible thermodynamics is used to explain observations from Cellmask™ experiments. In this expanded model, the entropy generation during water transport provides an additional "energy" to overcome the energy barrier in the formation of the transition state.

During slow freezing, the above thermodynamic mechanism would be reduced due to reduction in temperature as well as a reduction in rate of dehydration. We suggest that the stiffness of the cytoskeleton affects: (i) the morphology of the membrane in the dehydrated state, and (ii) the availability of membrane material for re-expansion of the cell either during return to isotonic conditions or during thawing.

6.2 THERMODYNAMIC MECHANISMS OF DAMAGE

We propose that the formation of surface defects and lipid desorption can be explained using a model based on thermodynamics and reaction rate theory. This mechanism, termed the "slow dehydration damage", is related to changes in hydration at the bilayer surface. This model can be expanded upon using non-equilibrium irreversible thermodynamics to qualitatively understand the damage caused when a large osmotic gradient is present. The second mechanism, termed the "fast dehydration damage", is thought to be due to the effect of water transport across the bilayer and its effect on the structure of the bilayer.

6.2.1 SLOW DEHYDRATION DAMAGE

In chapter 4 experiments with the FM1-43 dye show that an increase in osmotic pressure increased the rate at which the dye partitions into the membrane. We also observed that the rate at which CellMask desorbed from the membrane increased with an increase in osmotic pressure. In order to interpret this adsorption and desorption of lipid-like molecules from the membrane, the kinetic/thermodynamic model developed by Aniansson et al [166] that describes amphiphile monomer-micelle dissociation was used. This model was used previously in the literature to describe amphiphile desorption from micelles and bilayers [285, 286], as well as insertion of a fluorescent phospholipid derivative into the lipid bilayer [287]. In this model, the rate constant of lipid desorption, k_d, is given by

$$k_d = \frac{D}{l^2}\exp\left[-\Delta G_d^{\neq o} / RT\right] \tag{6.1}$$

Where D is the diffusion constant for the lipid leaving the bilayer, $\Delta G_d^{\neq o}$ is the maximum energy barrier to lipid dissociation, l is the width of the energy barrier. For reference, Nichols et al [285] used l = 0.7 Å for D = 5 x 10^{-6} cm^2s^{-1}. Similarly, the rate constant for adsorption is given by

$$k_a = \frac{D}{l^2}\exp\left[-\Delta G_a^{\neq o} / RT\right] \tag{6.2}$$

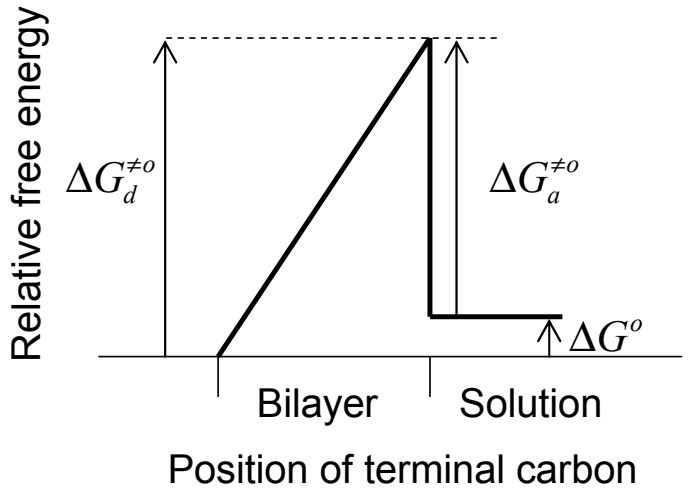

Figure 6.1 Free energy diagram describing lipid desorption/ adsorption process. Adapted from [285]. $\Delta G_d^{\neq o}$,and $\Delta G_a^{\neq o}$,represent the free energy for desorption and adsorption respectively.

where $\Delta G_a^{\neq o}$ is the maximum energy barrier to lipid adsorption. The energetics for lipid desorption/adsorption can be described by a free energy-reaction coordinate diagram (Figure 6.1). In this model the transition state formed at the top of the energy barrier is the same in either lipid desorption or lipid adsorption although the free energy contributions differ in each process. The transition state is taken to be when a lipid is almost totally out of the bilayer such that two cavities exist, one in the bilayer and one in the aqueous phase [285]. The formation of the transition state during desorption requires the disruption of lipid-lipid van der Waals forces and electrostatic head-group interactions which is enthalpically unfavorable [285-287]. Also, water-water hydrogen bonds must be broken to accommodate the lipid acyl chain when it is in the aqueous phase, an enthalpically unfavorable configuration [285-287]. There is also an unfavorable entropic contribution from the ordered water layer formation around the acyl chains [285-

287]. There is a favorable entropic contribution due to the disorder created in the bilayer. The formation of the transition state during the adsorption process involves disruption of the bilayer packing, removal of the ordered water molecules at the bilayer-solution interface and partial removal of the ordered water layer formation around the acyl chains, all of which are entropically favorable. As stated above for the desorption process, the disruption of the bilayer will be enthalpically unfavorable. These various contributions to the free energy of the transition state suggests that factors such as membrane phase, acyl chain length and water structure will affect the desorption and adsorption of lipids. This is in accordance with observation by Arroyo et al [75] where MC540 partitioning was dependent on whether the vesicle was in gel or liquid crystalline phase before osmotic shock.

In order to link the change in osmotic pressure with a change in the energy level of the transition state we use the Gibbs-Duhem equation. This approach is the indential to that employed by McGrath [129, 164] to model hemolysis of osmotically stressed erythrocytes except in his model only lipid desorption was assumed and analyzed. The Gibbs-Duhem equation is given by

$$0 = VdP - SdT - \sum_j n_j d\mu_j - Ad\gamma \tag{6.3}$$

For constant pressure and temperature and ignoring surface tension effects,

$$0 = -\sum_j n_j d\mu_j \tag{6.4}$$

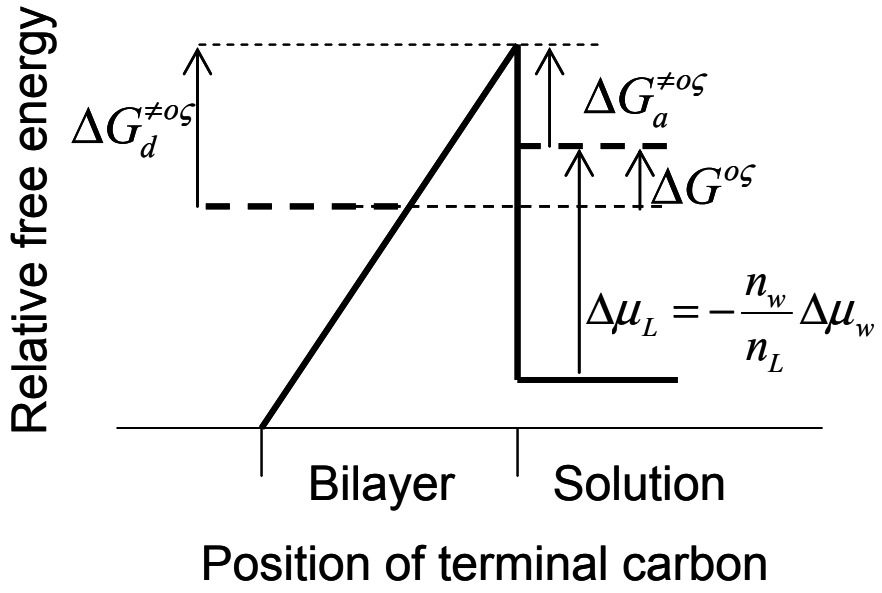

Figure 6.2 Free energy diagram describing lipid desorption/ adsorption process when there is a change in the chemical potential of water

In the membrane and in the solution, water is the dominant species on a molar basis and undergoes a large change in chemical potential with the addition of solute in the solution. Assuming negligible surface tension effects, the change in chemical potential for lipids either in the membrane or in solution is given by,

$$\Delta\mu_L = -\frac{n_w}{n_L}\Delta\mu_w \qquad (6.5)$$

Where μ_L represents the chemical potential of water and the ratio $\frac{n_w}{n_L}$ is the number of molecules of water per lipid that is involved in the formation of the transition state. This ratio will change according to the process, i.e. adsorption or desorption, since the formation of the transition state in each process differs.

Analyzing the adsorption process, we see from Figure 6.2 that if there is a change in the chemical potential of the water the new Gibb's free energy for the adsorption process, $\Delta G_a^{\neq \zeta o}$, is given by

$$\Delta G_a^{\neq \zeta o} = \Delta G_a^{\neq o} - \left(-\frac{n_w}{n_L} \Delta \mu_w \right) \tag{6.6}$$

For simplicity if we use the negative change in chemical potential of water (i.e. the reduction in the chemical potential of water), this becomes

$$\Delta G_a^{\neq \zeta o} = \Delta G_a^{\neq o} - \frac{n_w}{n_L} \Delta \mu_w \tag{6.7}$$

Substitution Eq. 6.7 into Eq. 6.2, we get

$$k_a = \frac{D}{l^2} \exp\left[-\Delta G_a^{\neq \zeta o} / RT \right] = \frac{D}{l^2} \exp\left[-\left(\Delta G_a^{\neq o} - \frac{n_w}{n_L} \Delta \mu_w \right) / RT \right] \tag{6.8}$$

Taking the negative natural log we get

$$-\ln k_a = \left(-\ln \frac{D}{l^2} + \frac{\Delta G_a^{\neq o}}{RT} \right) - \frac{1}{RT} \frac{n_w}{n_L} \Delta \mu_w \tag{6.9}$$

which is the equation of a straight line.

If we examine the partitioning of the FM1-43 dye into the membrane, we can determine the rate constant (k) of partitioning using

Table 6.1 Rate Constants for FM1-43 dye partitioning at various osmotic pressures for data shown in Figure 4.14

Osmotic Pressure [MPa]	10	15	20	30
Rate Constant [10^4 s^{-1}]	2.78	5.92	10.4	36.8

$$\frac{I - I_\infty}{I_i - I_\infty} = e^{-kt} \qquad (6.10)$$

where I_i and I_∞ are the intensities at t = 0 and t $\rightarrow \infty$, respectively. The rate constants obtained are given in Table 6.1. Since there was very little dye in the membrane, the measurements of fluorescence intensity relate only to how much dye partitioned into the

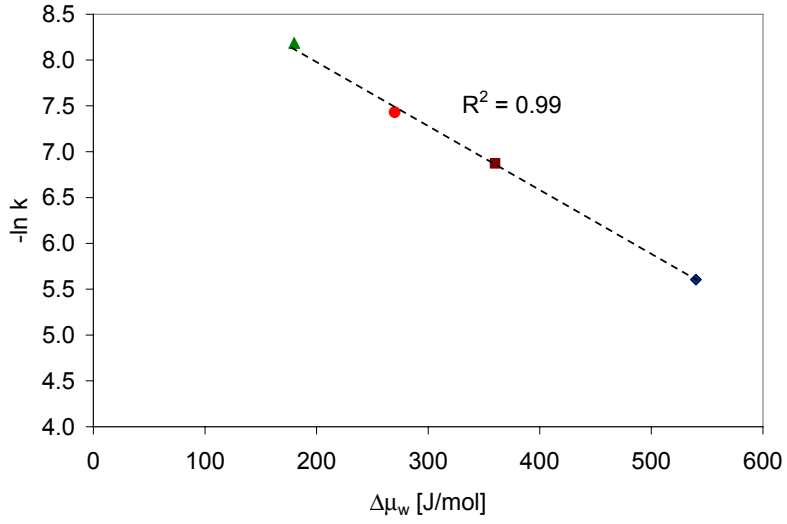

Figure 6.3 Plot of the negative natural log of the rate constant of FM1-43 dye insertion during osmotic stress versus the decrease in the chemical potential of water for (▲) 48.3% w/w (Π=10MPa), (●) 54.7% w/w (Π=15MPa), (■) 59.6% w/w (Π=20MPa), (◆) 67% w/w (Π=30MPa) PEG 600

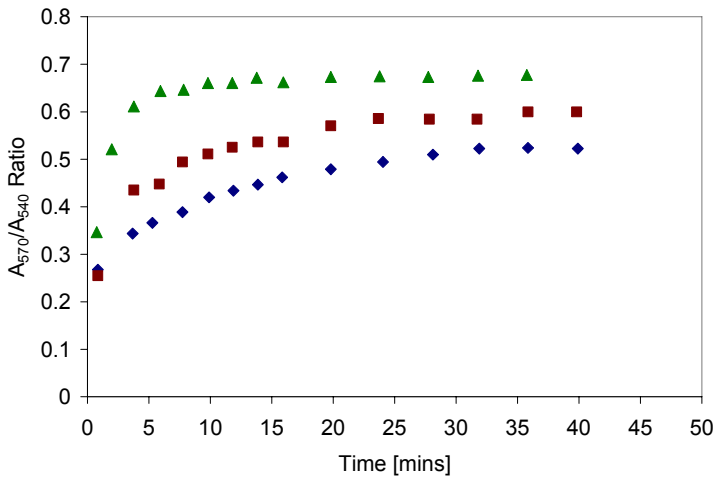

Figure 6.4 Abuin et al [247] data for partitioning of MC540 into DPPC vesicles. The amount of dye in the membrane is directly related to the A_{570}/A_{530} ratio.

membrane. When the negative natural logarithms of the rate constants are plotted with respect to the reduction in the chemical potential of water, where the reference state is pure water, a straight line is obtained with a coefficient of determination, R^2, value of 0.99 (Figure 6.3). This is highly indicative that the main driving force for the partitioning of the FM1-43 dye into the membrane during hyperosmotic stress in the chemical potential of water as predicted by Eq. 6.8.

In the literature, another dye, Merocyanine 540 (MC540), has shown a similar behavior with osmotically stressed large vesicles composed of dipalmitoylphosphatidylcholine (DPPC) lipids [247] (Figure 6.4). Using the data from the literature (Figure 6.4), the rate constants for MC540 partitioning into the lipid bilayer could also be obtained by fitting the data to Equation 6.1 (Figure 6.5). Again a very good coefficient of determination, R^2,

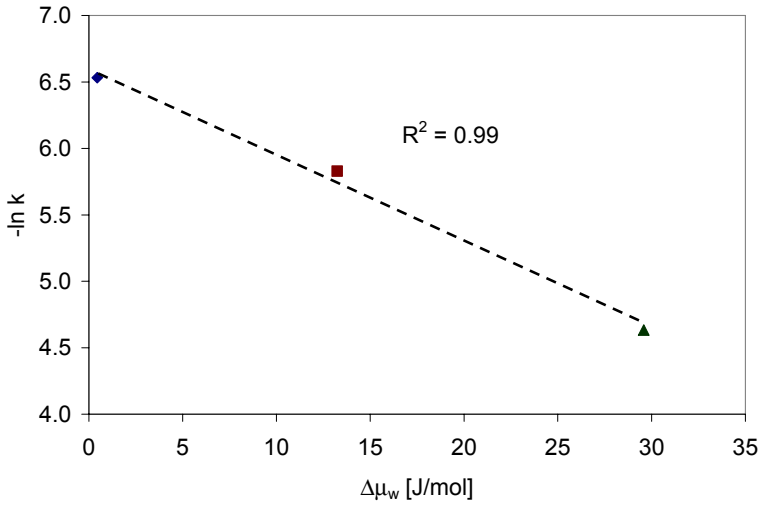

Figure 6.5 Plot of the negative natural log of the rate constant of MC540 dye insertion into DPPC vesicles [247] during osmotic stress versus the decrease in the chemical potential of water.

value was obtained (R^2 = 0.99) suggesting that the insertion of MC540 into the lipid bilayer with hyperosmotic stress follows the mechanism described by Eq. 6.8.

Given the high coefficient of determination for both FM1-43 data and MC540 data from the literature [247], we suggest that the change in the chemical potential of water during hyperosmotic stress is a major contributor for the formation of the transition state during either adsorption or desorption. This relation between the chemical potential of water and the formation of the transition state also explains the CellMask desorption kinetics observed during hyperosmotic stress. The rate constant for CellMask / lipid desorption (k_d) would be given by

$$k_d = \frac{D}{l^2}\exp\left[-\Delta G_d^{\neq\zeta o}/RT\right] = \frac{D}{l^2}\exp\left[-\left(\Delta G_d^{\neq o} - \frac{n_w}{n_L}\Delta\mu_w\right)/RT\right] \qquad (6.11)$$

which is the same in form as Eq. 6.8. However, as mentioned before, the ratio, $\frac{n_w}{n_L}$, will differ due to differences in the process of forming the transition state during desorption as compared to adsorption. Using Eq. 6.11 we can explain why at higher osmotic stress (i.e. larger values in the reduction of the chemical potential of water), there was an increased rate of desorption (k_d) of CellMask dye from the membrane. The lower values of final CellMask dye concentration in the membrane at 30 MPa versus 10 MPa indicate that equilibrium concentration of the dye in the membrane was dependent on osmotic pressure, i.e. $\Delta G^{\neq \zeta o}$ decreased with increasing osmotic pressure. Assuming that the change in the chemical potential of water is the dominant factor in the desorption process, the shift in equilibrium suggests that the ratio, $\frac{n_w}{n_L}$, was greater for the desorption process that the adsorption process.

6.2.1.1 Surface defects and lipid desorption

In Chapter 4, we stated that we used FM1-43 to investigate the formation of surface defects in the membrane with hyperosmotic stress, similar to what has been done in the literature using MC540 with osmotically stressed liposomes [75, 247]. However, using the above analysis we have shown the transfer of these dyes into the membrane is dependent on the chemical potential of water and its effect on the formation of the transition state. We therefore suggest that the formation of surface defects observed in the literature [79] is actually the formation of the transition state in the model. This implies

that both the formation of surface defects and lipid desorption with increasing osmotic pressures are due to the same mechanism. This mechanism also links other dehydration/ surface defect -induced changes to the membrane, such as fusion, increased permeability to solutes and increased susceptibility to amphipath insertion (see Chapter 1), directly to the decrease in the chemical potential of water.

6.2.1.2 Effect of osmolyte

From the above analysis, we observed that decrease in the Gibbs free energy of adsorption and desorption leads to an enhanced rate of transfer of lipids into and out of the membrane. The decrease in the Gibbs free energy was determined to be due to the reduction in the chemical potential of water due to presence of increasing concentrations of solutes. However, the presence of solutes can alter other properties of the aqueous phase. Surface tension is another property that is affected by the presence of solutes. If the solute causes a large increase in the surface tension then it is more difficult to make a cavity in the aqueous phase to accommodate the non-polar molecule. PEG has been shown to lower the surface tension of water [288]. Therefore, addition of PEG should favor dissolution of the acyl chain in the aqueous phase. This is one possible reason for the enhancement in lipid transfer between vesicles in the presence of PEG [289]. Conversely, increasing amounts of KCl (at low concentrations) have been shown to decrease the rate of transfer of pyrenePC [286] from vesicles. This was attributed to a "salting out" effect due to the increase in surface tension expected in the presence of KCl. It should be noted that surface tension is also dependent on temperature such that any

reduction in temperature would increase the surface tension of the aqueous phase [290] which would favor lipid adsorption into the bilayer.

In the FM1-43 and CellMask experiments we used PEG 600 as an osmolyte. PEG is not expected to interact directly with the membrane since it is excluded from the membrane surface [291]. However, other solutes such as trehalose, which can interact directly with lipids [292], will be expected to alter the magnitude of osmotic stress effect on lipid transfer. This is due to fact that direct interaction with the lipid would change the magnitude of the various contributions in forming the transition state, for example, the enthalpy associated with creating the cavity in the bilayer.

6.2.2 FAST DEHYDRATION DAMAGE

In Chapter 4 we observed that for experiments with Cellmask™ that the dye is seen to exit membrane during cell dehydration. With 48 % w/w PEG 600 the fluorescence continually decreases over a 10 minute period after the cell has dehydrated whereas for 67 % w/w PEG 600 there is very little change during the 10 minute period. This result indicates that the 67 % w/w PEG 600 reached equilibrium very quickly during the dehydration while 48 % w/w PEG 600 did not. It was also observed that slowly dehydrated cells retained a slightly (but significantly) greater amount of dye despite being exposed to a longer period of osmotic stress. Additionally, it was observed that at lower temperatures, dye first exited the cell followed by the dye repartitioning into the cell membrane. We suggest that based on results from Chapter 4 and data from the literature

that the chemical potential gradient across the membrane also affects the final membrane structure. This idea that changes/ damage to the membrane is caused by a large osmotic gradient has also been previously proposed and developed using mechanistic methods but evidence is inconclusive [57].

This analysis uses irreversible thermodynamics to analyze the membrane as the system during water transport. There are several assumptions made in this approach:

1. The entropy change accompanying a process occurring far removed from equilibrium can still be described by the equilibrium Gibbs relation.

2. Inhomogeneities and gradients of concentration, temperature and pressure .within the system can be ignored

For a system,

$$dS = dS_{ext} + dS_{\text{int}} \tag{6.12}$$

$$dS_{ext} = \frac{\delta Q}{T} \tag{6.13}$$

dS_{ext} = entropy entering system for a reversible process

dS_{int} = entropy generated within the system for an irreversible process

The Gibbs equation is given by,

$$TdS = dU + PdV - \sum_j \mu_j dn_j \tag{6.14}$$

Using irreversible thermodynamics for transport of dn moles of solute through a membrane from compartment I to compartment II,

$$dS = dS_I + dS_{II} \tag{6.15}$$

$$TdS = dU_I + dU_{II} + P_I dV + P_{II} dV_{II} - \mu_I dn_I - \mu_{II} dn_{II} \tag{6.16}$$

$$dQ = dU_I + dU_{II} + P_I dV + P_{II} dV_{II} \tag{6.17}$$

$$dS = \frac{\delta Q}{T} + \frac{\mu_I - \mu_{II}}{T} dn \tag{6.18}$$

$$dS_{\text{int}} = \frac{\mu_I - \mu_{II}}{T} dn \tag{6.19}$$

For the system,

$$\delta Q - TdS = \left(\mu_{II} - \mu_I\right) dn \,. \tag{6.20}$$

Using the definition of Gibbs free energy, $G = H - TS$, for an isothermal system,

$$dG = dH - TdS \tag{6.21}$$

For enthalpy,

$H = U + PV$, and (6.22)

$$dH = dU + PdV + VdP = \delta Q + VdP + \mu dN \,. \tag{6.23}$$

For constant pressure and constant N (N=number of lipid molecules),

$$dH = \delta Q \,. \tag{6.24}$$

Therefore,

$$dG = (\mu_{II} - \mu_I)dn = -TdS_{\text{int}} \,. \tag{6.25}$$

Dividing by dt, we get

$$-\frac{dG}{dt} = T\frac{dS_{\text{int}}}{dt} = \left(\mu_I - \mu_{II}\right)\frac{dn}{dt} \tag{6.26}$$

Using the terminology for water transport through a membrane used by Kadem and Katchalsky [67] and the relation of the flux to its force given by irreversible thermodynamics,

$$J = LX \tag{6.27}$$

the rate of dissipation of Gibbs free energy is given by

$$-\frac{dG}{dt} = L_p\left(\mu_{w,i} - \mu_{w,o}\right)^2 \tag{6.28}$$

where L_p is the hydraulic conductivity of the membrane and $\mu_{w,i}$ and $\mu_{w,o}$ represent the intraceullar and extracellular chemical potential of water.

As seen from above, the decrease in the Gibbs free energy during osmotically driven water transport goes into increasing the internal entropy of the membrane. Sogami et al [64] suggested that ΔS (change in entropy) values for permeation are related to the lipid chain disordering and they intimated that higher ΔS values may indicate irreversible

breaking of the membrane. This idea of increased disorder is supported by molecular dynamics simulations which demonstrate the necessity for the creation of free volume for transport through the lipid bilayer [65].

We expect that an increase in entropy of the membrane would increase the mobility of the lipids. We envisage that this increased mobility would provide a partial reduction in the energy barrier (i.e. increase the free energy of the lipids) thereby further favoring the formation of the transition state during lipid desorption. As a result of the transient nature of the irreversible thermodynamics mechanism we would expect that there would only be a temporary addition of "energy" (to get over the energy barrier) for lipid dissociation before the "slow dehydration damage" mechanism would take over. If the bilayer structure can dissipate energy effectively, for example by using aquaporins to transport water, then only the effect of the "slow dehydration damage" mechanism would be observed.

At very large osmotic gradients, membrane stability would be determined by the dissipation of the stored "energy". In a similar analysis for an ohmic resistor, the rate of change of Gibbs free energy would equal the power dissipation, $-\frac{dG}{dt} = T\frac{dS_{\text{int}}}{dt} = cV^2 = P$. One can imagine that if the voltage drop across the resistor was too great and there was insufficient dissipation of energy by heat transfer then the resistor would burn out. This dissipation of energy (in the form of excess entropy) is a general requirement for stable systems [293].

This model can be used to qualitatively interpret the results from the Cellmask™ experiments in Chapter 4. The difference in multi-step dehydration results versus a single "rapid" step can be understood from the point that the rapid dehydration would maximize the instantaneous entropy generated within the membrane and potentially accelerate the loss of lipids. Results from dehydration experiments at low temperatures can also be interpreted using this model. At low temperatures, the favorability of Cellmask™ in solution would decrease due to the increase in surface tension thereby shifting the equilibrium more to the bilayer. The favorability of Cellmask™ in the membrane may have also increased slightly due to the small phase change observed in FTIR and DCVJ data (see Chapter 5). It has been previously shown that for vesicles in the gel phase there is a reduction in lipid desorption [294]. When a sudden dehydration is imposed, it seems that the "fast dehydration damage" mechanism is temporarily able to increase the energy of the dye molecules to get over the energy barrier. However, once that mechanism is removed (after water transport has stopped) equilibrium is restored which is observed by an increase in fluorescence of the cells.

Both thermodynamic mechanisms basically describe destabilization of the membrane by lipid movement into and out of the bilayer. Even if this movement does not cause membrane rupture, it would certainly increase the chances of a non-functional membrane due to scrambling.

As an aside, MD simulations have shown that if a lipid is placed inside a bilayer it is possible to form pores [295]. The simulation also showed that the energetic cost of moving a lipid out of the bilayer was the same as putting the lipid in the middle of the

bilayer. Therefore, it may indeed be feasible that rapid water transport through the bilayer could provide enough energy to create pores as hypothesized by Muldrew et al [57].

6.3 DAMAGE DUE TO CELL SHRINKAGE AND CYTOSKELETON STIFFNESS

In Chapter 5 we observed that at higher freezing temperatures (-20 °C), cells in PEG 600 demonstrated a much higher viability than cells in PBS. This viability was slightly (but significantly) improved with Rho kinase inhibition. A similar result was obtained for osmotically stressed HFFs at 4°C (see Chapter 4), where it was observed that using a Rho kinase inhibitor at lower temperatures yielded higher viability. At lower freezing temperatures (-80 °C), the viability of cells in PEG 600 was not significantly different from those in media or PBS. However, the viability was again slightly (but significantly) improved with Rho kinase inhibition. These observations are similar to several reports in the literature where reducing the stiffness of the cytoskeleton has led to an increase in post-thaw viability [61-63]. This indicates that mechanical properties of the cytoskeleton affect the freeze/thaw outcome. We also observed that reducing cell shrinkage using PEG 200 gave a higher viability that PEG 600. In this section, we discuss possible links between cytoskeletal stiffness, cell shrinkage and membrane morphology and their effect on dehydration- and freeze/thaw-induced damage to the cell membrane.

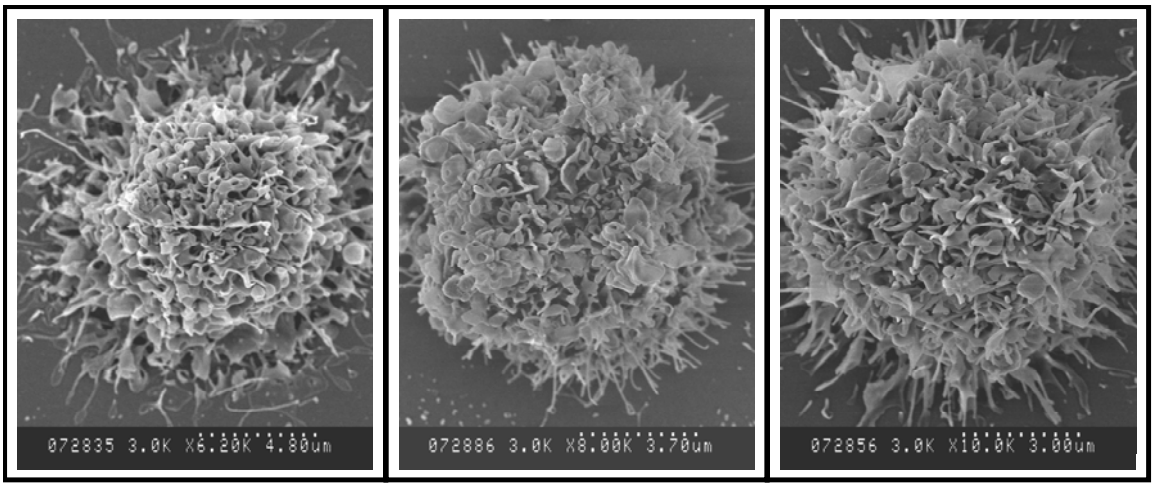

Figure 6.6 SEM images of cells that were pretreated with various drugs and then subjected to hyperosmotic stress at 4°C using 48% w/w PEG 600.

6.3.1 CELL STIFFNESS AND MEMBRANE MORPHOLOGY DURING DEHYDRATION

During dehydration-induced shrinkage, the excess membrane area of the cell transforms into microvilli/ tubular structures, blebs and lamellar-like projections. Using Y-27632, a Rho kinase inhibitor, a decrease in villi-like structures was observed at low temperatures (during hyperosmotic stress) and more lamellae-like structures were present. Inhibition of Rho kinase inhibits myosin motors as well as prevents actin bundling. Since the formation of a stable filopodia/ microvilli depends on bundled actin filaments this may be one mechanism by which Y27632 prevents formation of microvilli. However, myosin activity decreases with a decrease in temperature [296, 297] making this possibility unlikely. Another possible mechanism for formation of filopodia is due to actin polymerization at the tips, but both reports in literature [298] and our data (see Chapter

4) show that actin polymerization is inhibited at low temperatures, making this an unlikely possibility. Also due to the cell behaving as a strong glass under osmotic compression [299] we can expect that all biological processes would be greatly slowed including directed growth of microvilli or filopoida.

The lack of an active mechanism to form microvilli does not preclude its formation during osmotic stress. The formation of tubular structures has also been observed in shrinking giant vesicles [300] where there was no underlying cytoskeleton present. Their formation was attributed to spontaneous curvature generated by a transfer of lipids to the outer monolayer due to the water transport through the bilayer. We hypothesize that the formation of various structures formed during cell shrinkage is dependent on the stiffness of the membrane and the underlying support (the cortical cytoskeleton). This hypothesis is based on work by Pocivavsek et al [301] showing the formation of wrinkles versus folds is dependent on the ratio of the stiffness of the membrane and to that of the underlying support.

The differences in the dehydrated cell membrane morphology at 22 °C versus 4 °C support the hypothesis that cell stiffness affects membrane morphology in the dehydrated state. At low temperatures it is expected that the underlying cytoskeleton would be significantly stiffer. ATP depletion, which would occur a low temperatures [302], can cause stiffening of the actomyosin cytoskeleton since the ADP-bound myosin II to F-actin serves to cross-link filaments [303]. It has also been shown that α-actinin cross-linked actin filaments experience a large increase in stiffness at low temperatures *in vitro* [304]. The increase in cytoskeletal stiffness has been experimentally demonstrated using

magnetic twisting cytometry where alveolar epithelial cells exhibited a large, significant increase in stiffness when the temperature was lowered from 37 °C to 4 °C [251].

The hypothesis is further supported by data showing that pretreatment of cells with Y27632, which decreases the cortical stiffness, abrogated the formation of microvilli at lower temperatures. SEM images of cells treated with other cytoskeletal altering drugs that reduce the stiffness of the cytoskeleton (blebbistatin to inhibit myosin activity and cytochalasin D to depolymerize actin filaments) also showed a similar behavior, i.e. less microvilli (Figure 6.6). Cells treated with WGA, which increases membrane stiffness, also displayed different membrane morphology with the formation of thicker protrusions. This again supports the hypothesis that both the stiffness of the cytoskeleton and the membrane affect the membrane morphology during dehydration. The effect of WGA on the cell would likely increase during freeze/ thaw due to freeze concentration.

6.3.2 Membrane protrusions and membrane damage

In Chapter 4 we observed that higher viability was observed for cells that were osmotically stressed with sorbitol versus PEG 600. Even more significantly, in chapter 5 we observed that cells that underwent freeze/thaw in PEG 200 gave a higher viability than PEG 600 despite the increase in membrane-ice interactions with PEG 200. These results suggest that cell shrinkage is a factor for damage. In the literature damage due to cell shrinkage has been associated with vesiculation [141] and the resulting loss in membrane area. However, SEM images of dehydrated HFFs did not demonstrate vesicle

formation. SEM images showed that the type of protrusions formed during freezing with PEG 200 (bleb-like protrusions) were very different from those formed with PEG 600 (microvilli-like protrusions). We attribute this to the fact that PEG 200 enters the cell thereby lessening the volumetric reduction during freezing.

It was also observed that altering the structure of the cytoskeleton using Y27632 during osmotic stress experiments at 4°C both altered the type of membrane protrusions (i.e. eliminating the formation of microvilli) and increased viability. The link between the mechanical properties of the cytoskeleton and dehydrated membrane morphology may explain why reducing the stiffness of the cytoskeleton lessened the degree of damage that the cells sustain during freeze/thaw and osmotic stress experiments at low temperatures. Dobrinsky suggested that depolymerizing cytoskeletal elements prior to cryopreservation prevents irreparable damage to the cytoskeleton [160] but he did not suggest any link to membrane damage. Hosu et al [63] showed that disassembly of the actin cytoskeleton in mouse oocytes increased survival after freeze/thaw, i.e. reduced membrane damage. They speculated that this increased survival was a result of enhanced repair of the cell membrane due to disassembly of the actin cytoskeleton. While this might be a possibility in our experiments it does not resolve the mechanism of damage to the cell membrane.

We suggest that the formation of microvilli during freeze/thaw or during osmotic dehydration at low temperatures is linked to damage to the cell membrane. There are several (non-mutually exclusive) possibilities why the formation of microvilli is linked to cell damage. One, already mentioned in Chapter 5, is that the microvilli may not be retracted during cell expansion, effectively decreasing the membrane area. The retraction

of the microvilli would also be dependent on the membrane adhesion to the cytoskeleton and the cytoskeleton stiffness. If there was strong adhesion between the cytoskeleton and membrane then the membrane cannot easily "slip" to cover the expanding areas if the cell. In the case of fibroblasts there is strong adhesion between the cytoskeleton and membrane [305, 306] which would hamper retraction of microvilli during cell expansion. In addition, if the cytoskeleton was very stiff the retraction of microvilli would be hampered by the cytoskeleton inability to stretch and shear. The second possibility is that the microvilli are shed during expansion, again decreasing the membrane area. Thirdly, the microvilli may be more susceptible to damage during freeze thaw and during dehydration and rehydration. Whether microvilli are more susceptible to mechanical damage during osmotic stress or freeze/thaw is speculative at this point. However, microvilli have been shown to be susceptible to damage during sonication when cells are lightly fixed with glutaraldehyde; if there is no fixation the entire cell is damaged during sonication whereas only the microvilli remain susceptible to damage when the cells are fixed [307].

CHAPTER 7: CONCLUSION

This thesis demonstrates that there are multiple mechanisms behind the damage inflicted to the cell membrane during osmotic dehydration and slow freezing.

7.1 DAMAGE MECHANISMS FROM OSMOTIC STRESS

There were several mechanisms identified as being responsible for dehydration damage. It was observed that the membrane phase transition during drying had a negative impact on post rehydration viability (Chapter 2). We also identified that a suddenly applied osmotic stress was more deleterious to the membrane than gradual dehydration. Results and analysis from Chapters 4 & 6, suggested that the lowering of the chemical potential of water at the membrane interface destabilizes the membrane thereby promoting the formation of surface defects in the membrane and lipid dissolution. We suggest that both processes are linked to the same thermodynamic mechanism. We hypothesize that during rapid dehydration water transport through the membrane increases the internal entropy, which further destabilizes the membrane and accelerates lipid dissolution. We observed that damage to the cell membrane is exacerbated by cell shrinkage and cell stiffness. We demonstrated that the cytoskeleton has a significant role in determining membrane morphology upon shrinking. We suggest that cell shrinkage and cell stiffness exacerbate damage due to type of membrane protrusions formed during cell shrinkage, which subsequently affect the ability of the cell to successfully return to isotonic conditions.

7.2 POSSIBLE STRATEGIES TO ALLEVIATE DEHYDARTION DAMAGE

Based on the mechanisms identified, some strategies (some of which are already used) to lessen damage to the membrane during dehydration are:

1. Avoid the lyotropic phase transition – this can be accomplished either by directly stabilizing the lipid head groups (e.g. by using trehalose) or by dehydration of the membrane while in the gel phase (see Chapter 3).

2. Use solutions that increase the "salting out" effect, i.e. one that increases the surface tension. This would reduce the favorability of lipid monomer solvation.

3. Reduce the temperature of dehydration. This would slow down the rate of damage as well as increase the "salting out" effect.

4. Use high viscosity solutions or solutions that vitrify upon drying

5. Reduce the stiffness of the cytoskeleton by using drugs (see Chapter 5) or by preconditioning the cells to tune the stiffness of the cell. For example, exposure to hypoosmotic conditions would cause actin depolymerization thereby reducing the cell stiffness. Another suggestion to reduce cell stiffness is mechanical deformation of the cell immediately prior to freezing in order to break cross-links within the cell. This type of mechanical deformation has been previously accomplished using a microfluidic device with a narrow channel [308]

6. Provide an alternative path for water transport by increasing aquaporin content in the membrane [309]

7. Reduce hydraulic conductance of membrane by using cholesterol

8. Slowly dehydrate membrane to avoid large osmotic gradient

The last three suggestions are applicable to membrane damage that occurs when there is a large osmotic gradient present.

7.3 DAMAGE MECHANISMS FROM SLOW FREEZING

In addition to some of the dehydration damage mechanisms there were several other damage mechanisms identified during slow freezing. Many of them have already been identified as damage mechanisms such as ice-cell interaction, cell shrinkage and eutectic formation. However, new details regarding the effects of these mechanisms on the cell membrane were shown. It was demonstrated that the eutectic formation results in dehydration of the lipid bilayer which may contribute to changes in the post-thaw membrane structure. We observed that ice-cell interaction resulted in membrane damage and that the ice morphology could be altered using PVA to enhance the damage. As with osmotic stress experiment, we again observed that cell shrinkage and a stiff cytoskeleton promoted membrane damage.

7.4 POSSIBLE STRATEGIES TO ALLEVIATE SLOW FREEZING DAMAGE

Given the large body of literature dedicated to slow freezing of biological samples, new suggestions to reduce freeze/thaw damage are limited. Based on the mechanisms identified, some strategies to lessen damage to the membrane during slow freezing are:

1. Reduce ice-cell interaction – this can be accomplished by increasing the unfrozen fraction of the solution

2. Increase the strength of the membrane – this can be accomplished by using wheat germ agglutinin (see Chapter 5)

3. Eliminate eutectic formation either by eliminating use of salts that form a eutectic or use of trehalose to suppress eutectic formation (see Chapter 2)

4. Reduce the stiffness of the cytoskeleton by using drugs (see Chapter 5) or by osmotic preconditioning of the cells to tune the stiffness of the cell.

7.5 SUGGESTIONS FOR FUTURE WORK

While the evidence presented for the thermodynamic mechanism of damage to the membrane is promising, it is still not a proven mechanism. One experiment that would show evidence that is more conclusive would be a direct measurement of the amount of lipids extracted during osmotic stress. This would also help to gather more quantitative data on the amount of lipid the membrane can be expected to lose.

Another drawback in this study was that no information was gathered on possible membrane changes within the cell. During cell shrinkage, the membrane can either form protrusions or invaginations. In the methods used, we only looked at effects on the membrane surface. While this is likely acceptable for our model cell due to the dense

actin cytoskeleton acting as a barrier over short timescales, this will not be true for all cells. Therefore, future work investigating changes to the membrane should also include methods such as Transmission Electron Microscopy which can be used to look at changes inside the cell.

The effect of shear stress during hyperosmotic stress of suspended cells is another effect that should be investigated. This can be done qualitatively (the exact shear stress would be unknown) using the cell trapping device designed by Di Carlo et al [238], (to prevent cells from escaping). Using the techniques presented in this thesis to compare osmotic stress and freeze/ thaw damage along with this additional study could provide valuable information on the role of shear during cryopreservation.

Based on our findings, we suggest that the formation of membrane projections can exist without an active cytoskeletal response but that the type of projection is dependent on the structure of the cytoskeleton. This is a fascinating concept and could have implications in understanding how cells function.

7.6 FINAL CONCLUSION

Due to the complicated nature of the phenomena associated with dehydration and slow freezing, it is expected that there are more mechanisms, which were not investigated in this thesis. However, from the data presented in this thesis (and the literature over the past 40 years that was used to interpret the data) a more comprehensive picture of

damage during dehydration and slow freezing has started to emerge which will improve the science of biopreservation.

CHAPTER 8: BIBLIOGRAPHY

[1] A.A. Gage, J.M. Baust, J.G. Baust, Experimental cryosurgery investigations in vivo, Cryobiology 59 (2009) 229-243.

[2] R. Fleck, B. Fuller, 21 Cell Preservation, Medicines from animal cell culture (2007) 417-432.

[3] T.D.R. Lloyd, S. Orr, P. Skett, D.P. Berry, A.R. Dennison, Cryopreservation of hepatocytes: a review of current methods for banking, Cell and Tissue Banking 4 (2003) 3-15.

[4] E. Walters, Laboratory Animals: Cryopreservation of Oocytes and Sperm, Encyclopedia of Biotechnology in Agriculture and Food 352 - 354.

[5] T. Kanias, J.P. Acker, Mammalian Cell Desiccation: Facing the Challenges, Cell Preservation Technology 4 (2006) 253-277.

[6] M. Horbowicz, R.L. Obendorf, Seed desiccation tolerance and storability: Dependence on flatulence-producing oligosaccharides and cyclitols?review and survey, Seed Science Research 4 (1994) 385-405.

[7] M. Potts, Desiccation tolerance of prokaryotes, Microbiol. Rev 58 (1994) 775–805.

[8] A. Aksan, M. Toner, Roles of Thermodynamic State and Molecular Mobility in Biopreservation, in: J.D. Bronzino (Ed.), The Biomedical Engineering Handbook, vol. 3, Taylor & Francis, Boca Raton, 2006.

[9] M. Grunze, B. Deuticke, Changes of membrane permeability due to extensive cholesterol depletion in mammalian erythrocytes, Biochim Biophys Acta 356 (1974) 125-130.

[10] A. Carruthers, D.L. Melchior, Study of the relationship between bilayer water permeability and bilayer physical state, Biochemistry 22 (1983) 5797-5807.

[11] E. Evans, D. Needham, Giant vesicle bilayers composed of mixtures of lipids, cholesterol and polypeptides. Thermomechanical and (mutual) adherence properties, Faraday Discussions of the Chemical Society 81 (1986) 267-280.

[12] S.F. Pedersen, E.K. Hoffmann, J.W. Mills, The Cytoskeleton and Cell Volume Regulation, Comparative Biochemistry and Physiology Part A 130 (2001) 385-399.

[13] T. Le Bihan, D. Pelletier, P. Tancrède, B. Heppell, J.P. Chauvet, C.R. Gicquaud, Effect of the polar headgroup of phospholipids on their interaction with actin, Journal of Colloid And Interface Science 288 (2005) 88-96.

[14] E.E. Noiles, K.A. Thompson, B.T. Storey, Water Permeability, Lp, of the Mouse Sperm Plasma Membrane and Its Activation Energy Are Strongly Dependent on Interaction of the Plasma Membrane with the Sperm Cytoskeleton, Cryobiology 35 (1997) 79-92.

[15] T. Fujiwara, K. Ritchie, H. Murakoshi, K. Jacobson, A. Kusumi, Phospholipids Undergo Hop Diffusion in Compartmentalized Cell Membrane, The Journal of Cell Biology 157 (2002) 1071-1081.
[16] G.T. Charras, J.C. Yarrow, M.A. Horton, L. Mahadevan, T.J. Mitchison, Non-equilibration of hydrostatic pressure in blebbing cells, Nature 435 (2005) 365-369.
[17] G.J. Doherty, H.T. McMahon, Mediation, Modulation, and Consequences of Membrane-Cytoskeleton Interactions, Annual Review of Biophysics 37 (2008) 65-95.
[18] M.R. Kasschau, T.D. Ngo, L.M. Sperber, K.L. Tran, Formation of filopodia in earthworm (Lumbricus terrestris) coelomocytes in response to osmotic stress, Zoology 110 (2007) 66-76.
[19] H. Takamatsu, R. Takeya, S. Naito, H. Sumimoto, On the mechanism of cell lysis by deformation, Journal of Biomechanics 38 (2005) 117-124.
[20] J. Korlach, P. Schwille, W.W. Webb, G.W. Feigenson, Characterization of lipid bilayer phases by confocal microscopy and fluorescence correlation spectroscopy, Proceedings of the National Academy of Sciences 96 (1999) 8461.
[21] J. Wolfe, Z. Yan, J.M. Pope, Hydration forces and membrane stresses: cryobiological implications and a new technique for measurement, Biophysical Chemistry 49 (1994) 51-58.
[22] J.F. Nagle, H.L. Scott Jr, Lateral compressibility of lipid mono-and bilayers. Theory of membrane permeability, Biochim Biophys Acta 513 (1978) 236-243.
[23] H.T. McMahon, J.L. Gallop, Membrane curvature and mechanisms of dynamic cell membrane remodelling, Nature 438 (2005) 590-596.
[24] T. Taniguchi, Shape Deformation and Phase Separation Dynamics of Two-Component Vesicles, Physical Review Letters 76 (1996) 4444-4447.
[25] S.J. Marrink, J. Risselada, A.E. Mark, Simulation of gel phase formation and melting in lipid bilayers using a coarse grained model, Chemistry and Physics of Lipids 135 (2005) 223-244.
[26] T. Soderlund, J.M.I. Alakoskela, A.L. Pakkanen, P.K.J. Kinnunen, Comparison of the Effects of Surface Tension and Osmotic Pressure on the Interfacial Hydration of a Fluid Phospholipid Bilayer, Biophysical Journal 85 (2003) 2333-2341.
[27] G. Bryant, K.L. Koster, J. Wolfe, Membrane behaviour in seeds and other systems at low water content: the various effects of solutes, Seed Science Research 11 (2001) 17-26.
[28] J. Milhaud, New insights into water–phospholipid model membrane interactions, Biochimica et Biophysica Acta 1663 (2004) 19-51.
[29] R.I. MacDonald, Membrane fusion due to dehydration by polyethylene glycol, dextran, or sucrose, Biochemistry 24 (1985) 4058-4066.
[30] D. Hoekstra, Role of lipid phase separations and membrane hydration in phospholipid vesicle fusion, Biochemistry 21 (1982) 2833-2840.
[31] L. Beney, Y. Mille, P. Gervais, Death of Escherichia coli during rapid and severe dehydration is related to lipid phase transition, Applied Microbiology and Biotechnology 65 (2004) 457-464.

[32] P.L. Steponkus, M.F. Dowgert, R.Y. Evans, W. Gordon-Kamm, Cryobiology of isolated protoplasts, Plant Cold Hardiness and Freezing Stress 2 (1982) 459-474.
[33] P.L. Steponkus, D.V. Lynch, The behavior of large unilamellar vesicles of rye plasma membrane lipids during freeze/thaw-induced osmotic excursions, Cryo-Letters 10 (1989) 43-50.
[34] A.L. Bernard, M.A. Guedeau-Boudeville, L. Jullien, J.M. di Meglio, Raspberry vesicles, BBA-Biomembranes 1567 (2002) 1-5.
[35] J.H. Crowe, L.M. Crowe, R. Mouradian, Stabilization of Biological-Membranes at Low Water Activities, Cryobiology 20 (1983) 346-356.
[36] G. Bryant, J. Wolfe, Can hydration forces induce lateral phase separations in lamellar phases?, European Biophysics Journal 16 (1989) 369-374.
[37] G. Bryant, J.M. Pope, J. Wolfe, Low hydration phase properties of phospholipid mixtures, European Biophysics Journal 21 (1992) 223-232.
[38] G.J. Morris, Lipid loss and haemolysis by thermal shock: lack of correlation, Cryobiology 12 (1975) 192-201.
[39] P.L. Steponkus, Role of the plasma membrane in freezing Injury and cold acclimation, Annual Review of Plant Physiology 35 (1984) 543-584.
[40] W.J. Gordon-Kamm, P.L. Steponkus, Lamellar-to-hexagonal _II Phase Transitions in the Plasma Membrane of Isolated Protoplasts after Freeze-Induced Dehydration, P Natl Acad Sci USA 81 (1984) 6373-6377.
[41] L.M. Crowe, J.H. Crowe, Hydration-Dependent Hexagonal Phase Lipid in a Biological Membrane, Archives of Biochemistry and Biophysics 217 (1982) 582-587.
[42] J.H. Crowe, L.M. Crowe, Effects of dehydration on membranes and membrane stabilization at low water activities, Biological Membranes 5 (1984) 57–102.
[43] L.M. Crowe, C. Womersley, J.H. Crowe, D. Reid, L. Appel, A. Rudolph, Prevention of Fusion and Leakage in Freeze-Dried Liposomes by Carbohydrates, Biochimica Et Biophysica Acta 861 (1986) 131-140.
[44] E.A. Golovina, F.A. Hoekstra, M.A. Hemminga, Drying increases intracellular partitioning of amphiphilic substances into the lipid phase: impact on membrane permeability and significance for desiccation tolerance, Plant Physiology 118 (1998) 975–986.
[45] J. Crowe, F. Hoekstra, L. Crowe, Anhydrobiosis, Annu. Rev. Physiol. 54 (1992) 579-599.
[46] S.J. Webb, Bound Water in Biological Activity, Charles C. Thomas, Springfield, IL, 1965.
[47] J.H. Crowe, J.S. Clegg, Anhydrobiosis, 1973.
[48] J.H. Crowe, F. Tablin, W.F. Wolkers, K. Gousset, N.M. Tsvetkova, J. Ricker, Stabilization of membranes in human platelets freeze-dried with trehalose, Chem Phys Lipids 122 (2003) 41-52.
[49] Y. Mille, L. Beney, P. Gervais, Viability of Escherichia coli after combined osmotic and thermal treatment: a plasma membrane implication, Biochim Biophys Acta 1567 (2002) 41-48.

[50] M. Caffrey, The Combined and Separate Effects of Low Temperature and Freezing on Membrane Lipid Mesomorphic Phase Behavior: Relevance to Cryobiology, Biochimica et Biophysica Acta 896 (1987) 123-127.
[51] J.H. Crowe, L.M. Crowe, Membrane integrity in anhydrobiotic organisms: toward a mechanism for stabilizing dry cells, in: S. GN, O. CB, B. CL (Eds.), Water and Life, Springer-Verlag, Berlin, Germany, 1992, pp. 87–103.
[52] Y. Mille, L. Beney, P. Gervais, Magnitude and kinetics of rehydration influence the viability of dehydrated E. coli K-12, Biotechnology and Bioengineering 83 (2003) 578-582.
[53] L. Beney, H. Simonin, Y. Mille, P. Gervais, Membrane physical state as key parameter for the resistance of the gram-negative *Bradyrhizobium japonicum* to hyperosmotic treatments, Archives of Microbiology 187 (2007) 387-396.
[54] C. Laroche, P. Gervais, Achievement of rapid osmotic dehydration at specific temperatures could maintain high Saccharomyces cerevisiae viability, Applied Microbiology and Biotechnology 60 (2003) 743-747.
[55] S. Zawlodzka, H. Takamatsu, Osmotic injury of PC-3 cells by hypertonic NaCl solutions at temperatures above 0 °C, Cryobiology 50 (2005) 58-70.
[56] M.P. Sheetz, J.E. Sable, H.-G. Döbereiner, Continuous membrane-cytoskeleton adhesion requires continuous accommodation to lipid and cytoskeleton dynamics, Annual Review of Biophysics and Biomolecular Structure 35 (2006) 417-434.
[57] K. Muldrew, J. Schachar, P. Cheng, C. Rempel, S. Liang, R. Wan, The possible influence of osmotic poration on cell membrane water permeability, Cryobiology 58 (2009) 62-68.
[58] D. Raucher, M.P. Sheetz, Characteristics of a membrane reservoir buffering membrane tension, Biophysical journal 77 (1999) 1992-2002.
[59] J.-Y. Tinevez, U. Schulze, G. Salbreux, J. Roensch, J.-F.o. Joanny, E. Paluch, Role of cortical tension in bleb growth, Proceedings of the National Academy of Sciences 106 (2009) 18581-18586.
[60] C. Morisset, C. Gazeau, J. Hansz, J. Dereuddre, Importance of actin cytoskeleton behaviour during preservation of carrot cell suspensions in liquid nitrogen, Protoplasma 173 (1993) 35-47.
[61] M. Franco, P.J. Hansen, Effects of hyaluronic acid in culture and cytochalasin B treatment before freezing on survival of cryopreserved bovine embryos produced in vitro, In Vitro Cellular & Developmental Biology 42 (2006) 40-44.
[62] R.S. Prather, N.L. First, Effect of cytochalasin ß and demecolcine on freeze-thaw survival of murine embryos in vitro, The Journal of experimental zoology 239 (1986) 37-40.
[63] B.G. Hosu, S.F. Mullen, J.K. Critser, G. Forgacs, Reversible Disassembly of the Actin Cytoskeleton Improves the Survival Rate and Developmental Competence of Cryopreserved Mouse Oocytes, PLoS ONE 3 (2008).
[64] M. Sogami, S. Era, M. Murakami, Y. Seo, H. Watari, N. Uyesaka, Application of the transition state theory to water transport across cell membranes, BBA-Biomembranes 1511 (2001) 42-48.

[65] T. Xiang, B.D. Anderson, Molecular dissolution processes in lipid bilayers: A molecular dynamics simulation, The Journal of Chemical Physics 110 (1999) 1807.
[66] H.J. Galla, W. Hartmann, U. Theilen, E. Sackmann, On two-dimensional passive random walk in lipid bilayers and fluid pathways in biomembranes, Journal of Membrane Biology 48 (1979) 215-236.
[67] O. Kedem, A. Katchalsky, Thermodynamic analysis of the permeability of biological membranes to non-electrolytes, Biochim Biophys Acta 27 (1958) 229-246.
[68] F.W. Kleinhans, Membrane Permeabiliy Modeling - Kedem-Katchalsky vs a Two-Parameter Formalism, Cryobiology 37 (1998) 271-289.
[69] M.H. Jacobs, The simultaneous measurement of cell permeability to water and to dissolved substances, Journal of Cellular and Comparative Physiology 2 (1933) 427-444.
[70] J.N. Israelachvili, J. Mitchell, B.W. Ninham, Theory of Self-Assembly of Lipid Bilayers and Vesicles, Biochimica et Biophysica Acta. 470 (1977) 185-201.
[71] G. Cevc, Isothermal Lipid Phase Transitions, Chemistry and physics of lipids 57 (1991) 293-307.
[72] T. Fukuma, M.J. Higgins, S.P. Jarvis, Direct Imaging of Individual Intrinsic Hydration Layers on Lipid Bilayers at Angstrom Resolution, Biophys J 92 (2007) 3603.
[73] G.L. Jendrasiak, R.L. Smith, W. Shaw, The water adsorption characteristics of charged phospholipids, BBA-Biomembranes 1279 (1996) 63-69.
[74] A.S. Ulrich, A. Watts, Molecular response of the lipid headgroup to bilayer hydration monitored by 2H-NMR, Biophys J 66 (1994) 1441-1449.
[75] J. Arroyo, A.C.B. de Lopez, D.L. Bernik, E.A. Disalvo, Surface Packing of Lipid Bilayers in the Gel State Induced by Osmotic Stress As Measured by the Dimerization of Merocyanine 540, Journal of Colloid and Interface Science 203 (1998) 106-114.
[76] J.Y. Lehtonen, P.K. Kinnunen, Changes in the lipid dynamics of liposomal membranes induced by poly(ethylene glycol): free volume alterations revealed by inter- and intramolecular excimer-forming phospholipid analogs, Biophysical Journal 66 (1994) 1981-1990.
[77] J.X. Cheng, S. Pautot, D.A. Weitz, X.S. Xie, Ordering of water molecules between phospholipid bilayers visualized by coherent anti-Stokes Raman scattering microscopy, Proc Natl Acad Sci US A 100 (2003) 9826-9830.
[78] H. Binder, Water near lipid membranes as seen by infrared spectroscopy, European Biophysics Journal 36 (2007) 265-279.
[79] E.A. Disalvo, F. Lairion, F. Martini, E. Tymczyszyn, M. Frías, H. Almaleck, G.J. Gordillo, Structural and functional properties of hydration and confined water in membrane interfaces, Biochimica et Biophysica Acta (BBA) - Biomembranes 1778 (2008) 2655-2670.
[80] V.A. Raghunathan, J. Katsaras, Structure of the L_ {c^{'}} Phase in a Hydrated Lipid Multilamellar System, Physical Review Letters 74 (1995) 4456-4459.

[81] J.F. Nagle, Theory of the Main Lipid Bilayer Phase Transition, Annual Review of Physical Chemistry 31 (1980) 157-196.
[82] D.L. Melchior, J.M. Steim, Thermotropic Transitions in Biomembranes, Annual Review of Biophysics and Bioengineering 5 (1976) 205-238.
[83] T. Heimburg, Mechanical aspects of membrane thermodynamics. Estimation of the mechanical properties of lipid membranes close to the chain melting transition from calorimetry, BBA-Biomembranes 1415 (1998) 147-162.
[84] T. Heimburg, A Model for the Lipid Pretransition: Coupling of Ripple Formation with the Chain-Melting Transition, Biophysical Journal 78 (2000) 1154-1165.
[85] A.E. Oliver, L.M. Crowe, J.H. Crowe, Methods for dehydration-tolerance: Depression of the phase transition temperature in dry membranes and carbohydrate vitrification, Seed Science Research 8 (1998) 211-221.
[86] D. Needham, E. Evans, Structure and mechanical properties of giant lipid (DMPC) vesicle bilayers from 20. degree. C below to 10. degree. C above the liquid crystal-crystalline phase transition at 24. degree. C, Biochemistry 27 (1988) 8261-8269.
[87] M. Langner, S.W. Hui, Dithionite penetration through phospholipid bilayers as a measure of defects in lipid molecular packing, Chemistry and physics of lipids 65 (1993) 23-30.
[88] L.M. Hays, J.H. Crowe, W. Wolkers, S. Rudenko, Factors Affecting Leakage of Trapped Solutes from Phospholipid Vesicles during Thermotropic Phase Transitions, Cryobiology 42 (2001) 88-102.
[89] E.Z. Drobnis, L.M. Crowe, T. Berger, T.J. Anchordoguy, J.W. Overstreet, J.H. Crowe, Cold Shock Damage Is Due to Lipid Phase-Transitions in Cell-Membranes - a Demonstration Using Sperm as a Model, Journal of Experimental Zoology 265 (1993) 432-437.
[90] T. Takahashi, S. Noji, E.F. Erbe, R.L. Steere, H. Kon, Cold shock hemolysis in human erythrocytes studied by spin probe method and freeze-fracture electron microscopy, Biophysical Journal 49 (1986) 403-410.
[91] Mammalian cell membranes, London ; Boston : Butterworths, London ; Boston, 1976.
[92] S.J. Singer, G.L. Nicolson, The Fluid Mosaic Model of the Structure of Cell Membranes, Science 175 (1972) 720-731.
[93] G. van Meer, K. Simons, Viruses budding from either the apical or the basolateral plasma membrane domain of MDCK cells have unique phospholipid compositions, The EMBO Journal 1 (1982) 847.
[94] A. Kusumi, Y. Sako, Cell surface organization by the membrane skeleton, Current Opinion in Cell Biology 8 (1996) 566-574.
[95] K. Jacobson, E.D. Sheets, R. Simson, Revisiting the fluid mosaic model of membranes, Science 268 (1995) 1441-1442.
[96] J. Palek, K.E. Sahr, Mutations of the red blood cell membrane proteins: from clinical evaluation to detection of the underlying genetic defect, Blood 80 (1992) 308-330.

[97] D. Yarar, C.M. Waterman-Storer, S.L. Schmid, A Dynamic Actin Cytoskeleton Functions at Multiple Stages of Clathrin-mediated Endocytosis, Molecular Biology of the Cell 16 (2005) 964-975.
[98] M.P. Sheetz, Cell control by membraneâ€“cytoskeleton adhesion, Nat Rev Mol Cell Biol 2 (2001) 392-396.
[99] P.S. Rentsch, H. Keller, Suction pressure can induce uncoupling of the plasma membrane from cortical actin, European Journal of Cell Biology 79 (2000) 975-981.
[100] G.T. Charras, M. Coughlin, T.J. Mitchison, L. Mahadevan, Life and Times of a Cellular Bleb, Biophysical Journal 94 (2008) 1836-1853.
[101] J. Chen, M.C. Wagner, Altered membrane-cytoskeleton linkage and membrane blebbing in energy-depleted renal proximal tubular cells, Am J Physiol Renal Physiol 280 (2001) F619-627.
[102] X. Liu, R.G. Schnellmann, Calpain Mediates Progressive Plasma Membrane Permeability and Proteolysis of Cytoskeleton-Associated Paxillin, Talin, and Vinculin during Renal Cell Death, Journal of Pharmacology and Experimental Therapeutics 304 (2003) 63-70.
[103] S.R. Heidemann, S. Kaech, R.E. Buxbaum, A. Matus, Direct Observations of the Mechanical Behaviors of the Cytoskeleton in Living Fibroblasts, The Journal of Cell Biology 145 (1999) 109-122.
[104] R.M. Hochmuth, Micropipette aspiration of living cells, Journal of Biomechanics 33 (2000) 15-22.
[105] C.T. Lim, E.H. Zhou, S.T. Quek, Mechanical models for living cells--a review, Journal of Biomechanics 39 (2006) 195-216.
[106] C. Gicquaud, Actin conformation is drastically altered by direct interaction with membrane lipids: A differential scanning calorimetry study, Biochemistry 32 (1993) 11873-11877.
[107] C. Gicquaud, P. Wong, Mechanism of interaction between actin and membrane lipids: a pressure-tuning infrared spectroscopy study, Biochemical Journal 303 (1994) 769-774.
[108] B.F. Lillemeier, J.R. Pfeiffer, Z. Surviladze, B.S. Wilson, M.M. Davis, Plasma membrane-associated proteins are clustered into islands attached to the cytoskeleton, Proceedings of the National Academy of Sciences 103 (2006) 18992.
[109] J.W. Mills, E.M. Schwiebert, B.A. Stanton, The Cytoskeleton and Cell Volume Regulation, Cellular and Molecular Physiology of Cell Volume Regulation (1994).
[110] A.P. Liu, D.A. Fletcher, Actin Polymerization Serves as a Membrane Domain Switch in Model Lipid Bilayers, Biophysical Journal 91 (2006) 4064-4070.
[111] A.P. Liu, D.L. Richmond, L. Maibaum, S. Pronk, P.L. Geissler, D.A. Fletcher, Membrane-induced bundling of actin filaments, Nat Phys 4 (2008) 789-793.
[112] D.K. Hincha, R. Hofner, K.B. Schwab, U. Heber, J.M. Schmitt, Membrane rupture is the common cause of damage to chloroplast membranes in leaves injured by freezing or excessive wilting, Plant Physiol 83 (1987) 251-253.

[113] T. Senaratna, B.D. McKersie, Characterization of solute efflux from dehydration injured soybean (Glycine max L. Merr) seeds, Plant Physiology 72 (1983) 911–914.
[114] I. Puhlev, N. Guo, D.R. Brown, F. Levine, Desiccation Tolerance in Human Cells, Cryobiology 42 (2001) 207-217.
[115] J.H. Crowe, J.F. Carpenter, L.M. Crowe, The role of vitrification in anhydrobiosis, Annual Review of Physiology 60 (1998) 73-103.
[116] S. Garcia-Manyes, G. Oncins, F. Sanz, Effect of Temperature on the Nanomechanics of Lipid Bilayers Studied by Force Spectroscopy, Biophysical Journal 89 (2005) 4261-4274.
[117] S.B. Leslie, S.A. Teter, L.M. Crowe, J.H. Crowe, Trehalose Lowers Membrane Phase-Transitions in Dry Yeast-Cells, Biochim. Biophys. Acta-Biomembr. 1192 (1994) 7-13.
[118] H.H. Mantsch, A. Martin, D.G. Cameron, Characterization by infrared spectroscopy of the bilayer to nonbilayer phase transition of phosphatidylethanolamines, Biochemistry 20 (1981) 3138-3145.
[119] D. Van Bilsen, F.A. Hoekstra, L.M. Crowe, J.H. Crowe, Altered Phase Behavior in Membranes of Aging Dry Pollen May Cause Imbibitional Leakage, Plant Physiology 104 (1994) 1193.
[120] T.J. McIntosh, A.D. Magid, S.A. Simon, Steric repulsion between phosphatidylcholine bilayers, Biochemistry 26 (1987) 7325-7332.
[121] T. Ito, M. Yamazaki, S. Ohnishi, Osmoelastic coupling in biological structures: a comprehensive thermodynamic analysis of the osmotic response of phospholipid vesicles and a reevaluation of the" dehydration force" theory, Biochemistry 28 (1989) 5626-5630.
[122] P.J. Quinn, A lipid-phase seaparation model of low-temerature damage to biological membranes, Cryobiology 22 (1985) 128-146.
[123] F.E. De Leeuw, H.-C. Chen, B. Colenbrander, A.J. Verkleij, Cold-induced ultrastructural changes in bull and boar sperm plasma membranes, Cryobiology 27 (1990) 171-183.
[124] M. Yamazaki, T. Ito, Deformation and instability of membrane structure of phospholipid vesicles caused by osmophobic association: mechanical stress model for the mechanism of poly (ethylene glycol)-induced membrane fusion, Biochemistry 29 (1990) 1309-1314.
[125] S.A. Safran, T.L. Kuhl, J.N. Israelachvili, Polymer-Induced Membrane Contraction, Phase Separation, and Fusion via Marangoni Flow, Biophysical Journal 81 (2001) 659-666.
[126] J. Lee, B.R. Lentz, Outer Leaflet-Packing Defects Promote Poly(ethylene glycol)-Mediated Fusion of Large Unilamellar Vesiclesâ€ Biochemistry 36 (1997) 421-431.
[127] G. Cevc, H. Richardsen, Lipid vesicles and membrane fusion, Advanced Drug Delivery Reviews 38 (1999) 207-232.

[128] Y. Mille, L. Beney, P. Gervais, Compared tolerance to osmotic stress in various microorganisms: Towards a survival prediction test, Biotechnology and Bioengineering 92 (2005) 479-484.
[129] J.J. McGrath, The kinetics and thermodynamics of human erythrocyte freeze-thaw damage at sub-optimal cooling rates, Mechanical Engineering, vol. PhD., MIT, 1977.
[130] J. Chakrabarty, D. Banerjee, D. Pal, J. De, A. Ghosh, G.C. Majumder, Shedding off specific lipid constituents from sperm cell membrane during cryopreservation, Cryobiology 54 (2007) 27-35.
[131] N.K. Rastogi, A. Angersbach, D. Knorr, Synergistic effect of high hydrostatic pressure pretreatment and osmotic stress on mass transfer during osmotic dehydration, Journal of Food Engineering 45 (2000) 25-31.
[132] J. Antheunisse, L. Arkesteijn-Dijksman, Rate of drying and the survival of microorganisms, Antonie van Leeuwenhoek 45 (1979) 177-184.
[133] L. Beney, I.M. de Maranon, P.-A. Marechal, S. Moundanga, P. Gervais, Osmotic destruction of Saccharomyces cerevisiae is not related to a high water flow rate across the membrane, Biochemical Engineering Journal 9 (2001) 205-210.
[134] J.H. Crowe, L.M. Crowe, D. Chapman, Preservation of Membranes in Anhydrobiotic Organisms - the Role of Trehalose, Science 223 (1984) 701-703.
[135] X.H. Liu, A. Aksan, M.A. Menze, S.C. Hand, M. Toner, Trehalose loading through the mitochondrial permeability transition pore enhances desiccation tolerance in rat liver mitochondria, BBA-Biomembranes 1717 (2005) 21-26.
[136] S.B. Leslie, E. Israeli, B. Lighthart, J.H. Crowe, L.M. Crowe, Trehalose and Sucrose Protect Both Membranes and Proteins in Intact Bacteria During Drying, Applied and Environmental Microbiology 61 (1995) 3592-3597.
[137] H. Oldenhof, W.F. Wolkers, F. Fonseca, S. Passot, M. Marin, Effect of Sucrose and Maltodextrin on the Physical Properties and Survival of Air-Dried Lactobacillus bulgaricus: An in Situ Fourier Transform Infrared Spectroscopy Study, Biotechnology Progress 21 (2005) 885-892.
[138] M.M. Norris, A. Aksan, K. Sugimachi, M. Toner, 3-O-Methyl-D-Glucose Improves Desiccation Tolerance of Keratinocytes, Tissue Engineering 12 (2006) 1-7.
[139] P. Mazur, S. Leibo, E.H.Y. Chu, A Two-Factor Hypothesis of Freezing Injury, Experimental Cell Research 71 (1972) 345-355.
[140] H.T. Meryman, Osmotic stress as a mechanism of freezing injury, Cryobiology 8 (1971) 489-500.
[141] P.L. Steponkus, Behaviour of the plasma membrane during osmotic excursions, in: C.R. Hawes, J.O.D. Coleman, D.E. Evans (Eds.), Endocytosis, Exocytosis, and Vesicle Traffic in Plants, Society for Experimental Biology, London, UK, 1991, pp. 103-128.
[142] P. Mazur, K.W. Cole, Roles of unfrozen fraction, salt concentration, and changes in cell volume in the survival of frozen human erythrocytes, Cryobiology 26 (1989) 1-29.

[143] H. Ishiguro, B. Rubinsky, Mechanical Interactions between Ice Crystals and Red Blood Cells during Directional Solidification, Cryobiology 31 (1994) 483-500.
[144] A. Hubel, E.G. Cravalho, B. Nunner, C. Körber, Survival of directionally solidified B-lymphoblasts under various crystal growth conditions, Cryobiology 29 (1992) 183-198.
[145] J.E. Lovelock, The denaturation of lipid-protein complexes as a cause of damage by freezing, Proceedings of the Royal Society of London. Series B, Biological Sciences 147 (1957) 427-433.
[146] B. Han, J.C. Bischof, Direct cell injury associated with eutectic crystallization during freezing, Cryobiology 48 (2004) 8-21.
[147] P. Mazur, Freezing of Living Cells: Mechanisms and Implications, American Journal of Physiology 247 (1984) C125-C142.
[148] K. Shimada, E. Asahina, Visualization of intracellular ice crystals formed in very rapidly frozen cells at -27 °C, Cryobiology 12 (1975) 209-218.
[149] N. Fuller, R.P. Rand, Water in Actin Polymerization, Biophysical Journal 76 (1999) 3261-3266.
[150] C. Di Ciano-Oliveira, A.C.P. Thirone, K. Szaszi, A. Kapus, Osmotic Stress and the Cytoskeleton: The R(h)ole of Rho GTPases, Acta Physiologica 187 (2006) 257-272.
[151] C. Di Ciano, Z. Nie, K. Szaszi, A. Lewis, T. Uruno, X. Zhan, O.D. Rotstein, A. Mak, A. Kapus, Osmotic stress-induced remodeling of the cortical cytoskeleton, American Journal of Physiology- Cell Physiology 283 (2002) 850-865.
[152] H. Aizawa, M. Katadae, M. Maruya, M. Sameshima, K. Murakami-Murofushi, I. Yahara, I. Yahara, Hyperosmotic stress-induced reorganization of actin bundles in Dictyostelium cells over-expressing cofilin, Genes to Cells 4 (1999) 311-324.
[153] R. Tharmann, M.M.A.E. Claessens, A.R. Bausch, Micro- and Macrorheological Properties of Actin Networks Effectively Cross-Linked by Depletion Forces, Biophysical Journal 90 (2006) 2622-2627.
[154] T. Ito, M. Yamazaki, The" Le Chatelier's Principle"-Governed Response of Actin Filaments to Osmotic Stress, Journal of physical chemistry. B, Condensed matter, materials, surfaces, interfaces, & biophysical chemistry 110 (2006) 13572-13581.
[155] P.A. Janmey, The Cytoskeleton and Cell Signaling: Component Localization and Mechanical Coupling, Physiological Reviews 78 (1998) 763-781.
[156] H.F. Cantiello, A.G. Prat, J.V. Bonventre, C.C. Cunningham, J.H. Hartwig, D.A. Ausiello, Actin-binding protein contributes to cell volume regulatory ion channel activation in melanoma cells, Journal of Biological Chemistry 268 (1993) 4596-4599.
[157] K.J. Bibby, C.A. McCulloch, Regulation of cell volume and [Ca2+] i in attached human fibroblasts responding to anisosmotic buffers, American Journal of Physiology- Cell Physiology 266 (1994) 1639-1649.
[158] F. Guilak, G.R. Erickson, H.P. Ting-Beall, The Effects of Osmotic Stress on the Viscoelastic and Physical Properties of Articular Chondrocytes, Biophysical Journal 82 (2002) 720-727.

[159] P.S. Niranjan, The polymerization of actin: Thermodynamics near the polymerization line, The Journal of Chemical Physics 119 (2003) 4070.
[160] J.R. Dobrinsky, Cellular approach to cryopreservation of embryos, Theriogenology 45 (1996) 17-26.
[161] B.L. Liu, J. McGrath, Response of cytoskeleton of murine osteoblast cultures to two-step freezing, Acta Biochimica et Biophysica Sinica 37 (2005) 814-818.
[162] C. Wang, L. Zhang, M. Yuan, Y. Ge, Y. Liu, J. Fan, Y. Ruan, Z. Cui, S. Tong, S. Zhang, The microfilament cytoskeleton plays a vital role in salt and osmotic stress tolerance in Arabidopsis, Plant Biology 12 70-78.
[163] K. Muldrew, L.E. McGann, The osmotic rupture hypothesis of intracellular freezing injury, Biophys J 66 (1994) 532-541.
[164] J.J. McGrath, Thermodynamic modelling of membrane damage, in: G.J. Morris, A. Clarke (Eds.), Effects of low temperatures on biological membranes, Academic Press, London, 1981, pp. 335-417.
[165] S. Leekumjorn, A.K. Sum, Molecular Dynamics Study on the Stabilization of Dehydrated Lipid Bilayers with Glucose and Trehalose, The Journal of Physical Chemistry B 112 (2008) 10732-10740.
[166] E.A.G. Aniansson, S.N. Wall, M. Almgren, H. Hoffmann, I. Kielmann, W. Ulbricht, R. Zana, J. Lang, C. Tondre, Theory of the kinetics of micellar equilibria and quantitative interpretation of chemical relaxation studies of micellar solutions of ionic surfactants, The Journal of Physical Chemistry 80 (1976) 905-922.
[167] B.J. Fuller, A.N. Lane, E.E. Benson, Life in the Frozen State, CRC Press, Boca Raton, 2004.
[168] P.L. Steponkus, D.V. Lynch, Freeze/Thaw-Induced Destabilization of the Plasma Membrane and the Effects of Cold Acclimation, Journal of Bioenergetics and Biomembranes 21 (1989) 21-41.
[169] A. Eroglu, M.J. Russo, R. Bieganski, A. Fowler, S. Cheley, H. Bayley, M. Toner, Intracellular trehalose improves the survival of cryopreserved mammalian cells, Nature Biotechnology 18 (2000) 163-167.
[170] A. Eroglu, M. Toner, T.L. Toth, Beneficial Effect of Microinjected Trehalose on the Cryosurvival of Human Oocytes, Fertility and Sterility 77 (2002) 152-158.
[171] J.H. Crowe, L.M. Crowe, Membrane Stabilization at Low Water Activities, Cryobiology 19 (1982) 670-670.
[172] T. Arakawa, S.N. Timasheff, Preferential interactions of proteins with salts in concentrated solutions, Biochemistry 21 (1982) 6545-6552.
[173] S.N. Timasheff, Protein Hydration, Thermodynamic Binding, and Preferential Hydration, Biochemistry 41 (2002) 13473-13482.
[174] A. Charrier, F. Thibaudau, Main Phase Transitions in Supported Lipid Single-Bilayer, Biophysical Journal 89 (2005) 1094-1101.
[175] C.B. Fox, G.A. Myers, J.M. Harris, Temperature-Controlled Confocal Raman Microscopy to Detect Phase Transitions in Phospholipid Vesicles, Applied Spectroscopy 61 (2007) 465-469.

[176] D.K. Hincha, M. Hagemann, Stabilization of model membranes during drying by compatible solutes involved in the stress tolerance of plants and microorganisms, Biochem. J 383 (2004) 277-283.
[177] S. Kint, P.H. Wermer, J.R. Scherer, Raman Spectra of Hydrated Phospholipid Bilayers. 2. Water and Head-Group Interactions, Journal of Physical Chemistry 96 (1992) 446-452.
[178] M.R. Morrow, J.P. Whitehead, D. Lu, Chain-length dependence of lipid bilayer properties near the liquid crystal to gel phase transition, Biophysical Journal 63 (1992) 18-27.
[179] G. Bryant, K.L. Koster, Dehydration of solute–lipid systems: hydration forces analysis, Colloids and Surfaces B: Biointerfaces 35 (2004) 73-79.
[180] L. Cruzeiro-Hanson, O.G. Mouritsen, Passive ion Permeability of Lipid Membranes Modelled via Lipid-domain Interfacial Area, Biochimica et Biophysica Acta 944 (1988) 63-72.
[181] T.H. Haines, Water Transport Across Biological Membranes, FEBS Letters 346 (1994) 115-122.
[182] D. Papahadjopoulos, K. Jacobson, S. Nir, T. Isca, Phase Transitions in Phospholipid Vesicles, Biochimica et Biophysica Acta 311 (1973) 330-348.
[183] F.A. Hoekstra, W.F. Wolkers, J. Buitink, E.A. Golovina, J.H. Crowe, L.M. Crowe, Membrane stabilization in the dry state, Pergamon-Elsevier Science Ltd, 1997, pp. 335-341.
[184] R. Lewis, B.D. Sykes, R.N. McElhaney, Thermotropic phase behavior of model membranes composed of phosphatidylcholines containing cis-monounsaturated acyl chain homologs of oleic acid: differential scanning calorimetric and phosphorus-31 NMR spectroscopic studies, Biochemistry 27 (1988) 880-887.
[185] F.M. Harris, K.B. Best, J.D. Bell, Use of laurdan fluorescence intensity and polarization to distinguish between changes in membrane fluidity and phospholipid order, BBA-Biomembranes 1565 (2002) 123-128.
[186] D. Chapman, J. Urbina, K.M. Keough, Biomembrane Phase Transitions: Studies of Lipid-water systems using differential scanning calorimetry, Journal of Biological Chemistry 249 (1974) 2512-2521.
[187] W.F. Wolkers, L.M. Crowe, N.M. Tsvetkova, F. Tablin, J.H. Crowe, In situ assessment of erythrocyte membrane properties during cold storage, Mol. Membr. Biol. 19 (2002) 59-65.
[188] V. Ragooonanan, M. J., D.R. Bond, A. Aksan, Roles of Membrane Structure and Phase Transition on the Hyperosmotic Stress Survival of Geobacter sulfurreducens, Biochimica et Biophysica Acta (BBA)-Biomembranes 1778 (2008) *2283-2290*.
[189] S.K. Balasubramanian, W.F. Wolkers, J.C. Bischof, Membrane Hydration Correlates to Cellular Biophysics During Freezing in Mammalian Cells, Biochem. et Biophys. Acta (In Review) (2008).
[190] W.F. Wolkers, S.K. Balasubramanian, E.L. Ongstad, H.C. Zec, J.C. Bischof, Effects of freezing on membranes and proteins in LNCaP prostate tumor cells, Biochimica et Biophysica Acta 1768 (2007) 728-736.

[191] A.C. Biondi, G.A. Senisterra, E.A. Disalvo, Permeability of Lipid Membranes Revised in Relation to Freeze-Thaw Processes, Cryobiology 29 (1992) 323-331.
[192] F.A. Hoekstra, J.H. Crowe, L.M. Crowe, Effect of Sucrose on Phase-Behavior of Membranes in Intact Pollen of Typha-Latifolia L, as Measured with Fourier-Transform Infrared-Spectroscopy, Plant Physiol. 97 (1991) 1073-1079.
[193] C. Laroche, H. Simonin, L. Beney, P. Gervais, Phase transitions as a function of osmotic pressure in Saccharomyces cerevisiae whole cells, membrane extracts and phospholipid mixtures, Biochimica et Biophysica Acta (BBA)-Biomembranes 1669 (2005) 8-16.
[194] C.M. Scherber, J.L. Schottel, A. Aksan, Membrane phase behavior of Escherichia coli during desiccation, rehydration, and growth recovery, Biochimica et Biophysica Acta (BBA) - Biomembranes 1788 (2009) 2427-2435.
[195] A.S. Ulrich, M. Sami, A. Watts, Hydration of DOPC bilayers by Differential Scanning Calorimetry, Biochimica Et Biophysica Acta 1191 (1994) 225-230.
[196] Y.-D. Zhang, Y. Lu, S.-X. Hu, M. Li, Thermotropic Phase Behavior of Multilamellar Membranes of Dioleoylphosphatidylcholine, The Journal of Physical Chemistry B 114 (2010) 2153-2157.
[197] K. Brandenburg, U. Seydel, Infrared spectroscopy of glycolipids, Chem. Phys. Lipids 96 (1998) 23-40.
[198] J.R. Silvius, Lipid-protein interactions, by PC Jost and OH Griffith, A Wiley-Interscience Publication, John Wiley & Sons, New York 2 (1982) 265.
[199] R.J. Mashl, H.L. Scott, S. Subramaniam, E. Jakobsson, Molecular Simulation of Dioleoylphosphatidylcholine Lipid Bilayers at Differing Levels of Hydration, Biophysical Journal 81 (2001) 3005-3015.
[200] R.L. Biltonen, A statistical-thermodynamic view of cooperative structural changes in phospholipid bilayer membranes: their potential role in biological function, Journal of chemical thermodynamics 22 (1990) 1-19.
[201] P. Ni, J. Ding, B. Rao, In situ cryogenic Raman spectroscopic studies on the synthetic fluid inclusions in the systems H_2O and NaCl-H_2O, Chinese Science Bulletin 51 (2006) 108-114.
[202] A. Nilsson, A. Holmgren, G. Lindblom, An FTIR Study of the Hydration and Molecular Ordering at Phase Transitions in the Monooleoylglcerol/Water Systems, Chemistry and Physics of Lipids 71 (1994) 119-131.
[203] W. Pohle, C. Selle, H. Fritzsche, H. Binder, Fourier Transform Infrared Spectrsocsopy as a Probe for the Study of the Hydration of Lipid Self-Assemblies. I. Methodology and General Phenomena, Biospectroscopy 4 (1998) 267-280.
[204] R.A. Callow, J.J. McGrath, Thermodynamic modeling and cryomicroscopy of cell-size, unilamellar, and paucilamellar liposomes, Cryobiology 22 (1985) 251-267.
[205] J. Kristiansen, Leakage of a trapped fluorescent marker from liposomes: Effects of eutectic crystallization of NaCl and internal freezing, Cryobiology 29 (1992) 575-584.

[206] K. Izutsu, S. Yoshioka, S. Kojima, Effect of cryoprotectants on the eutectic crystallization of NaCl in frozen solutions studied by differential scanning calorimetry (DSC) and broad-line pulsed NMR, Chemical & pharmaceutical bulletin 43 (1995) 1804-1806.
[207] A.K. Sum, R. Faller, J.J. de Pablo, Molecular Simulation Study of Phospholipid Bilayers and Insights of the Interactions with Disaccharides, Biophysical Journal 85 (2003) 2830-2844.
[208] D.R. Bond, D.R. Lovley, Electricity Production by *Geobacter Sulfurreducens* Attached to Electrodes, Applied and Environmental Microbiology 69 (2003) 1548-1555.
[209] J.R. Lloyd, D.R. Lovley, L.E. Macaskie, Biotechnological application of metal-reducing microorganisms, Adv Appl Microbiol 53 (2003) 85-128.
[210] D.R. Lovley, Dissimilatory Fe (III) and Mn (IV) reduction, Microbiology and Molecular Biology Reviews 55 (1991) 259.
[211] D.R. Lovley, Microbial fuel cells: novel microbial physiologies and engineering approaches, Current Opinion in Biotechnology 17 (2006) 327-332.
[212] M.E. Hernandez, D.K. Newman, Extracellular electron transfer, Cellular and Molecular Life Sciences (CMLS) 58 (2001) 1562-1571.
[213] J.D. Wall, L.R. Krumholz, Uranium Reduction, Annu. Rev. Microbiol 60 (2006) 149-166.
[214] M.C. Flickinger, J.L. Schottel, D.R. Bond, A. Aksan, L.E. Scriven, Painting and printing living bacteria: Engineering nanoporous biocatalytic coatings to preserve microbial viability and intensify reactivity, Biotechnology Progress 23 (2007) 2-17.
[215] M.J. Wilkins, F.R. Livens, D.J. Vaughan, J.R. Lloyd, The Impact of Fe (III)-reducing Bacteria on Uranium Mobility, Biogeochemistry 78 (2006) 125-150.
[216] D.R. Bond, D.E. Holmes, L.M. Tender, D.R. Lovley, Electrode-reducing microorganisms that harvest energy from marine sediments, Science 295 (2002) 483-485.
[217] A. Shantaram, H. Beyenal, R. Raajan, A. Veluchamy, Z. Lewandowski, Wireless Sensors Powered by Microbial Fuel Cells, Environmental Science and Technology 39 (2005) 5037-5042.
[218] S. Srikanth, E. Marsili, M.C. Flickinger, D.R. Bond, Electrochemical characterization of *Geobacter sulfurreducens* cells immobilized on graphite paper electrodes, Biotechnol Bioeng 99 (2007) 1065-1073.
[219] V.S. Thiagarajan, Z. Huang, L.E. Scriven, J.L. Schottel, M.C. Flickinger, Microstructure of a biocatalytic latex coating containing viable *Escherichia coli* cells, Journal of Colloid And Interface Science 215 (1999) 244-257.
[220] O.K. Lyngberg, D.J. Stemke, J.L. Schottel, M.C. Flickinger, A single-use luciferase-based mercury biosensor using *Escherichia coli* HB101 immobilized in a latex copolymer film, Journal of Industrial Microbiology and Biotechnology 23 (1999) 668-676.
[221] O.K. Lyngberg, C.P. Ng, V.S. Thiagarajan, L.E. Scriven, M.C. Flickinger, Engineering the Microstructure and Permeability of Thin Multilayer Latex

Biocatalytic Coatings Containing E. coli, Biotechnology Progress 17 (2001) 1169-1179.
[222] J.H. Crowe, L.M. Crowe, J.F. Carpenter, S.J. Prestrelski, F.A. Hoekstra, P. de Araujo, A.D. Panek, Anhydrobiosis: cellular adaptation to extreme dehydration, Handbook of Physiology 2 (1997) 1445–1477.
[223] J.H. Crowe, L.M. Crowe, F.A. Hoekstra, Phase-transitions and permeability changes in dry membranes during rehydration, J. Bioenerg. Biomembr. 21 (1989) 77-91.
[224] C. Laroche, H. Simonin, L. Beney, P. Gervais, Phase transitions as a function of osmotic pressure in *Saccharomyces cerevisiae* whole cells, membrane extracts and phospholipid mixtures, BBA-Biomembranes 1669 (2005) 8-16.
[225] E.Z. Drobnis, L.M. Crowe, T. Berger, T.J. Anchordoguy, J.W. Overstreet, J.H. Crowe, Cold shock damage is due to lipid phase-transitions in cell-membranes - A demonstration using sperm as a model, J. Exp. Zool. 265 (1993) 432-437.
[226] G. Anderle, R. Mendelsohn, Thermal denaturation of globular proteins. Fourier transform-infrared studies of the amide III spectral region, Biophysical Journal 52 (1987) 69-74.
[227] E. Goormaghtigh, J.M. Ruysschaert, V. Raussens, Evaluation of the Information Content in Infrared Spectra for Protein Secondary Structure Determination, Biophysical Journal 90 (2006) 2946-2957.
[228] C.A. Morgan, N. Herman, P.A. White, G. Vesey, Preservation of micro-organisms by drying; A review, Journal of Microbiological Methods 66 (2006) 183-193.
[229] H. Susi, D.M. Byler, Protein structure by Fourier transform infrared spectroscopy: second derivative spectra, Biochem Biophys Res Commun 115 (1983) 391-397.
[230] W.F. Wolkers, S.A. Looper, R.A. Fontanilla, N.M. Tsvetkova, F. Tablin, J.H. Crowe, Temperature dependence of fluid phase endocytosis coincides with membrane properties of pig platelets, BBA-Biomembranes 1612 (2003) 154-163.
[231] L.M. Crowe, J.H. Crowe, A. Rudolph, C. Womersley, L. Appel, Preservation of freeze-dried liposomes by trehalose, Archives of Biochemistry and Biophysics 242 (1985) 240-247.
[232] M.J. Blandamer, J. Engberts, P.T. Gleeson, J.C.R. Reis, Activity of water in aqueous systems; A frequently neglected property, Chemical Society Reviews 34 (2005) 440-458.
[233] D.P. Siegel, The Modified Stalk Mechanism of Lamellar/Inverted Phase Transitions and Its Implications for Membrane Fusion, Biophysical Journal 76 (1999) 291-313.
[234] G. Charras, E. Paluch, Blebs lead the way: how to migrate without lamellipodia, Nat Rev Mol Cell Biol 9 (2008) 730-736.
[235] J.A. Cooper, Effects of cytochalasin and phalloidin on actin, vol. 105, Rockefeller Univ Press, 1987, pp. 1473-1478.
[236] A.F. Straight, A. Cheung, J. Limouze, I. Chen, N.J. Westwood, J.R. Sellers, T.J. Mitchison, Dissecting Temporal and Spatial Control of Cytokinesis with a Myosin II Inhibitor, Science 299 (2003) 1743-1747.

[237] M. Uehata, T. Ishizaki, H. Satoh, T. Ono, T. Kawahara, T. Morishita, H. Tamakawa, K. Yamagami, J. Inui, M. Maekawa, Calcium sensitization of smooth muscle mediated by a Rho-associated protein kinase in hypertension, Nature 389 (1997) 990-993.
[238] D. Di Carlo, N. Aghdam, L.P. Lee, Single-Cell Enzyme Concentrations, Kinetics, and Inhibition Analysis Using High-Density Hydrodynamic Cell Isolation Arrays, Analytical Chemistry 78 (2006) 4925-4930.
[239] T.J. Mitchison, G.T. Charras, L. Mahadevan, Implications of a poroelastic cytoplasm for the dynamics of animal cell shape, Seminars in Cell & Developmental Biology 19 (2008) 215-223.
[240] D. Raucher, M.P. Sheetz, Cell Spreading and Lamellipodial Extension Rate Is Regulated by Membrane Tension, J. Cell Biol. 148 (2000) 127-136.
[241] R.A. Böckmann, A. Hac, T. Heimburg, H. Grubmüller, Effect of Sodium Chloride on a Lipid Bilayer, Biophysical Journal 85 (2003) 1647-1655.
[242] R. VaÌ□cha, S.W.I. Siu, M. Petrov, R.A. BoÌˆckmann, J. Barucha-Kraszewska, P. Jurkiewicz, M. Hof, M.L. Berkowitz, P. Jungwirth, Effects of Alkali Cations and Halide Anions on the DOPC Lipid Membraneâ€ The Journal of Physical Chemistry A 113 (2009) 7235-7243.
[243] S. Garcia-Manyes, G. Oncins, F. Sanz, Effect of Ion-Binding and Chemical Phospholipid Structure on the Nanomechanics of Lipid Bilayers Studied by Force Spectroscopy, Biophysical Journal 89 (2005) 1812-1826.
[244] V.L. Sukhorukov, D. Imes, M.W. Woellhaf, J. Andronic, M. Kiesel, R. Shirakashi, U. Zimmermann, H. Zimmermann, Pore size of swelling-activated channels for organic osmolytes in Jurkat lymphocytes, probed by differential polymer exclusion, Biochimica et Biophysica Acta (BBA) - Biomembranes 1788 (2009) 1841-1850.
[245] P.A. Marechal, I.M. de Marañon, P. Molin, P. Gervais, Yeast cell responses to water potential variations, International Journal of Food Microbiology 28 (1995) 277-287.
[246] A. Zweifach, FM1-43 reports plasma membrane phospholipid scrambling in T-lymphocytes, Biochem. J. 349 (2000) 255-260.
[247] E.B. Abuin, A.M. Campos, E.A. Lissi, E.A. Disalvo, Osmotic Response of Large Unilamellar Vesicles of Phosphatidylcholine: Factors Determining the Rate of the Process and the Properties of the Shrunken Vesicles, Journal of Colloid and Interface Science 171 (1995) 406-412.
[248] E.A. Disalvo, A.M. Campos, E. Abuin, E.A. Lissi, Surface changes induced by osmotic shrinkage on large unilamellar vesicles, Chemistry and Physics of Lipids 84 (1996) 35-45.
[249] W.J. Betz, F. Mao, C.B. Smith, Imaging exocytosis and endocytosis, Current Opinion in Neurobiology 6 (1996) 365-371.
[250] M.M.G. Krishna, N. Periasamy, Fluorescence of organic dyes in lipid membranes: Site of solubilization and effects of viscosity and refractive index on lifetimes, Journal of Fluorescence 8 (1998) 81-91.

[251] R.W. Stroetz, N.E. Vlahakis, B.J. Walters, M.A. Schroeder, R.D. Hubmayr, Validation of a new live cell strain system: characterization of plasma membrane stress failure, J Appl Physiol 90 (2001) 2361-2370.
[252] H. Takamatsu, S. Zawlodzka, Contribution of extracellular ice formation and the solution effects to the freezing injury of PC-3 cells suspended in NaCl solutions, Cryobiology 53 (2006) 1-11.
[253] A.A. Gurtovenko, J. Anwar, Modulating the Structure and Properties of Cell Membranes: The Molecular Mechanism of Action of Dimethyl Sulfoxide, Journal of Physical Chemistry B 111 (2007) 10453-10460.
[254] C. Vincent, S.J. Pickering, M.H. Johnson, Dimethylsulfoxide Affects The Organization Of Microfilaments In The Mouse Oocyte, Molecular Reproduction And Development 26 (1990) 227-235.
[255] C. Vincent, G. Pruliere, E. Pajotaughy, Effects Of Cryoprotectants On Actin-Filaments During The Cryopreservation Of One-Cell Rabbit Embryos Cryobiology 27 (1990) 9-23.
[256] C.C. Cunningham, Actin polymerization and intracellular solvent flow in cell surface blebbing, J. Cell Biol. 129 (1995) 1589-1599.
[257] P. Nicotera, P. Hartzell, G. Davis, S. Orrenius, The formation of plasma membrane blebs in hepatocytes exposed to agents that increase cytosolic Ca2+ is mediated by the activation of a non-lysosomal proteolytic system, FEBS Letters 209 (1986) 139-144.
[258] E.A. Disalvo, Thermodynamic factors determining the permeability barrier properties of lipid bilayers, Chemistry and Physics of Lipids 37 (1985) 385-397.
[259] K. Arnold, L. Pratsch, K. Gawrisch, Effect of poly(ethylene glycol) on phospholipid hydration and polarity of the external phase, Biochimica et Biophysica Acta (BBA) - Biomembranes 728 (1983) 121-128.
[260] S. Dupont, L. Beney, J.-F. Ritt, J. Lherminier, P. Gervais, Lateral reorganization of plasma membrane is involved in the yeast resistance to severe dehydration, Biochimica et Biophysica Acta (BBA) - Biomembranes 1798 (2010) 975-985.
[261] V.L. Sukhorukov, W.M. Arnold, U. Zimmermann, Hypotonically induced changes in the plasma membrane of cultured mammalian cells, Journal of Membrane Biology 132 (1993) 27-40.
[262] N. Groulx, F. Boudreault, S. Orlov, R. Grygorczyk, Membrane Reserves and Hypotonic Cell Swelling, Journal of Membrane Biology 214 (2006) 43-56.
[263] L.R. Maki, E.L. Galyan, M.M. Chang-Chien, D.R. Caldwell, Ice nucleation induced by Pseudomonas syringae, Applied and Environmental Microbiology 28 (1974) 456-459.
[264] P. Mazur, W.F. Rall, N. Rigopoulos, Relative contributions of the fraction of unfrozen water and of salt concentration to the survival of slowly frozen human erythrocytes, Biophys J 36 (1981) 653-675.
[265] M.I. Gibson, C.A. Barker, S.G. Spain, L. Albertin, N.R. Cameron, Inhibition of Ice Crystal Growth by Synthetic Glycopolymers: Implications for the Rational Design of Antifreeze Glycoprotein Mimics, Biomacromolecules 10 (2008) 328-333.

[266] T. Inada, S.-S. Lu, Inhibition of Recrystallization of Ice Grains by Adsorption of Poly(Vinyl Alcohol) onto Ice Surfaces, Crystal Growth & Design 3 (2003) 747-752.
[267] P.L. Davies, C.L. Hew, Biochemistry of fish antifreeze proteins, FASEB J. 4 (1990) 2460-2468.
[268] M.A. Haidekker, E.A. Theodorakis, Molecular rotors—fluorescent biosensors for viscosity and flow, Organic & Biomolecular Chemistry 5 (2007) 1669-1678.
[269] S. Sawada, T. Iio, Y. Hayashi, S. Takahashi, Fluorescent rotors and their applications to the study of G-F transformation of actin, Analytical Biochemistry 204 (1992) 110-117.
[270] K. Luby-Phelps, D.L. Taylor, F. Lanni, Probing the structure of cytoplasm, J. Cell Biol. 102 (1986) 2015-2022.
[271] M.A. Haidekker, N. L'Heureux, J.A. Frangos, Fluid shear stress increases membrane fluidity in endothelial cells: a study with DCVJ fluorescence, American Journal of Physiology 278 (2000) H1401-1406.
[272] C. Ballestrem, B. Wehrle-Haller, B.A. Imhof, Actin dynamics in living mammalian cells, Journal of cell science 111 (1998) 1649-1658.
[273] E. Evans, A. Leung, Adhesivity and rigidity of erythrocyte membrane in relation to wheat germ agglutinin binding, The Journal of Cell Biology 98 (1984) 1201-1208.
[274] R.A. Anderson, R.E. Lovrien, Erythrocyte membrane sidedness in lectin control of the Ca2+-A23187-mediated diskocyte [rlarr2] echinocyte conversion, Nature 292 (1981) 158-161.
[275] S. Lin, W.H. Huestis, Wheat germ agglutinin stabilization of erythrocyte shape: role of bilayer balance and the membrane skeleton, Biochimica et Biophysica Acta (BBA) - Biomembranes 1233 (1995) 47-56.
[276] M.P. Christopher, K. Predrag, N. Ian, Effect of Polyethylene Glycol on the Microstructure of Freeze-Cast Alumina, Journal of the American Ceramic Society 91 (2008) 3185-3190.
[277] H. Ishiguro, B. Rubinsky, Influence of antifreeze proteins on the freezing of suspensions of human red blood cells with glycerol and the viabiliy of cells, in: L. Fletcher, T. Aihara (Eds.), ASME/JSME Thermal Engineering Conference, vol. 4, ASME, Lahaina, Hawaii, 1995, pp. 561-566.
[278] J.F. Carpenter, T.N. Hansen, Antifreeze protein modulates cell survival during cryopreservation: mediation through influence on ice crystal growth, Proceedings of the National Academy of Sciences of the United States of America 89 (1992) 8953-8957.
[279] C.P. Sharma, M. Szycher, Blood compatible materials and devices: perspectives towards the 21st century, CRC, 1991, pp. 123-130.
[280] V. Ragoonanan, J. Malsam, D.R. Bond, A. Aksan, Roles of membrane structure and phase transition on the hyperosmotic stress survival of Geobacter sulfurreducens, Biochim Biophys Acta 1778 (2008) 2283-2290.

[281] S.K. Balasubramanian, W.F. Wolkers, J.C. Bischof, Membrane hydration correlates to cellular biophysics during freezing in mammalian cells, Biochimica et Biophysica Acta (BBA) - Biomembranes 1788 (2009) 945-953.
[282] A.S. Sechi, J. Wehland, The actin cytoskeleton and plasma membrane connection: PtdIns(4,5)P(2) influences cytoskeletal protein activity at the plasma membrane, J Cell Sci 113 (2000) 3685-3695.
[283] L.E. McGann, H. Yang, M. Walterson, Manifestations of cell damage after freezing and thawing, Cryobiology 25 (1988) 178-185.
[284] R. Hamm, Delocalization of Mitochondrial Enzymes During Freezing and Thawing of Skeletal Muscle, Proteins at Low Temperatures, American Chemical Society, Washington, D.C., 1979, pp. 191-204.
[285] J.W. Nichols, Thermodynamics and kinetics of phospholipid monomer-vesicle interaction, Biochemistry 24 (1985) 6390-6398.
[286] J.D. Jones, T.E. Thompson, Mechanism of spontaneous, concentration-dependent phospholipid transfer between bilayers, Biochemistry 29 (1990) 1593-1600.
[287] M.S.C. Abreu, M.J. Moreno, W.L.C. Vaz, Kinetics and Thermodynamics of Association of a Phospholipid Derivative with Lipid Bilayers in Liquid-Disordered and Liquid-Ordered Phases, Biophysical Journal 87 (2004) 353-365.
[288] Y. Kita, T. Arakawa, T.-Y. Lin, S.N. Timasheff, Contribution of the Surface Free Energy Perturbation to Protein-Solvent Interactions, Biochemistry 33 (1994) 15178-15189.
[289] S.W. Burgess, D. Massenburg, J. Yates, B.R. Lentz, Polyethylene glycol-induced lipid mixing but not fusion between synthetic phosphatidylcholine large unilamellar vesicles, Biochemistry 30 (1991) 4193-4200.
[290] S.J. Palmer, The effect of temperature on surface tension, Physics Education 11 (1976) 119.
[291] K. Arnold, O. Zschoernig, D. Barthel, W. Herold, Exclusion of poly(ethylene glycol) from liposome surfaces, Biochimica et Biophysica Acta (BBA) - Biomembranes 1022 (1990) 303-310.
[292] C.S. Pereira, R.D. Lins, I. Chandrasekhar, L.C.G. Freitas, P.H. Hunenberger, Interaction of the Disaccharide Trehalose with a Phospholipid Bilayer: A Molecular Dynamics Study, Biophysical Journal 86 (2004) 2273-2285.
[293] B.H. Lavenda, Concepts of stability and symmetry in irreversible thermodynamics. I, Foundations of Physics 2 (1972) 161-179.
[294] L.R. McLean, M.C. Phillips, Kinetics of phosphatidylcholine and lysophosphatidylcholine exchange between unilamellar vesicles, Biochemistry 23 (1984) 4624-4630.
[295] D.P. Tieleman, S.-J. Marrink, Lipids Out of Equilibrium:â€‰ Energetics of Desorption and Pore Mediated Flip-Flop, Journal of the American Chemical Society 128 (2006) 12462-12467.
[296] J.J. Blum, Interaction between myosin and its substrates, Archives of Biochemistry and Biophysics 87 (1960) 104-119.

[297] M. Anson, Temperature dependence and arrhenius activation energy of F-actin velocity generated in vitro by skeletal myosin, Journal of Molecular Biology 224 (1992) 1029-1038.
[298] P.S. Niranjan, P.B. Yim, J.G. Forbes, S.C. Greer, J. Dudowicz, K.F. Freed, J.F. Douglas, The polymerization of actin: Thermodynamics near the polymerization line, The Journal of Chemical Physics 119 (2003) 4070.
[299] E.H. Zhou, X. Trepat, C.Y. Park, G. Lenormand, M.N. Oliver, S.M. Mijailovich, C. Hardin, D.A. Weitz, J.P. Butler, J.J. Fredberg, Universal behavior of the osmotically compressed cell and its analogy to the colloidal glass transition, Proceedings of the National Academy of Sciences 106 (2009) 10632-10637.
[300] E. Boroske, M. Elwenspoek, W. Helfrich, Osmotic shrinkage of giant egg-lecithin vesicles, Biophysical Journal 34 (1981) 95-109.
[301] L. Pocivavsek, R. Dellsy, A. Kern, S. Johnson, B. Lin, K.Y.C. Lee, E. Cerda, Stress and Fold Localization in Thin Elastic Membranes, Science 320 (2008) 912-916.
[302] A. Kemp Jr, G.S.P. Groot, H.J. Reitsma, Oxidative phosphorylation as a function of temperature, Biochimica et Biophysica Acta (BBA) - Bioenergetics 180 (1969) 28-34.
[303] D. Smith, F. Ziebert, D. Humphrey, C. Duggan, M. Steinbeck, W. Zimmermann, J. Käs, Molecular Motor-Induced Instabilities and Cross Linkers Determine Biopolymer Organization, Biophysical Journal 93 (2007) 4445-4452.
[304] J. Xu, D. Wirtz, T.D. Pollard, Dynamic cross-linking by α-actinin determines the mechanical properties of actin filament networks, Journal of Biological Chemistry 273 (1998) 9570-9576.
[305] D. Raucher, T. Stauffer, W. Chen, K. Shen, S. Guo, J.D. York, M.P. Sheetz, T. Meyer, Phosphatidylinositol 4,5-Bisphosphate Functions as a Second Messenger that Regulates Cytoskeleton-Plasma Membrane Adhesion, Cell 100 (2000) 221-228.
[306] I. Titushkin, M. Cho, Distinct membrane mechanical properties of human mesenchymal stem cells determined using laser optical tweezers, Biophysical journal 90 (2006) 2582-2591.
[307] B. Kaur, J.M. Graham, C.A. Pasternak, Isolation of microvilli from mammalian cells, FEBS Letters 85 (1978) 353-356.
[308] S. Gabriele, A.-M. Benoliel, P. Bongrand, O. Théodoly, Microfluidic Investigation Reveals Distinct Roles for Actin Cytoskeleton and Myosin II Activity in Capillary Leukocyte Trafficking, Biophysical Journal 96 (2009) 4308-4318.
[309] R.A. Marinelli, L. Pham, P. Agre, N.F. LaRusso, Secretin Promotes Osmotic Water Transport in Rat Cholangiocytes by Increasing Aquaporin-1 Water Channels in Plasma Membrane, Journal of Biological Chemistry 272 (1997) 12984-12988.